Investigation of Radial Flow Ejector Performance Through Experiments and Computational Simulations

A Thesis submitted by

Hadi Rahimi, M Eng

For the award of

Doctor of Philosophy

2017

Dedication

To my family Maryam and Arvin

To Dad and Mam

To my brothers and my sister

Abstract

Adjustability in ejector geometry is desirable to extend the operating range of ejectors at different working conditions. Current approaches to geometric adjustability in the throat sizes of conventional axial ejectors have the disadvantage of blocking the flow path by positioning additional components in the high-speed flow. Furthermore, a viable mechanical system is not available for altering the diameters of the nozzle and ejector throat while providing gas-tight seals and a smooth surface throughout. An alternative concept, the radial ejector, has been created which makes possible a practical ejector that can readily achieve variable geometry without introducing additional flow blockage in the center of the high-speed flow. Such a radial configuration allows geometry adjustment during operation to achieve optimum performance at a range of different operating conditions without additional pressure losses from high-speed flow blockage. The radial ejector conceived, designed, commissioned and evaluated in this thesis was formed from two disk-like surfaces for both the primary nozzle and the ejector body enabling the radial ejector to operate with different flow areas by simply changing the separation of the ejector duct walls or the nozzle plates. Conventional axial flow ejector design procedures were adapted in the design process, and benchmarking against an experimental axial ejector was also performed. Air was employed as the working fluid to improve fabrication options and allow experiments to be performed with an open system. The radial ejector has a nozzle throat area of 8.8 mm^2 and a nozzle exit area of 180 mm^2, giving a nozzle area ratio of 20.4, and an ejector physical throat area of 520 mm^2, giving the ejector area ratio of 59. Experimental results show that the radial ejector produced entrainment ratios between 0.95 and 0.24 and critical pressure lift ratios around 1.5 for expansion ratios between 50 and 139. The relationships between the entrainment ratio and critical exit pressure and primary, secondary and exit pressures were similar to conventional axial ejectors. Similarly, trends observed in the measurements of wall pressure for the radial ejector configuration were generally consistent

with those for axial flow ejectors. Based on the experimental data from the critical mode ejector operation and based on an isentropic flow calculation, a secondary stream Mach number of around 0.7 was determined at the physical throat of the ejector. When ejector operation transitioned from the critical to the subcritical mode, wall pressures in the throat and at locations upstream of the throat increased, leading to a peak in pressure prior to the final pressure rise in the diffuser. Comparing the experimental results with the simulations show that the entrainment ratio achieved from the radial ejector prototype agreed well. The entrainment ratio performance also closely matched that of a quasi-one-dimensional gas dynamic model with an error level less than 10%. Computational Fluid Dynamic (CFD) analysis based on the k-epsilon standard turbulence model showed that simulations of entrainment ratio and critical back pressure were in reasonable agreement with the experimental results with an average discrepancy of less than 16%. Using the k-omega SST turbulence model, it was demonstrated that adjustability in the radial ejector is viable and by increasing the separation of the ejector duct walls from 2.2 mm to 3 mm, an increase of 34% in entrainment ratio can be achieved. A critical back pressure increase of 40% was achieved by reducing the separation of the ejector duct walls from 3 mm to 2.2 mm. However, as there are systematic differences between the measurements and the computational simulations using either the k-omega SST or the k-epsilon standard model, the overall reliability of the CFD simulations is questionable. The main issue for the current prototype radial ejector is the low critical exit pressure relative to expected performance from an equivalent axial flow ejector. More experiments and simulation are required to improve this aspect of the radial ejector performance. The radial ejector geometry is required to be optimized and many different flow features need extensive investigation to identify ways to achieve better performance and expand the adjustability options in the radial ejector.

Certification of Thesis

This thesis is entirely the work of Hadi Rahimi except where otherwise acknowledged. The work is original and has not previously been submitted for any other award, except where acknowledged.

Student and supervisors signatures of endorsement are held at USQ.

David Buttsworth

Principal Supervisor

Ray Malpress

Associate Supervisor

Acknowledgment

I would like to express my deepest gratitude to Professor David Buttsworth, my principal supervisor, for his persistence and support. This work would not have been possible without his guidance and encouragement. I would also like to acknowledge the support of my associate supervisor, Dr Ray Malpress, for his knowledge and mental and physical support in design and conducting the experiments. His instant response to all my questions and requests is highly appreciated.

In addition, I would like to acknowledge the support given by my colleagues: Drs Rishabh Choudhury, Khalid Saleh, John Leis, Ahmad Sharifian, Kavous Ariafar, and Mr Dean Beliveau, Chris Galligan and Adrian Blokland who generously shared their expertise and technical knowledge.

I would also like to thank my wife, Maryam, for her generous support specifically at the beginning of my study. I could never forget her helping hands. I would also like to thank my son, Arvin, for his companionship during my study at home and at my office. I also could not forget the support and encouragement of my sister and my brothers.

Finally, my dearest father and mother, I could not express what you have done to build me. I can only say thank you.

Hadi Rahimi

Table of Contents

List of Figures

List of Tables

Symbols, Acronyms & Abbreviations

d diameter, case of axial ejector

h separation of upper and lower surfaces, case of radial ejector

L length, case of axial ejectors

R radius, case of radial ejector; gas constant

p pressure

ω entrainment ratio, $\dot{m}_s/\dot{m}_p$

θ ejector contraction half-angle

Superscript

$*$ primary nozzle throat condition

Subscript

0 ejector at primary nozzle exit; stagnation value

$crit$ critical diffuser exit value

p primary stream

s secondary stream

t ejector throat

$exit$ exit of the primary nozzle

d exit of the diffuser

max maximum

mal malfunction

φ thrust augmentation

T_E ejector thrust

T_N nozzle thrust

J_T steady-state momentum flux due to the secondary flow

ER entrainment ratio

Q_e evaporator instantaneous heat, heat load

Q_g generator instantaneous heat, heat load

Δh_e evaporator specific enthalpy

Δh_g generator specific enthalpy

T temperature

γ ratio of specific heat

M Mach number

Chapter 1

Introduction

1.1 Ejector Theory and Application

Ejectors are simple devices that use a high pressure source to raise the pressure of a low pressure fluid; ejectors are effectively pumps without moving parts. Sir Charles Parsons invented an ejector for removing air from steam engine condensers around 1901 and Maurice Leblanc was the first user of a steam ejector in a jet refrigeration system in 1910 [1]. In its simplest form, the ejector (or jet-pump) refrigerator has the same basic components as a conventional vapour compression unit, but the vapour-compressor is replaced by a pump, a boiler and an ejector [2]. Figure 1-1 depicts a block diagram of a basic steam ejector refrigerator. A boiler, evaporator, condenser, expansion valve, and pump are the main parts of this system [3]. Industrial applications for pumping take advantage of ejectors' long service life, resistance to wear and capability to pump from low pressures. Ejector systems typically have low maintenance costs.

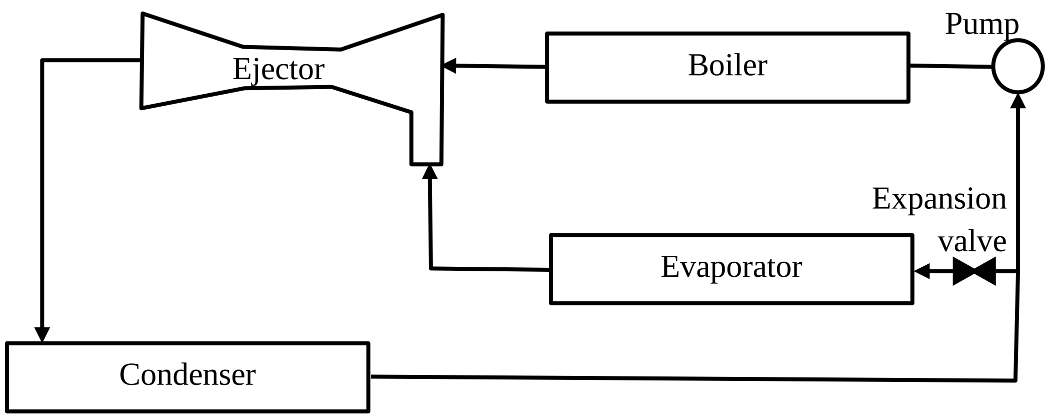

Figure 1-1: Block diagram of a steam jet refrigerator cycle.

Ejectors consist of four main parts: the nozzle, mixing chamber, throat and diffuser. Motive high-pressure fluid or primary flow is supplied to the nozzle, producing a high velocity flow. In the case of gas or vapour-driven ejectors, the nozzle makes use of a converging/diverging profile to convert the high pressure and low velocity fluid into a very high velocity stream with low static pressure. Figure 1-2 shows the cross section of a typical ejector and its main parts.

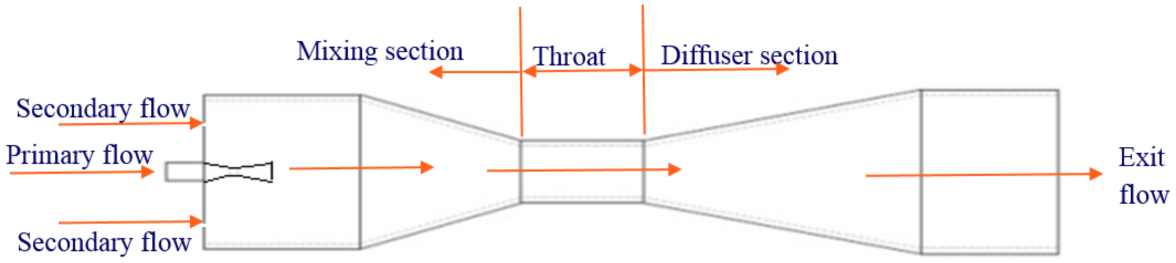

Figure 1-2: Typical ejector cross section showing flow directions.

Ejectors employ a jet of high pressure primary fluid, making use of mixing and pressure effects to induce a low pressure secondary flow in order to compress it to a higher pressure. Industries with low quality heat sources can readily make use of ejectors. As the primary fluid is expanded through the nozzle, a partial vacuum motivates the secondary flow, which is entrained by mixing with the primary flow, and when the mixed flow decelerates, the pressure of the mixture is raised to that of the exit flow [4]. Imparting momentum from the primary flow to the secondary flow occurs by two mechanisms: (1) shear stresses between the two flows as a result of turbulence and viscosity; and (2) in the case of unsteady flow fields, pressure exchange due to interface pressure forces applying between the primary and secondary fluids [5].

Ejector design is not a new field of research. For many years, different types of ejectors have been developed for different applications. The majority of ejectors have been designed with a similar axial flow pattern in which the primary (motive) and secondary (propelled) fluid enter a shaped pipe and move in the direction of the ejector axis.

A conventional jet pump (a typical ejector) cross-section with pressure and velocity profiles for the case of a steam ejector is shown in Figure 1-3. As the primary and secondary streams mix in the mixing area, they pass through the throat, experiencing a thermodynamic shock process [6] which suddenly increases the pressure [7].

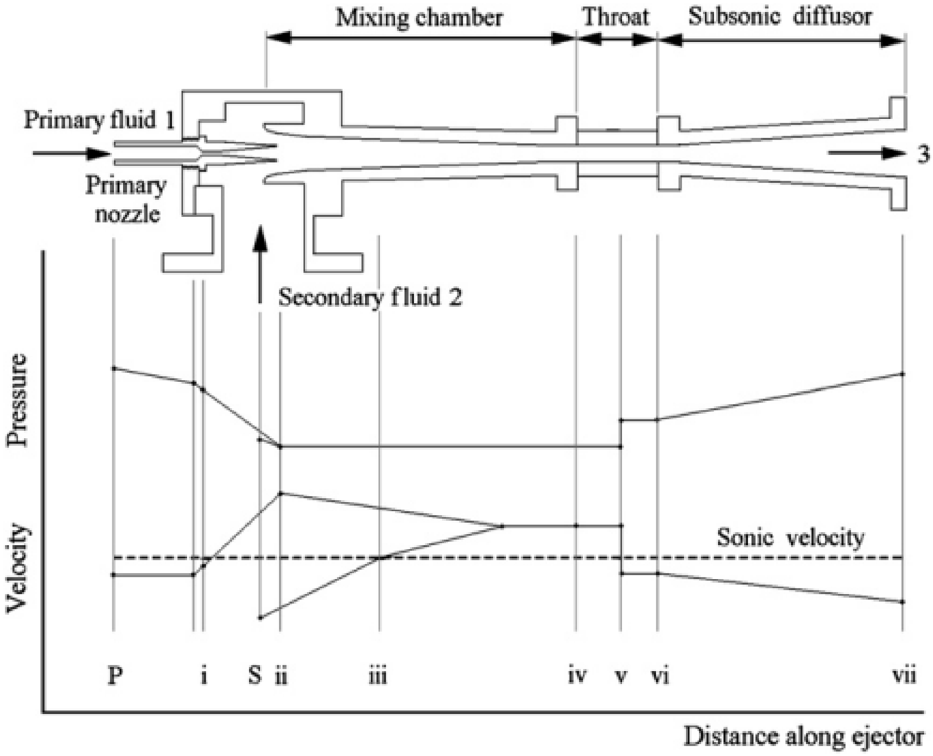

Figure 1-3: A typical cross-section, pressure and velocity profile of a steam ejector [7].

1.2 Ejector Performance

To quantify a system in terms of the energy consumption and effectiveness, a measure of performance is required. Ejector performance is evaluated in different terms in the literature. One important term is entrainment ratio ($ER = \omega \ = \frac{\dot{m}_s}{\dot{m}_p}$) where $\dot{m}_s$ and $\dot{m}_p$ are secondary and primary mass flow rates, respectively. For an ejector in a refrigeration system, ω is related to the coefficient of performance (COP) of a cooling cycle through the enthalpy change in the evaporator and generator as [8]:

$$COP = \frac{Q_e}{Q_g} = \omega \times \frac{\Delta h_e}{\Delta h_g}$$

Figure 1-4 shows a model axial ejector performance curve. The axial ejector characteristic curve (entrainment ratio vs outlet pressure) is often divided by researchers into critical, subcritical and malfunction modes [9] and [10]. If the ejector outlet pressure is less than the critical pressure, the entrainment ratio remains constant and increasing the outlet pressure does not have any effect on the entrainment ratio. As the outlet pressure increases beyond the critical pressure, entrainment ratio linearly decreases, according to the model, to reach zero when outlet pressure reaches the malfunction or back flow pressure. Any increase beyond the malfunction pressure causes back flow to the ejector secondary inlet resulting in no useful function.

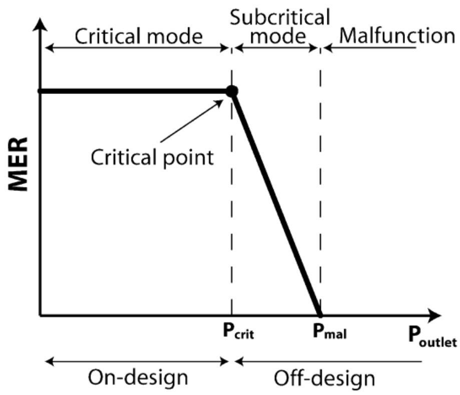

Figure 1-4: A model axial ejector characteristic curve [9].

The ejector performance is influenced by the mixing process, friction and flow separation [4], [11], [12]. Many studies have focused on the optimisation of the ejector geometry and operating conditions to achieve higher performance.

1.3 Objectives of the Thesis

For many years, different ejector arrangements and designs have been developed for different applications. The majority of designed ejectors follow a similar concept: the primary (motive) and secondary (propelled) fluid move axially in an axisymmetric arrangement. The author of this thesis suggests a new concept: a radial flow pattern for ejector applications. In this new radial configuration, the primary supply expands in the supersonic radial flow nozzle, and this expanding disk of primary flow entrains the secondary flow from the inlets positioned on either side of the expanding primary flow. The objective of this study is to investigate this new radial flow ejector concept through experiments, a quasi-one-dimensional gas dynamic model, and computational simulations using Ansys-Fluent software.

1.4 Scope of the Thesis

The scope of the project has been limited to the design and evaluation of a prototype radial flow ejector. The performance of the ejector has been targeted close to the ejector system designed by [13]. As the radial flow ejector is a new concept, to simplify fabrication, the design has been based on using air as the working fluid and operates as an open system. The system development has been limited to prototyping the radial nozzle, radial ejector, motive, exhaust and suction flow piping systems. Other components normally used in a steam refrigeration system such as evaporator, condenser, and generator have not been in the scope of this project.

1.5 Overview of the Thesis

The present introduction to the research area is followed by a literature review. The main body of the thesis is composed of 5 discrete pieces of work, two of which have been published as conference papers, and three of which are prepared in the format of papers and are in the processes of being prepared for publication. Following the main body of the thesis, a concluding chapter is presented where the general findings are summarised and recommendations have been made for future studies.

1.5.1 Chapter 2: Literature Review

The literature review focusses on methods employed for ejector performance improvement. It includes the effects of operating conditions on ejector performance, and the effects of geometry and flow characteristic in ejectors. The use of CFD in ejector design is also reviewed.

1.5.2 Chapter 3: Investigation of Radial Flow Ejector Concept Through CFD Analysis

The basis of this chapter is a conference paper:

> Rahimi, H., Malpress, R. and Buttsworth, D., Investigation of radial flow ejector concept through CFD analysis. 20th Australian Fluid Mechanics Conference, Perth, Australia, 5-8 December 2016.

This chapter discusses a CFD analysis of the radial ejector and compares this concept with an equivalent axial ejector. The same operating conditions and CFD settings were used for the simulation of the ejector performance in both cases. A k-omega SST turbulence model was employed in this study.

1.5.3 Chapter 4: CFD Study of a Variable Flow Geometry Radial Ejector

The basis of this chapter is a conference paper:

> Rahimi, H., Buttsworth, D. and Malpress, R., CFD study of variable flow geometry radial ejector. 4th International Conference of Fluid Flow, Heat and Mass Transfer (FFHMT'17). Toronto, Canada, 22-23 August 2017.

This chapter discusses a CFD study of a variable geometry radial ejector in which the ejector throat size was changed by adjusting the separation of the plates forming the ejector duct. Three different ejectors with different throat separations were compared in terms of entrainment ratio variation with ejector outlet pressure. A k-omega SST turbulence model was used in this study.

1.5.4 Chapter 5: Radial Ejector: a New Concept in Ejector Design

The work presented in this chapter is intended to introduce the radial ejector concept to a wider audience than can be reached through the conference publications presented in Chapters 3 and 4. The main methods of design, fabrication and evaluation of the prototype are discussed. Experimental results are appraised and compared with a quasi-one-dimensional model previously calibrated to axial flow ejector results.

1.5.5 Chapter 6: Experimental Investigation of Radial Ejector Performance

Work in Chapter 5 demonstrated the radial ejector has comparable performance to an equivalent axial flow ejector in terms of entrainment ratio, but the critical back pressure for the radial ejector was low relative to the equivalent axial flow ejector. However, the computational simulation work reported in Chapter 3 indicated that radial ejector should have critical back pressures that are comparable to the equivalent axial flow ejectors. Therefore, an understanding of the flow within the radial ejector is sought by presenting and analysing static pressure measurements within the radial ejector duct over the different operating conditions.

1.5.6 Chapter 7: CFD Simulation of Radial Flow Air Ejector Experiments

This chapter presents CFD analysis of the radial flow air ejector using Ansys Fluent software. The computational simulations are compared with experimental data for entrainment ratio, critical back pressure, and static pressure measured in the radial flow ejector. The computational simulations presented in Chapters 3 and 4 used the k-omega SST turbulence model, but generated critical pressures results that did not accurately reflect experimental data presented in Chapter 5. Therefore, the k-epsilon turbulence model was used in this work to further explore the reason for the discrepancy in the critical back pressure.

1.5.7 Chapter 8: Conclusion

The last chapter presents the overall conclusions and outcomes of this research study and recommendations for future works.

Chapter 2

Literature Review

2.1 Scope of Review

The primary goal of research in the area of ejectors is to improve their performance and efficiency and different approaches have been adopted in pursuit of this goal [14], [15]. Among the findings, working condition optimization, geometry optimization, variable geometry [16], [17], [8], and oscillatory primary stream pressure [18], [19] are identified as potential methods to improve performance and efficiency. Most existing ejectors have an axisymmetric and axial flow path, and the general arrangement is illustrated in Figure 1-2.

The limits of improving axial ejector performance by optimising nozzle and duct shapes and the position of the nozzle have probably been reached. Little work has been completed on implementing the concept of variable geometry because the inherent form of axial ejectors impedes the effective, efficient and practical application of most variable geometry concepts. Radial ejectors could offer the capacity to easily alter the nozzle and ejector throat areas by simply changing the separation of the nozzle surfaces and/or the duct walls. Such ejectors have not been studied extensively. Consequently, the vast majority of existing literature on ejectors does not:

1- Provide reliable analytical design tools for radial ejectors

2- Experimentally investigate radial ejector performance in the context of analytical design strategies

3- Numerically investigate radial ejector performance using CFD

As such, the review of the literature relevant to the concept of a radial ejector focusses on analytical, experimental, and computational work that contributes to a general understanding of axial flow ejector performance, the need for improved performance from ejectors, and how the performance of such ejectors may be augmented.

2.2 Ejector Operating Conditions

The operating condition needs to be carefully defined in order to design a suitable ejector. The entrainment ratio is the ratio of mass flow rate in the secondary stream to that in the primary stream, and normally the designer seeks to maximise this parameter, but the design is constrained by the necessary operating conditions. The expansion ratio, which is the ratio of the primary pressure to the secondary pressure, is a key parameter in designing the ejector. Another key parameter is the compression ratio (also known as the pressure lift ratio), which is the ratio of the pressure at the outlet of the ejector to the secondary pressure [14]. Normally this compression ratio is defined in terms of the critical value because the pressure that is imposed at the outlet of the ejector significantly influences the ejector entrainment ratio for pressures higher than the critical values [8].

Eames et al. [2] experimentally investigated a steam ejector refrigeration system, demonstrating that that COP is dependent on the temperatures of the boiler and evaporator and independent of condenser temperature until a certain condenser temperature is reached and COP decreases dramatically thereafter [2]. Figure 2-1 shows the variation of COP with condenser pressure from their work.

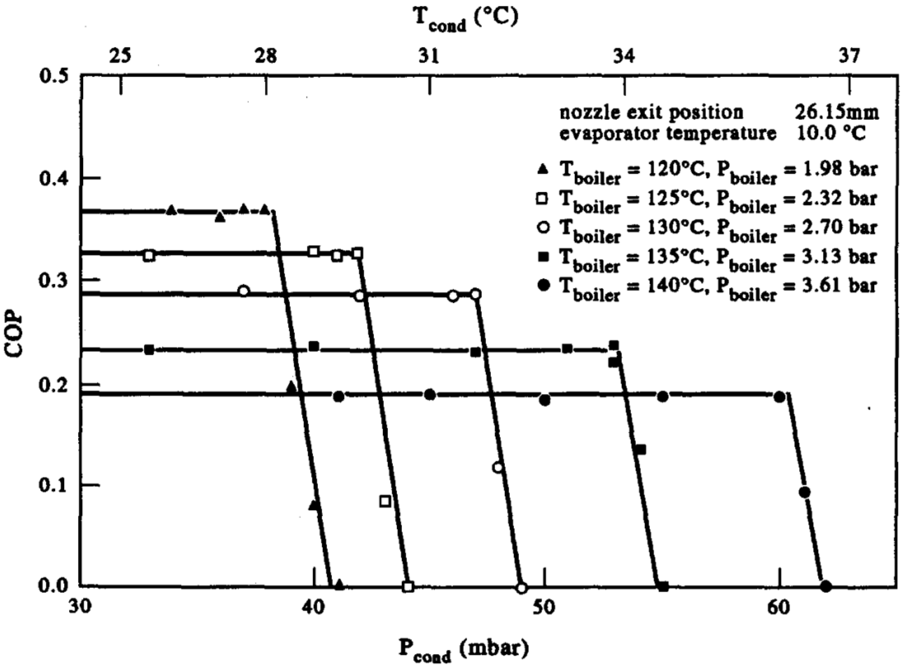

Figure 2-1: COP variations with condenser pressure over a range of boiler pressure at the evaporator temperature of 10 ^{o}C in a steam ejector refrigeration system [2].

Yapici and Yetisen [20] experimentally investigated an ejector refrigeration system powered by low-grade heat with R11 as the working fluid. A range of temperatures from 88.5 to 102^{o}C was used for the vapour generator and a range of 0 to 16^{o}C for the evaporator. A COP up to 0.25 was achieved. The cooling capacity and COP increase with evaporator temperature at constant vapour generator temperature and condenser pressure in a fixed area ejector as illustrated in Figure 2-2.

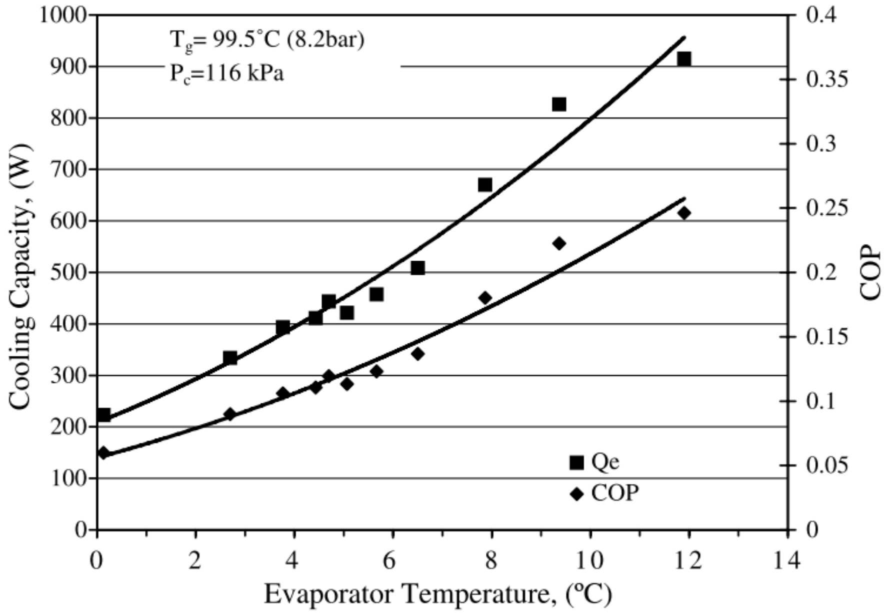

Figure 2-2: Cooling capacity and COP variation with evaporator temperature [20].

Chunnanond et al. [21] studied the effect of operating condition on the ejector performance for a steam ejector. They observed that for a constant evaporator condition, the primary flow conditions influenced the COP and critical back pressure and related these changes to a so-called effective area in the mixing chamber: by increasing the primary pressure, the effective area available for the secondary stream is reduced and therefore a lower COP is obtained [21]. Figure 2-3 illustrates the concept of the effective area for a typical ejector.

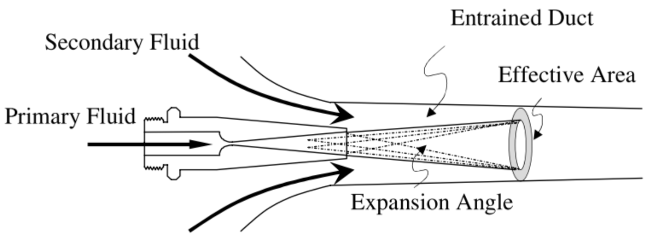

(a)

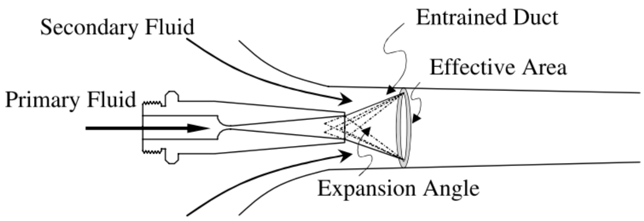

(b)

Figure 2-3: Effect of the operating conditions on the available flow cross sectional area for the secondary stream [21]: (a) low primary pressure; (b) high primary pressure.

Chunnanond and Aphornratana [21] stated that many factors can affect the COP including operating conditions, size and position of the nozzle. They conducted experiments using boiler temperatures 110-150^{o}C, evaporator temperatures 5-15^{o}C, and condenser pressures 25-60 mbar and demonstrated that COP increases as the boiler pressure decreases. The COP can increase along with the critical condenser pressure for the case of the system operating at a higher evaporator temperature [21]. A summary of the COP variation with operating condition reported in the literature is presented in Table 2-1.

Table 2-1: Summary of results regarding COP variation with operating conditions

Conclusion	Achieved COP	Reference
As the boiler pressure decreases, COP increases and critical back pressure decreases As the evaporator pressure increases, COP and critical back pressure increases	0.28 to 0.48	[21]
Every ejector with a specific geometry and configuration works best (achives a maximum COP) at an optimum boiler temperature for given condenser and evaporator temperatures	0.03 to 0.16	[22]
Increasing ejector area ratio and expansion ratio and decreasing compression ratio leads to increase in COP	0.12 to 0.29	[23]
Increasing generator temperature beyond a specific limit results in diminished COP	0.12 to 0.39	[24]

For convenience, many researchers use air as the working fluid in their ejector studies. In most air ejectors, the temperature of primary, secondary and exit are very close to the ambient conditions [9], [25], [26]. Figure 2-4 presents typical characteristic curves for an air ejector operating with primary pressures ranging from 1 to 5 bar and a secondary pressure of 1 bar [9]. This figure clearly shows the effect of different primary pressures on the performance of the air ejector. For a constant secondary pressure, the entrainment ratio decreases with increasing primary pressure. Similar results are achieved by other researchers [25], [26].

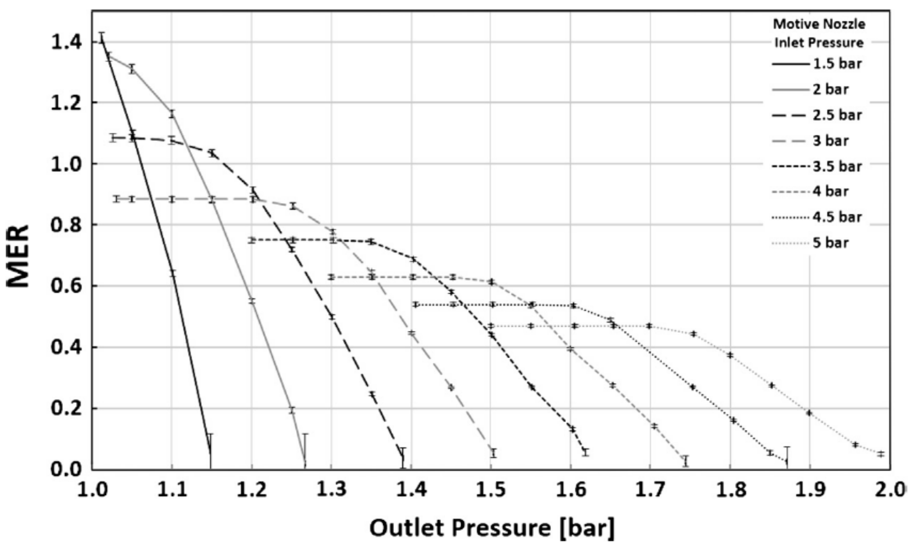

Figure 2-4: Air ejector characteristic curves for primary pressures ranging from 1.5 to 5 bar and secondary pressure of 1 bar over a range of outlet pressures [9].

In another study [27], Bartosiewicz et al. investigated different expansion ratios (the ratio of primary to secondary pressure) on the behavior of an ejector. It was concluded that, the best pressure ratio for their ejector was between 7 and 8. Figure 2-5 shows the sonic lines for different expansion ratio cases from computational simulations. The higher expansion ratios lead to under-expansion of the primary flow and limits the available flow cross sectional area for the secondary flow. Low expansion ratios leads to a large separation and the secondary flow not being choked.

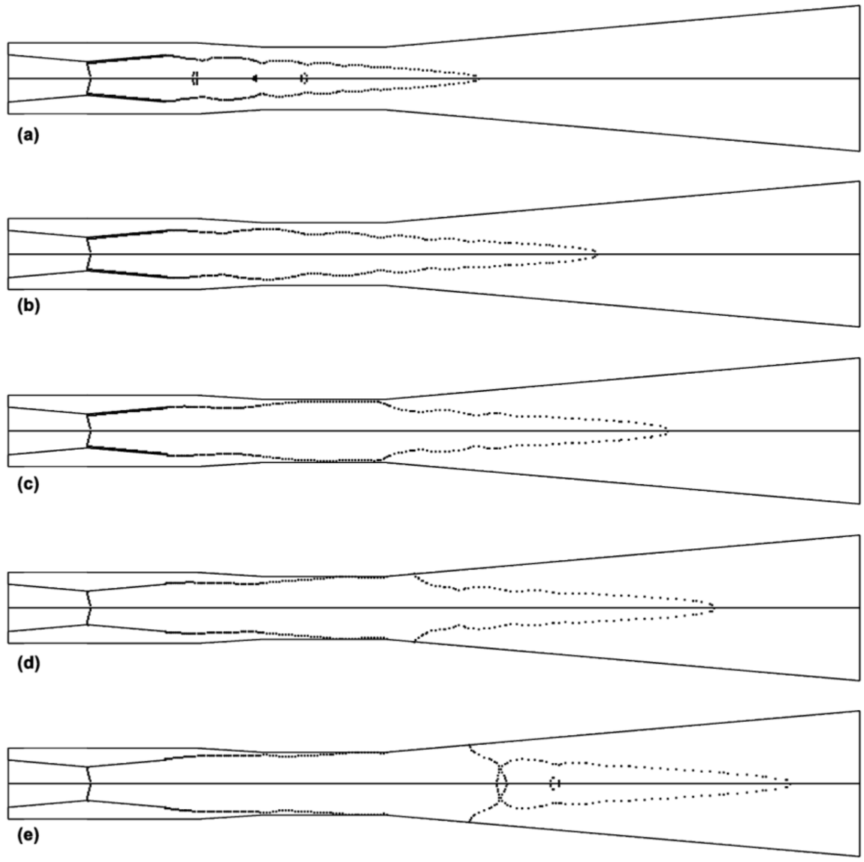

Figure 2-5: Sonic lines for (a) Pp/Ps=5, (b) Pp/Ps =6, (c) Pp/Ps =7, (d) Pp/Ps =8 and (e) Pp/Ps =10 for air ejector by CFD analysis [27].

2.3 Motivation for Variable Geometry

Working fluid properties, operating conditions and the ejector geometry are the main factors influencing the ejector performance. The influence of geometrical parameters has been investigated experimentally [28], [29] and numerically [8], [30], [31], [32]. It has been stated that the optimal ejector geometry is significantly dependent on the operating conditions. An ejector with a fixed geometry works best in a narrow range of operating condition [8]. Having adjustability in the ejector throat size during operation is a solution for extending the range of operating conditions. This becomes more important for ejectors driven by variable thermal energy sources. For example, if using solar energy to drive ejector systems, or in vehicle fuel cell applications for recirculating hydrogen, the ejector input energy sources will not be constant for long periods of time, or even if the ejector energy input is a constant for a modest period of time, it is possible that different outputs are required for optimal system performance. In the case of the solar ejector systems, the solar heat input varies throughout the day and is also dependent on the daily or seasonal radiation [33], [34]. In vehicle fuel cell systems, if the ejector is used to control the mass flow rate, it might be necessary to have a constant output mass flow rate while the primary stream condition is fluctuating [35]. Therefore ejectors used in such systems need to be adjustable to have optimum performance for different situations.

Existing technical solutions for adjusting the ejector area ratio mostly involve inserting shaped blockages upstream [17], [8], [36] or downstream [35] of the nozzle. This provides a convenient adjustment in the physical throat size of the nozzle or ejector in axisymmetric, axial flow ejectors. Many papers employed such flow blockage features on the ejector centreline [8], [37], [38], [39], [40]. However, the major drawback resulting from such methods in axial ejectors is the loss of total pressure that arises due the blockage of the high speed primary stream.

To design an ejector with the capacity to independently adjust both the primary nozzle throat and the ejector throat areas without introducing blockage on the centre line of the nozzle, a new configuration is needed.

2.4 Geometric Modifications for Enhanced Performance

With respect to ejector geometry, the parameters which need consideration are the area ratio (area of the ejector throat to the primary nozzle throat area), nozzle exit position, primary nozzle throat and exit diameter, ejector duct throat area and diffuser geometries [14].

2.4.1 Basic Ejector Geometric Features

2.4.1.1 Primary Nozzle

The primary nozzle is a supersonic nozzle which consists of an inlet, converging section, throat and diverging section [41]. The design of a supersonic nozzle has a signifcant influence on its performance. The major parameters for a nozzle are the design mass flow rate, $\dot{m}_p$, the exit area and the divergent angle. The nozzle area expansion ratio, the ratio of exit area to throat area, A/A^* essentially dictates the exit Mach number of the nozzle [42], and nozzle area ratios between 7 and 144 are reported for different ejector applications [43], [16] and [28].

The inlet section of a supersonic nozzle is important for creating uniform flow. It has been determined by [41] that the length of the inlet section should be more than 10 times the throat diameter, and while larger inlet diameters are also beneficial, limitations of manufacturing techniques and the particular nozzle application should also be considered.

The speed of the flow at the nozzle throat is sonic (Mach number equal to 1). With increases in the stagnation pressure, the flow velocity remains constant but the mass flow through the throat increases [41].

The effect of different nozzle divergent angles on the shock phenomena has been numerically investigated in [44]: the authors compare different divergent angles including 4, 7, 10, 13, and 15^o, and demonstrate that oblique shocks appear in the nozzles with lower divergent angles. As the divergent angle is increased, the position of the oblique shocks moves toward the nozzle exit and the shock is completely eleminated with the divergent angle of 15^o [44].

Eight different primary nozzles with different throat diameters between 1.4 and 2.6 mm have been used in an experimental study [16]. Some results which are presented in Figure 2-6 show that the nozzle with the largest throat diameter obviously supplies more fluid mass flow rate, resulting in less secondary fluid being moved because of less flow area being available for the secondary flow in the mixing chamber. Larger nozzle throat diameter can also lead to a higher exit pressure, so the critical condenser pressure increases [16].

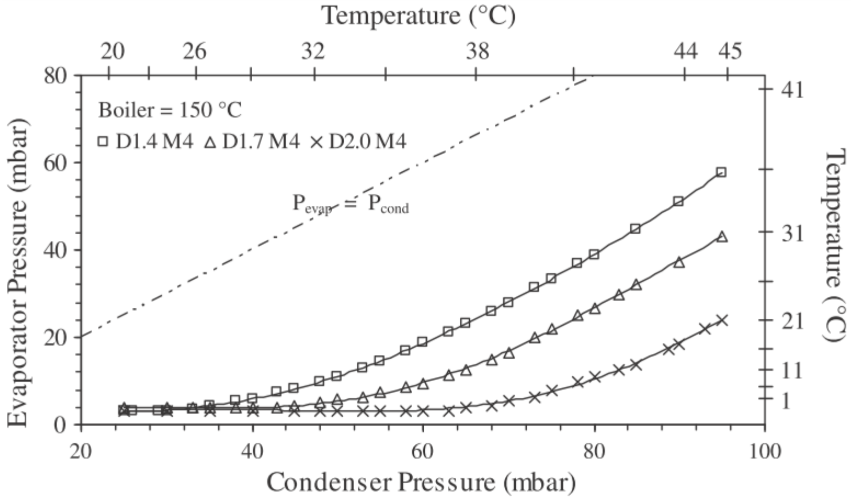

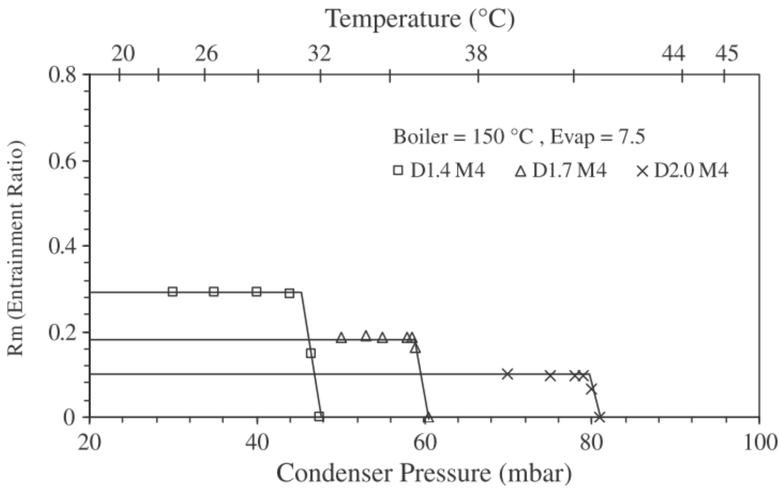

Figure 2-6: Variation of the minimum suction pressure and the entrainment ratio with the nozzle's throat diameter [16].

2.4.1.2 Ejector Duct

The length of ejectors is an important parameter for ejector design [12]. The length of an ejector can influence both COP and the pressure lift ratio. There are many suggestions regarding the appropriate ejector throat length ranging from 4 to 14 times throat diameter. A throat length between 7 to 9 times the throat diameter is reported to be the optimum [11]. Sun [39] stated that the optimum length of the ejector is influenced by operating conditions and argued that if the condenser temperature increases the lengh of the ejector should be increased. Sun also claimed that different condenser temperatures need different nozzle and diffuser diameters to achieve optimum performance. The critical exit pressure decreases with decreasing throat length [45], but there is not complete agreement between researchers regarding the effect of ejector length on ejector performance. In the work of [46], it is claimed that a larger compression ratio is achieved by using a smaller ejector [46].

It has been identified that the contour of the convergent section of a constant pressure ejector should be changed so the total pressure in this section remains constant [47]. This means that for different operating conditions, it is necessary to have different contours. Not working at optimum operating conditions potentially leads to low efficiency [47].

The total mixing chamber and throat length, which is the distance from the nozzle exit to the start of the diffuser should be in the range of 5 to 10 times the ejector throat diameter [48], [49], [50]. The convergent half angle of the duct is recommended to be between 2 and 10 degrees [48], [49], [50]. It was also concluded that the optimum ejector area ratio depends on operating conditions for a steam ejector [32], [51]. The optimum area ratio is related to the type of working fluid as well [52]. The influence of the area ratio on COP has been the topic of many research studies [16], [53], [54].

2.4.2 Constant Rate of Momentum Change Ejector Design

Eames [55] introduced the so-called constant rate of momentum change (CRMC) method for designing an ejector, noting that the thermodynamic shock, which occurs in the diffuser, brings about a sudden decrease in total pressure and as a result, affects the achievable compression ratio. The aim of the CRMC method was to produce a diffuser without a thermodynamic shock occurring, or at least to minimize the pressure losses associated with such a compression process. According to the theory, as the momentum of the flow changes at a constant rate while passing through the diffuser, the static pressure can rise gradually from the entry to the exit. The author argued that this method can lead to a higher performance in comparison to conventional designs [55]. Figure 2-7 shows typical cross sections of the conventional and CRMC ejectors.

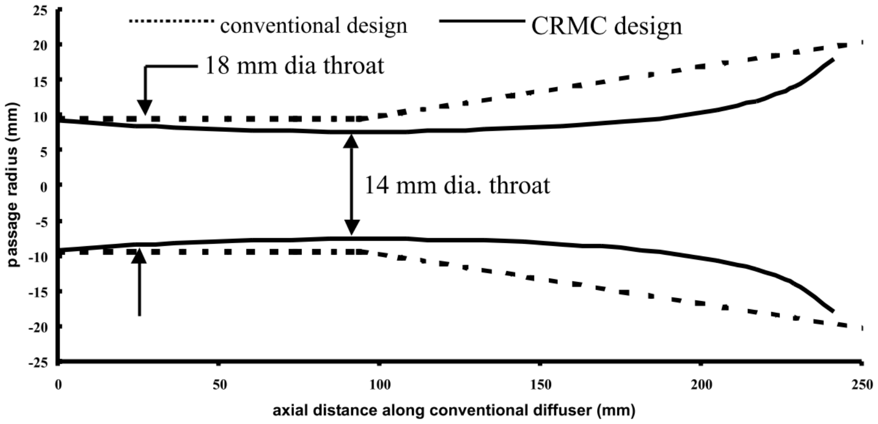

Figure 2-7: Comparison between profiles of conventional and CRMC ejectors [55].

Chandra and Ahmed [3] conducted an experimental and CFD study based on the CRMC design theory. They compared the design based on CRMC method with a conventional ejector with a constant area throat section. They concluded that the CRMC ejector had better performance in comparison to the conventional ejector used in the study. However, due to not chocking the secondary flow, this improvement has not been realized in all operating conditions [3]. They supposed that the shock compression process had been removed by the CRMC design and proceeded to conclude that by removing the shock process in the variable area ejector, the lift ratio can be increased significantly.

2.4.3 Primary Nozzle Position and Design

2.4.3.1 Primary Nozzle Position

The position of the primary nozzle influences ejector performance. Chunnanond et al. [21] improved ejector performance by using a smaller nozzle and retracting the nozzle upstream of the mixing chamber. Smaller primary nozzles positioned upstream of the mixing chamber will increase the distance over which jet mixing can occur prior to the diffuser thereby improving the

COP and cooling capacity. Figure 2-8 shows the effects of the primary nozzle position on the ejector performance.

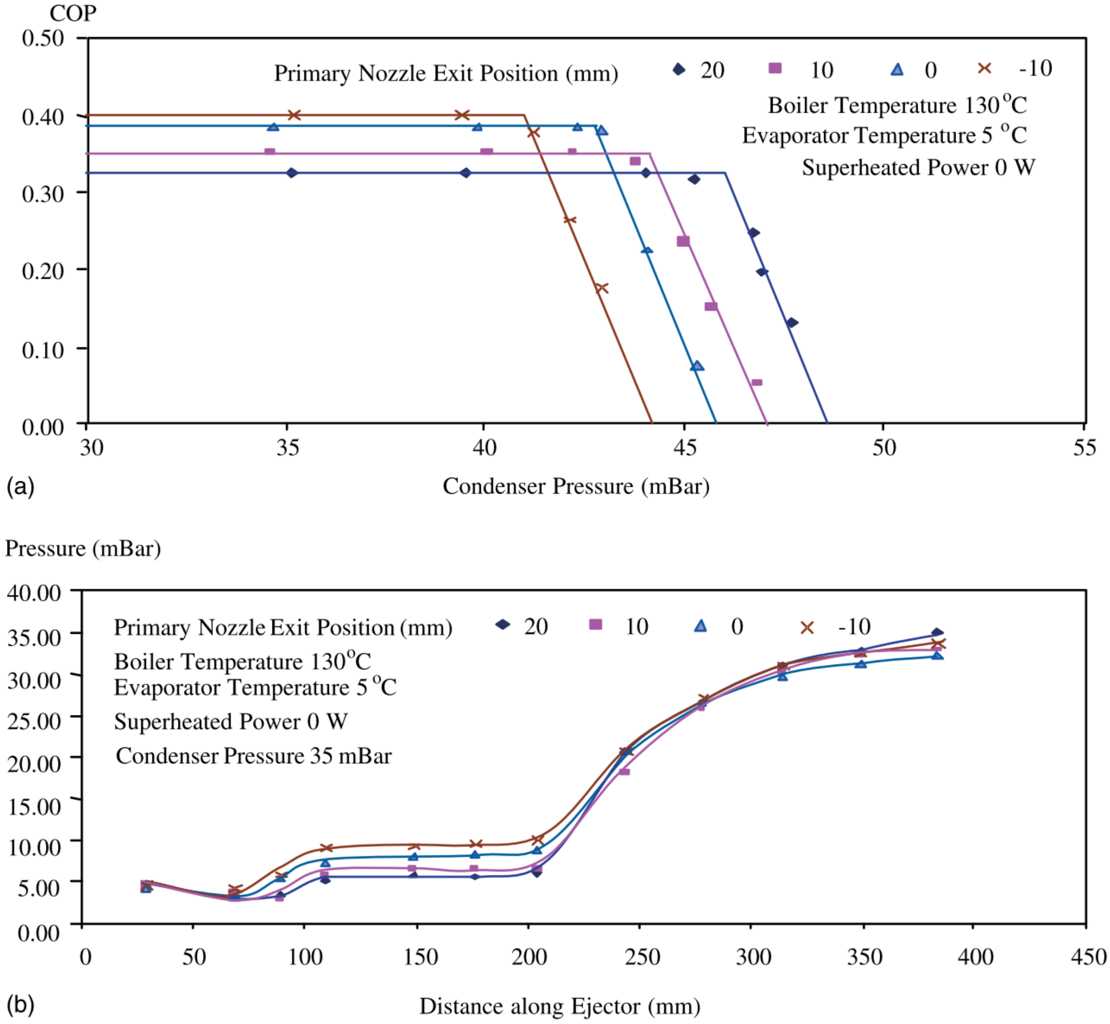

Figure 2-8: Effect of primary nozzle position on the performance and static pressure along the ejector [21].

Chunnanond et al. [21] conclude that two main parameters influence the COP. The first is the amount of secondary fluid which is related to the COP and cooling capacity, and the second is the momentum of the mixed stream, which has an impact on the maximum achievable condenser pressure. Lower boiler pressure, smaller nozzles and a larger nozzle distance from the mixing chamber can lead to less expansion of the primary jet and as a result, a larger amount of secondary fluid can be entrained and higher COP can be achieved [21].

Eames et al. [43] designed and evaluated a jet pump chiller for air conditioning and industrial applications based on two different ejector designs: one based on the original constant rate of momentum change (CRMC) design method, and the other optimized using CFD results. The main difference between the two ejectors is the area ratio between the diffuser and primary nozzle throats. Both designs have employed the same primary nozzles, the position of which can be adjusted axially [43]. The authors have demonstrated that the position of the primary nozzle is very important and determined the optimum positions for both designs experimentally [43]. Figure 2-9 shows the effect of nozzle exit position on the COP for the ejector.

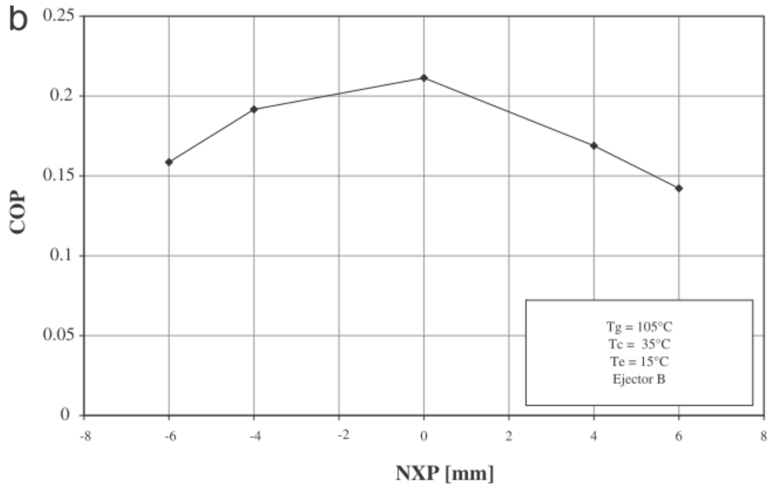

Figure 2-9: Variation in COP for different nozzle exit positions for the ejector designed using CRMC method [43].

2.4.3.2 Primary Nozzle Shape

The shape of the primary nozzle also affects ejector performance. Chang and Chen [56] used a petal nozzle in a steam-jet refrigeration system to increase the performance of the system. They applied different operating conditions including generator, evaporator and condenser temperatures for investigating the nozzle behaviour. They also evaluated the area ratio on the ejector performance. A conical nozzle with the same Mach number was also used for comparison, as illustrated in Figure 2-10. The findings show that the performance of a petal nozzle is better than a conical nozzle: the ejector with petal nozzle can work at a higher critical back pressure [56].

Different nozzle geometries have been investigated in [57]: two circular, two elliptical, a square, and two exotic nozzles were used. It was concluded that each nozzle shape works most effectively at different but specific Mach numbers [57]. Figure 2-11 shows different nozzle shapes employed in ejector systems in various studies in order to improve ejector performance.

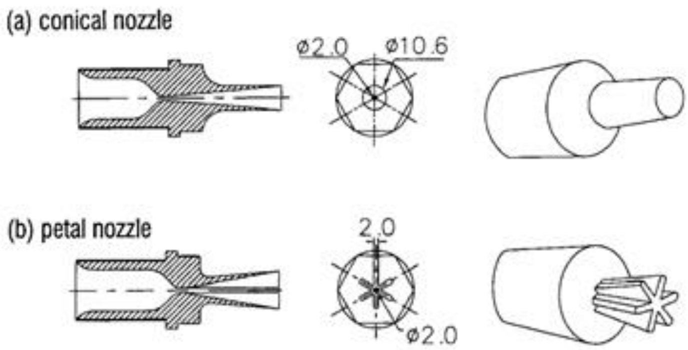

Figure 2-10: Conical and petal nozzle geometry used by [56].

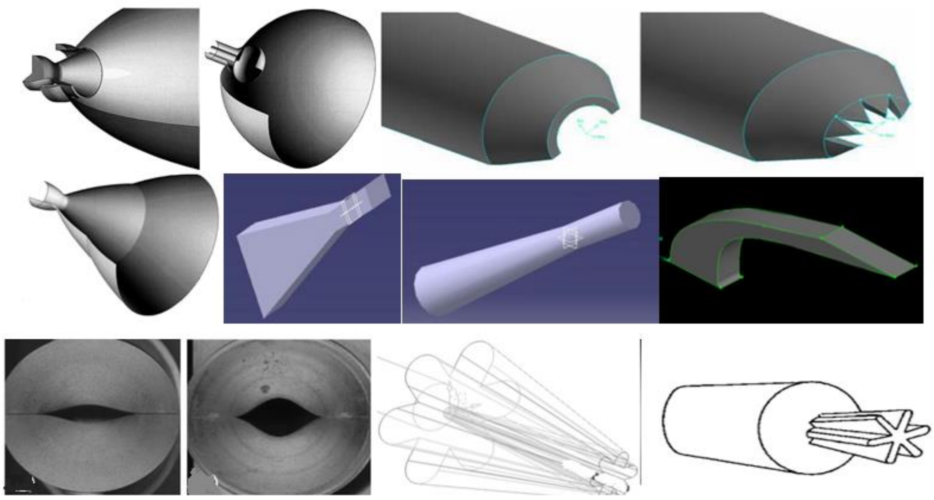

Figure 2-11: Samples of supersonic nozzle shapes employed by researchers in attempts to improve ejector performance [58, 59, 60, 61, 62, 63].

2.4.3.3 Nozzle and Ejector Centre Body Inserts

Various studies have investigated options for centre body inserts both upstream and downstream of the nozzle. For example, a conical insert shown in Figure 2-12 which moves axially in the ejector and changes the flow area of the nozzle exit and adjusts the ejector area ratio has been studied [35]. The secondary mass flow rate and the critical pressure lift ratio are both strongly affected by the ejector throat area ratio [35]. As the cone-cylinder shape was positioned in the centre and downstream of the primary nozzle, the passage of the high speed flow into the ejector throat was blocked to some degree and additional frictional losses are expected. The losses associated with the deflection and blockage of the primary flow by the cone-cylinder were not reported in the work.

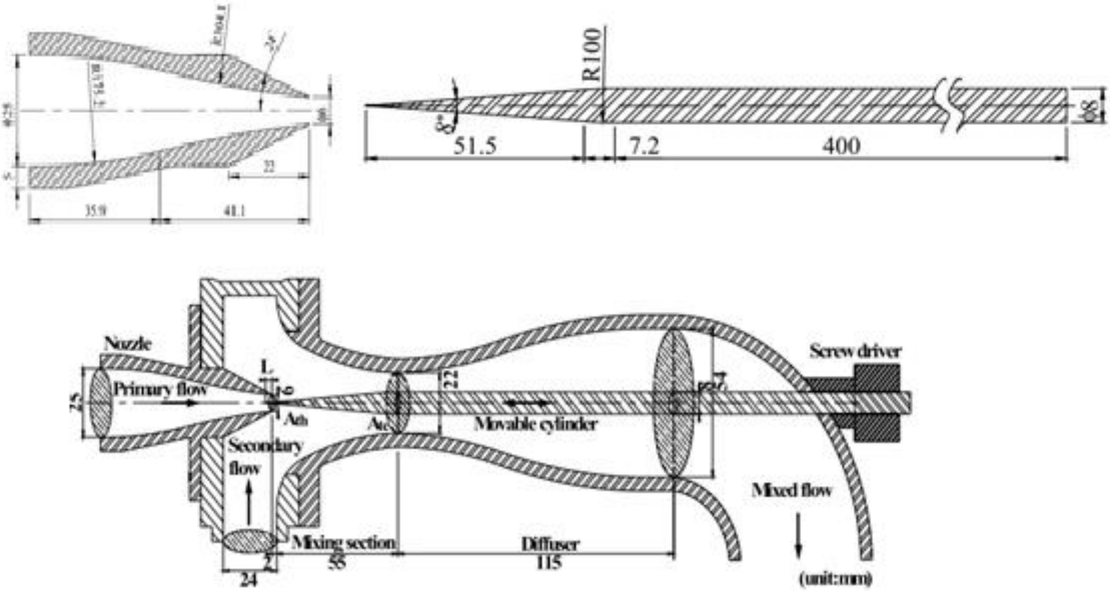

Figure 2-12: Variable nozzle-ejector configuration [35].

Ejector nozzles with pintle adjustment from upstream of the primary nozzle throat have been investigated by other researchers [17], [8] and [36] and this configuration avoids the high speed flow deflection and blockage that occurs with the arrangement of [35]. Moving a spindle located upsteam of the nozzle has shown good results in controlling the primary mass flow rate [17], [8] and [36] and hence influenced the entrainment ratio and critical back pressure. By increasing the mass flow rate, higher critical back pressure was achieved and by decreasing the primary mass flow rate, the entrainment ratio increased [17], [8].

2.4.4 Unsteady Flow Ejectors

The net rate of energy acquired by a fluid particle while traversing a flow field is the summation of the energy transfer via heat transfer, the work of shear forces (laminar and turbulent), and the work of pressure forces [64]. The energy that is directly exchanged between the primary and secondary flows is potentially improved in unsteady flow ejectors because the pressure exchange mode of energy transfer is only available in unsteady flows.

Different methods have been used in order to create unsteady behaviour in the primary flow. In the work of [18], ejector performance with a pulsating primary flow established using a synthetic jet generator based on two loud speakers has been investigated, as illustrated in Figure 2-13. The synthetic jet system was employed in the primary flow supply line just before the nozzle and it was found that higher compression ratio and efficiency were achieve using this system.

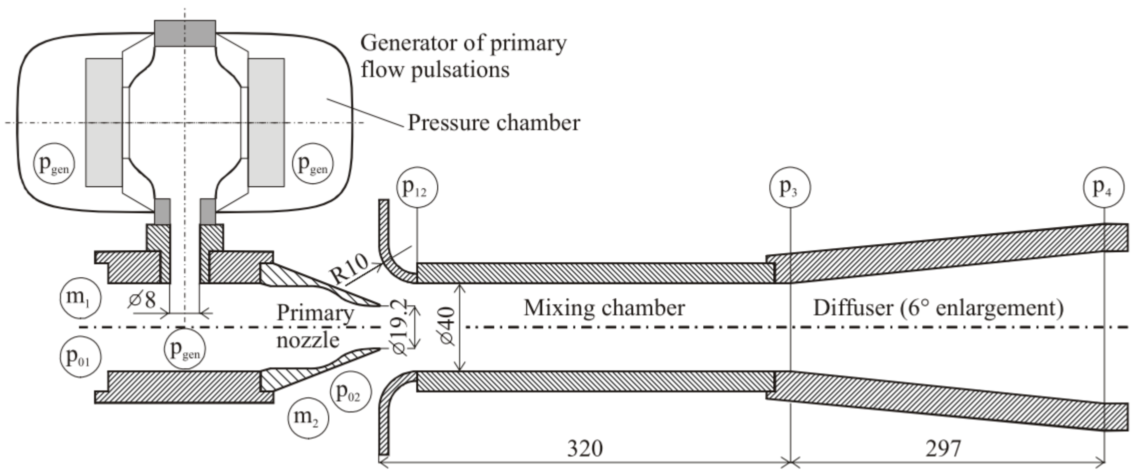

Figure 2-13: A synthetic jet system for generating oscillation of the primary flow [18].

In another study focussed on mixing augmentation of jets in supersonic flows [65], a wall-mounted cavity was used, as illustrated in Figure 2-14, for creating unsteady behaviour in the flow. The growth rate of the mixing layers in compressible flows is low in comparison to equivalent subsonic mixing layers [65]. The experimental and theoretical data show that this cavity is helpful for mixing enhancement of supersonic flows [65].

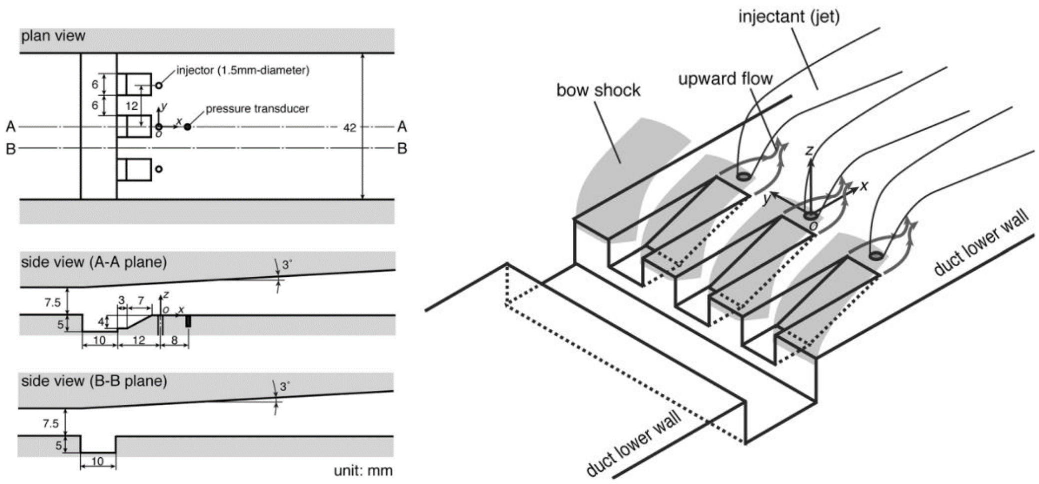

Figure 2-14: A wall-mounted cavity system for mixing enhancement in supersonic flow [65].

Thrust augmentation of a supersonic ejector through unsteady flow was studied in [66] and Figure 2-15 shows a rotary valve system used for generating flow pulsation in the ejector system. Thrust augmentation, φ, is defined as $\varphi = T_E / (T_N + J_T)$, where T_E is ejector thrust, T_N is the nozzle thrust and J_T is the steady-state momentum flux due to the secondary flow. Experimental data shows that the thrust augmentation was influenced by L/d (the length of the ejector to the diameter of the nozzle), frequency, secondary flow Mach number and pulse strength. Both frequency and pulse strength have a positive effect on thrust augmentation.

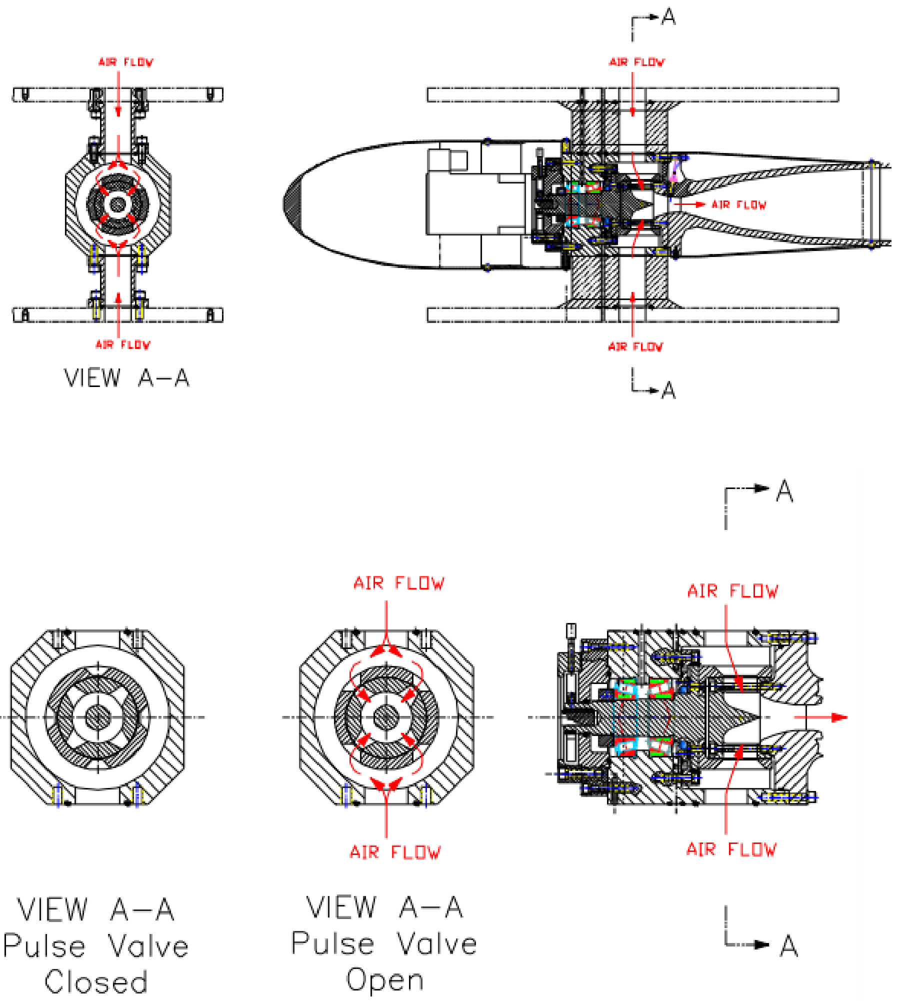

Figure 2-15: Pulse valve mechanism used for generating oscillatory behaviour in primary flow [66].

A rotor-vane ejector using pressure-exchange concepts was investigated under both rotating and non-rotating conditions by Hong et al. [5], as illustrated in Figure 2-16. The pressure exchange process in which momentum from the primary flow is imparted to the secondary flow, is only available in an oscillatory (unsteady) flow, and in contrast to the work of turbulent shear stresses of conventional steady flow ejectors, pressure exchange can theoretically be reversible, isentropic and inherently non-dissipative [5]. Because the rotary vane was installed at the nozzle exit in an area of supersonic flow, shock losses will be present in this arrangement. The authors state that as this configuration is a new design, the mechanics of flow in this ejector is unknown. They fabricated 22 different vanes to evaluate different features of the flow in this ejector. They discussed opportunities to decrease limitations and achieve enhanced ejector performance. However, they recommended that many other parameters have to be investigated to obtain a suitable vane geometry.

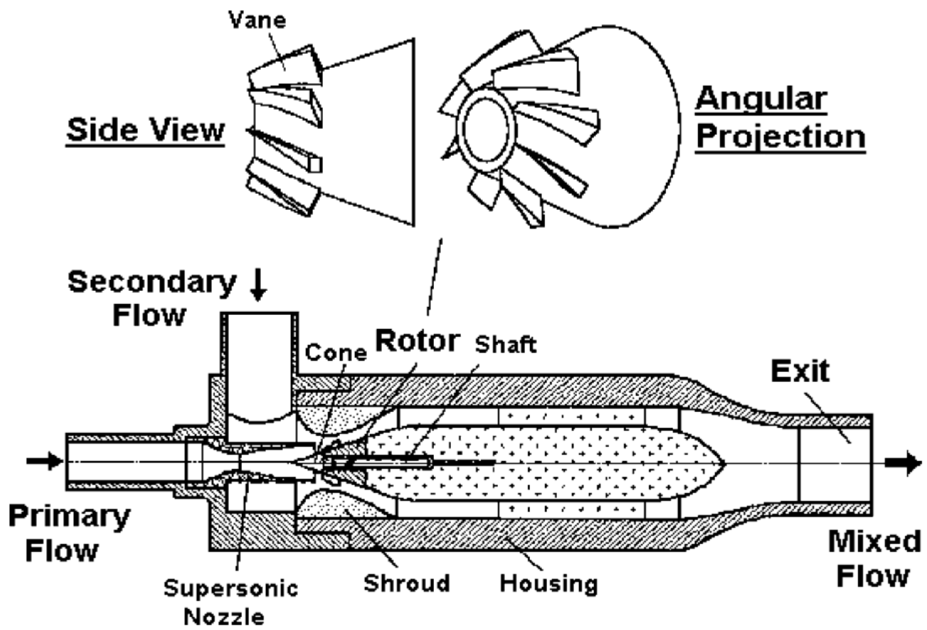

Figure 2-16: Rotor-vane pulsation system for a pressure-exchange ejector [5].

Earlier development of the pressure-exchange ejector concept was performed by Garris et al. [67] who introduced a radial arrangement and implemented a rotary nozzle as illustrated in Figure 2-17. The pressure exchange ejector configuration was intended to work on an entirely different principal relative to steady flow ejectors [67]. The authors sought to improve the COP by reducing the entropy rise normally associated with the dissipative shocks in the compression process of a conventional ejector through the use of a rotary nozzle radial ejector [67]. The authors could not confirm their findings because the earlier concepts were not successful because of mechanical failure [67], [69] due to very high rotary speed (about 50000 rpm). Work on the rotary nozzle radial ejector concept exposed many problems with this concept, including mechanical failures, vibration, and a requirement of high precision components resulting in high costs.

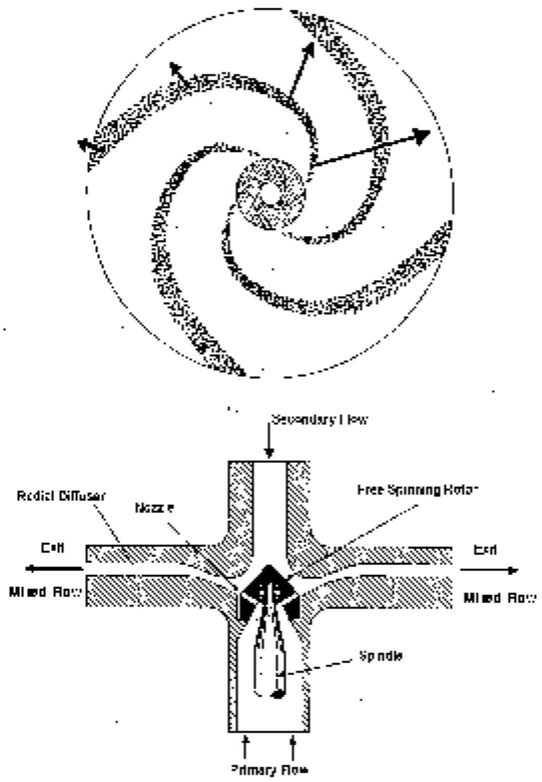

Figure 2-17: The rotary nozzle radial ejector concept of Garris et al. [67].

The Mach number effects of an unsteady ejector using the radial flow diffuser on fluid-to-fluid interactions have been investigated by Ababneh et al. [68] who argued that previous experimental studies on a similar configuration did not give meaningful data because of mechanical problems including failures in thrust bearings, seals and vibration and instabilities. In the study by Ababneh et al. [68], numerical simulations were performed on a configuration with 8 nozzles and a spin angle of 10^o from the meridian plane as illustrated in Figure 2-18, however, they did not support their findings with experimental data.

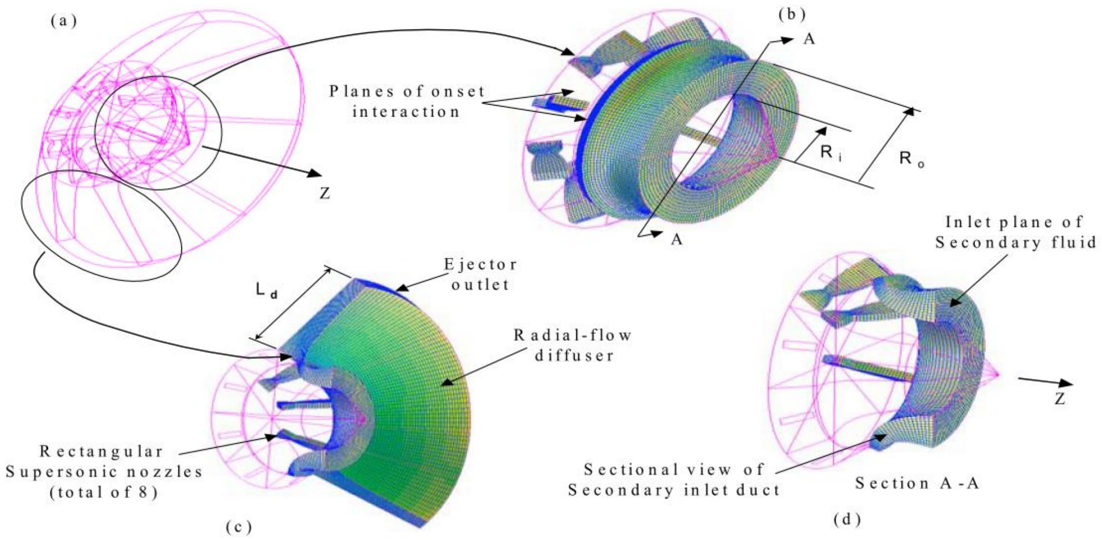

Figure 2-18: The radial flow pressure-exchange ejector of Ababneh et al. [68].

2.4.5 Earlier Radial Ejector without Rotary Parts

A radial ejector without rotary parts was designed and evaluated by [69]. In this concept, the flow is sandwiched between two flat plates. The primary flow enters the ejector duct from one side of the radial ejector and secondary flow from the other side. This concept is shown in Figure 2-19. As it can be seen from this figure, at any selected separation of the diffuser plates, the spool location controls the primary and secondary mass flow rates. By moving the spool and adjusting the separation of the diffuser plates, the ejector worked as a variable geometry ejector and this concept has been successful in acting similarly to an ejector and working as a variable geometry ejector. The performance of the ejector is highly dependent on the spool position and the diffuser plate separation. Having the high speed primary flow adjacent to one of the diffuser plates is likely to induce relatively high frictional losses. The momentum dissipated through such frictional losses is therefore not available to be transferred into the acceleration of the secondary stream, potentially resulting in compromised performance relative to a configuration in which the primary flow is not in direct contact with the diffuser plate.

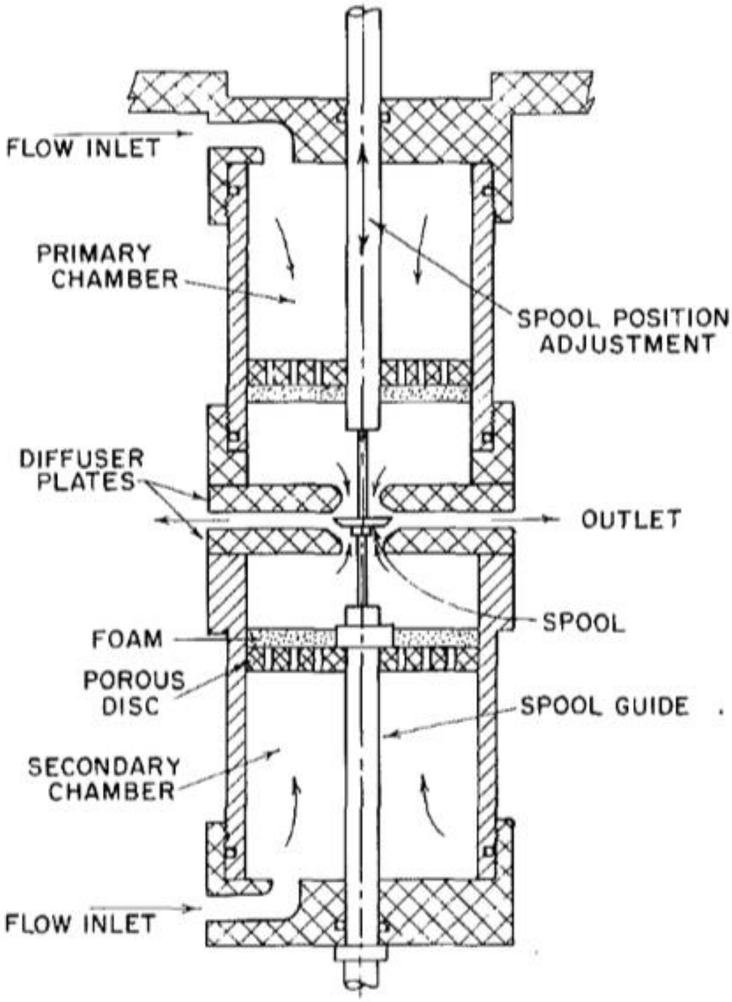

Figure 2-19: Sketch of variable geometry radial ejector [69].

2.5 Computational Fluid Dynamics

Computational Fluid Dynamics (CFD) has been proven as a successful tool in ejector flow analysis and performance improvement. This is achieved by the ability of CFD to simulate the flow field inside complex geometries.

Many researchers have performed CFD simulations [26], and have reported that the CFD analysis can predict the ejector performance with acceptable accuracy. Most of the studies achieved results showing an average error level of less than 10% [17], [26]. However, in some cases, larger discrepancies were reported [17] where the simulated entrainment ratio was not within 20% of experimental data. Ansys Fluent has been widely used for CFD simulation by researchers for ejector analysis. Table 2-2 shows a summary of the literature review regarding the use of Fluent in ejector simulations.

Table 2-2: Summary of literature review regarding the use of Fluent

Researcher	Fluent package	Number of elements	Turbulent model	Model
Varga et al. (2013)	Ansys Fluent 12	26889 to 20080	RNG k-ε	2 D
Kim et al. (2006)	Fluent	3781 and 3858 to 11200	k-omega	2 D
Chandra and Ahmed (2014)	Fluent	-	realizable k-ε	2D
Ababneh et al. (2009)	Fluent 6.2.16	-	-	2D - 3D
Sharifi et al. (2013)	Fluent 6.0	25780	-	2 D
Yazdani et al. (2012)	Fluent 12	80000	k-ε and Shear Stress (SST)	2D
Yen et al. (2013)	Fluent 6.3	50000	realizable k-ε turbulence	2D
Zhu et al. (2009)	Fluent 6.2	20000-54000	-	2D
Yadav and Patwardhan (2008)	Fluent 6.2.	-	standard k-ε turbulence k=ε=0.1	2D

As seen from the table, different turbulence models have been used in the literature. Bartosiewicz et al. [27] compared k-ω, k-ω SST and RNG turbulence models and concluded that k-ω SST performed better in comparison to other models. They argue that each turbulence model might have a different prediction of flow features and this finding may not be applicable to other cases. Hemidi et al. [26] concluded that over a range of operating conditions, the overall results show that k-ω model agreed better with ejector experimental data in comparison with k-ω SST model. Application of CFD in analysing radial ejectors is limited. A rotary nozzle semi-radial ejector consisting of 8 nozzles with spine angle of 10^{o} was investigated by the Fluent package and although there was the lack of experimental data on the actual configuration, validation of the results of the CFD simulations was achieved by comparing the CFD results with a proven analytical solution and conducting a mesh dependency analysis [67].

2.6 Conclusion

Many attempts have been made to improve supersonic ejector performance. Different approaches have been adopted in pursuit of this goal. Among the findings, variable geometry and oscillatory primary stream pressure are identified as potential methods to improve performance and efficiency. It is also concluded that operating conditions significantly affect the ejector performance in terms of entrainment ratio and pressure lift.

Most existing ejectors have an axisymmetric and axial flow path. Many researchers have adjusted the location of the primary nozzle and even altered the primary nozzle throat area but the form of axial ejectors impedes the effective, efficient and practical application of variable geometry concepts.

Radial ejector concepts have previously appeared in the literature, but primarily in the context of unsteady flow ejectors relying on pressure work to achieve the compression effect. One aim of such work has been to remove the strong normal shock in the diffuser section of typical ejectors. Researchers continued working on rotary concepts to achieve a positive effect from the oscillatory behaviour in the primary flow. The earlier concepts were not successful because of mechanical failure from the very high rotary speeds.

The radial ejector concept proposed in this thesis is similar to the axial flow ejector but transformed into a radial arrangement. The concept does not employ a rotary nozzle. The design of the radial flow ejector adopts certain geometric characteristics of a conventional ejector arrangement and an existing physical axial flow ejector was used as a benchmark. The radial ejector introduced herein offers the capacity to easily alter the nozzle and ejector throat areas by simply changing the separation of the nozzle surfaces and/or the duct walls.

Computational Fluid Dynamic (CFD) simulation has been proven as a successful tool in ejector flow analysis and performance improvement. Many researchers have used CFD models and reported that the CFD analysis can predict the ejector performance with acceptable accuracy. Ansys Fluent has been widely used by researchers for ejector analysis. This CFD tool has been used in this study in order to analyse the radial ejector performance and flow features inside the radial ejector.

Chapter 3

Investigation of Radial Flow Ejector Concept through CFD Analysis

To achieve higher performance from ejectors at some working conditions, it may be possible to develop practical ejectors that use variable geometry. However, most existing ejectors typically use an axisymmetric and axial flow path and this form restricts the practical implementation of variable geometry. A new ejector configuration that employs a radial flow path potentially allows for a variable geometry ejector in a practical configuration. For such a radial flow configuration, it is conceivable that geometric adjustment of the ejector could be made during operation in order to optimize performance over a range of different conditions. This radial flow ejector concept has been investigated using Computational Fluid Dynamic (CFD) analysis with Ansys Fluent software. Two dimensional (axisymmetric) CFD models were generated to compare the radial flow concept and an equivalent axial flow configuration. The CFD results reveal that the radial flow configuration is viable and can produce comparable performance to axial flow ejectors.

3.1 Introduction

To improve ejector performance through simulation of ejector flow behaviour, Computational Fluid Dynamics (CFD) has been widely employed in recent decades. Many researchers have reported the validation of CFD models using experimental data [26], [30], [70]. It has been claimed that CFD analysis can predict ejector performance with an acceptable error [71]; representative average error levels in some of the simulations are reported to be less than 10% [17], [26], although, higher magnitudes of error have been reported in [17] where the simulated entrainment ratio was only within 20% of the experimental data. CFD simulation using commercial software such as Fluent should at least be sufficiently reliable to determine the viability of the radial flow ejector concept.

The idea of a radial ejector was first introduced by Ng and Otis [69] in 1979 and in their ejector arrangement, the secondary flow entered the radial diffuser from below, and the primary flow entered the radial diffuser from above such that the high speed primary flow was adjacent to the upper diffuser plate. In an other radial ejector concept introduced in 2009, an ejector was arranged with eight rotary nozzles and a radial diffuser. Although there was lack of experimental data on the actual configuration, validation of the results of the CFD simulations were achieved by comparing the CFD results with a proven analytical solution and conducting a mesh dependency analysis [72], [18].

The radial ejector concept proposed in this paper is similar to the axial flow ejector, but transformed into a radial arrangement. The concept does not employ a rotary nozzle and unlike prior radial ejector work, the primary nozzle is centred within the ejector duct so that secondary flow is entrained from both sides. The design of the radial flow ejector adopts certain geometric characteristics of a conventional ejector arrangement and an existing physical axial flow ejector was used as a benchmark. The radial ejector introduced herein offers the capacity to easily alter the nozzle and ejector throat areas by simply changing the separation of the nozzle surfaces and/or the duct walls. This paper introduces this radial ejector arrangement and presents a comparative CFD analysis of the radial ejector concept and an equivalent axial concept.

3.2 Methodology

Established axial flow ejector design procedures based on empirical results and one-dimensional gas dynamic relations were adopted where possible during the design of the radial flow path, but significant departures from these established strategies have been necessary to achieve the desired performance in the radial configuration. In the radial configuration, the primary supply expands in the supersonic radial flow nozzle, and this expanding disk of primary flow entrains the secondary flow from the inlets positioned on either side of the expanding primary flow. An illustration showing flow paths in the radial ejector is presented in Figure 3-1.

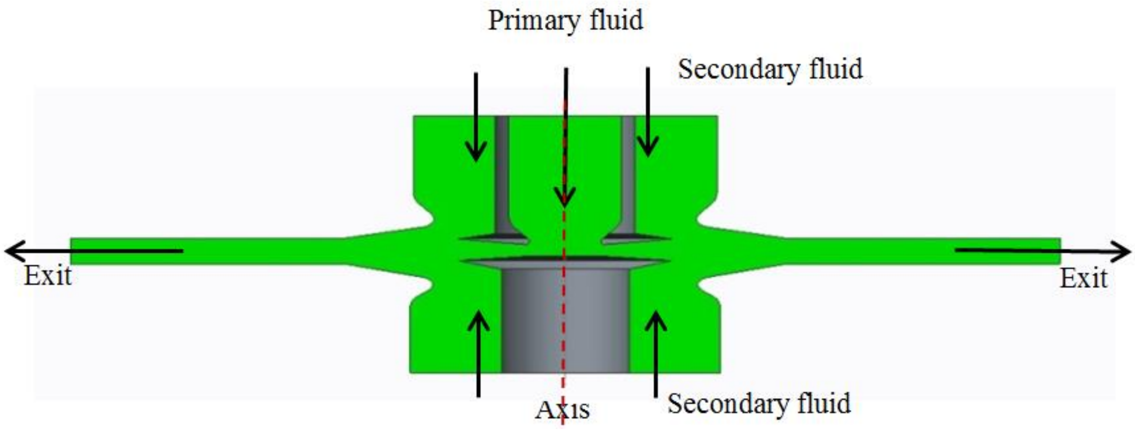

Figure 3-1: Illustration of flow inlets and outlets within a radial ejector.

The design of the radial ejector in this work loosely follows the semi-empirical design method for axial flow ejectors specified in [50] with necessary modifications to accommodate the radial nature of the flow.

Table 3-1 presents the geometric characteristics of the axial and radial ejector designed for this work. The target was to design a radial ejector equivalent to a benchmark axial ejector, which in the present work was the steam ejector design in [13]. However, some of the radial ejector features could not be completely equivalent to the axial flow benchmark case.

Table 3-1: Geometric characteristics of the radial ejector and the equivalent axial ejector.

Characteristic	Radial flow	Axial flow
Nozzle throat area (mm^2)	8.792	8.54
Nozzle exit area (mm^2)	179	154
Nozzle area ratio	20	18
Divergent part length (mm)	9.5	59.5
Divergent half angle	5^o	5^o
Ejector throat area (mm^2)	498	506
Ejector area ratio	58.24	59
Ejector convergent half angle	9^o	10^o
Ejector divergent half angle	0^o	3.5^o

3.3 CFD Model Arrangement and Validation

Two CFD models were created, one for the axial benchmark configuration and the other for the radial design that was intended to produce similar performance. Ansys Fluent 14.5 was used for the CFD simulation. A mesh independence analysis was performed for both cases. CFD simulations in the benchmark axial ejector configuration have previously been validated, including an assessment of mesh independence [13]. In the work of [13], the performance of course, medium and fine meshes was examined and the medium mesh with 19832 elements showed differences in static pressure and mass flow rate of less than 0.5% in comparison with the fine mesh. A similar mesh arrangement was also used in this paper for the axial ejector. For the radial design, different meshes of between 30000 and 80000 elements were produced. Based on the mesh independence analysis, the number of elements chosen for the simulations reported in this chapter was 51451, because static pressure results and entrainment ratio results are in agreement with results from the mesh with 79979 elements to within 0.45 %. As the radial ejector has a complicated shape and there was no experimental or numerical background for this design, a relatively fine mesh was applied.

Ansys Fluent 14.5 employs a finite volume technique in order to convert all governing equations to algebraic forms and the resulting equations of mass, momentum and energy are solved in this CFD model. The k-ω SST turbulence model has been very effective in other ejector simulations [15] and was employed in this work. All of the applied equations are reported in [73]. The CFD analysis was conducted using 2D models with air treated as an ideal gas in a compressible steady-state axisymmetric model. The primary and secondary inlets were set as 'pressure-inlet'. The ejector exit was set as 'pressure-outlet'. Primary pressures of 160, 200 and 250 kPa were selected for the motive fluid conditions. The secondary pressures of 1.8, 2.5 and 3.2 kPa were used for the secondary inlet condition. Different outlet pressures ranging from 2 to 7 kPa were used. A density-based implicit solver was chosen. This solver has been shown to be a suitable solver for supersonic flow fields [74], [75]. A second order upwind scheme was selected to discretise the equations to achieve higher accuracy at cell faces [73]. To define convergence of the solution, all residuals for calculations must fall to a specific level [75], which, for the present work was specified as less than 10^{-5}.

CFD simulations of the axial flow ejector configuration have been validated experimentally in the case of steam flows by [13] and [73]. The same CFD modelling has been used for the axial and radial configurations in the present work: the choice of solver, the turbulence model, the working fluid, the boundary conditions and convergence criteria were the same for both configurations. Furthermore, similar levels of mesh independence have been demonstrated for both the axial and radial configurations. Therefore it is expected that simulation results from the radial flow ejector configuration will reflect the real flow through such an ejector to a degree similar to that achieved with the axial flow ejector simulations.

3.4 Results and Discussion

Figure 3-2 shows the Mach number contours of axial and radial patterns obtained by the CFD analysis. The primary pressure, secondary pressure and exit pressure were set at 160, 1.8 and 2.5 kPa respectively. The simulation results produce the expected features including the sonic velocity at the nozzle throat and supersonic flow in the divergent section of the nozzle. The nozzle exit Mach number is slightly higher than 4.9 for the axial ejector and about 4.4 for radial ejector. The nozzle for the radial ejector actually had a slightly higher area ratio than the axial ejector, yet the nozzle exit Mach number is lower. The origin of this difference appears to be flow separation from the nozzle wall towards the exit of the radial nozzle that does not occur to the same extent in the case of the axial nozzle as illustrated in Figure 3-2, generally consistent with analytical results based on the geometric area ratio for the nozzles.

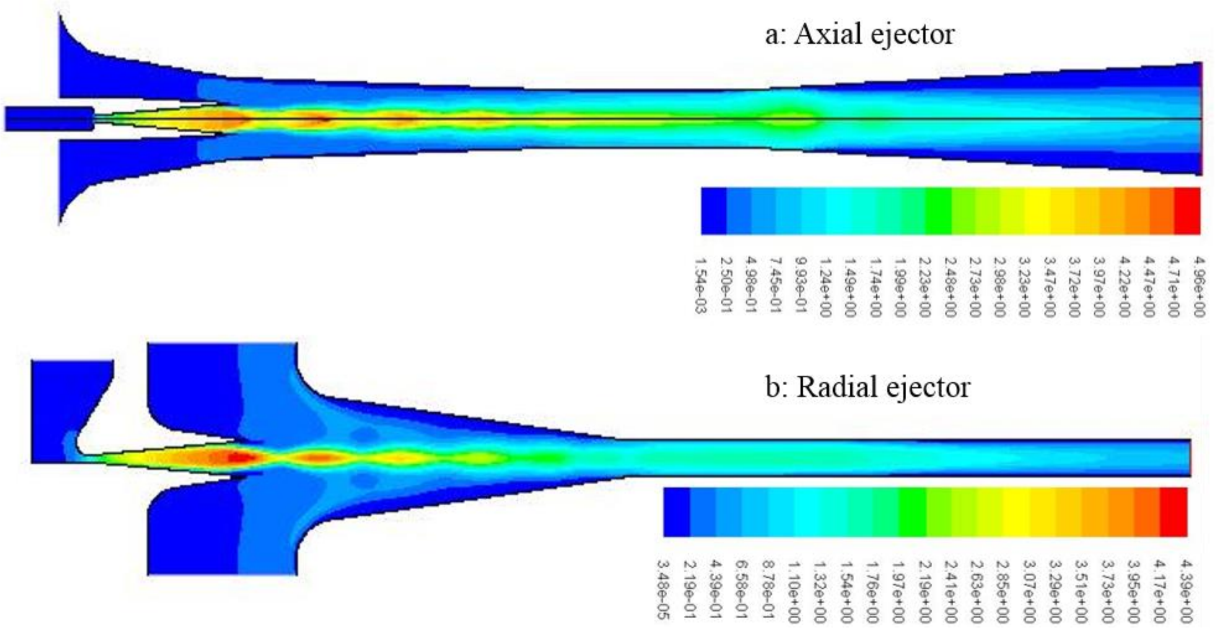

Figure 3-2: Contours of Mach number in the radial and axial configurations for primary pressure of 160 kPa, secondary pressure of 1.8 kPa and exit pressure of 2.5 kPa. The physical scale of the radial ejector illustrated here is approximately 7 times that of the axial ejector shown.

To evaluate the exit pressure effects, the primary pressure and secondary pressure were maintained at 160 kPa and 1.8 kPa while the ejector exit pressure was varied from 1.8 to 5 kPa. The performance of the ejectors in terms of the entrainment ratio was defined from these simulations. The ejector entrainment ratio is the mass flow rate of the secondary stream divided by the mass flow rate of the primary stream. Figure 3-3 shows the characteristic curves (entrainment ratio versus exit pressure) for axial and radial configurations for primary and secondary pressures of 160 and 1.8 kPa, respectively. At this working condition, the maximum entrainment ratio of the radial configuration was about 2% lower than the axial configuration. The critical pressure (where the entrainment ratio starts to decrease) and the malfunction pressure (where the entrainment ratio drops to zero) for the radial configuration were both slightly lower than axial configuration. It was shown that the total length of the ejector plays an important role in establishing the critical and malfunction pressures [50], [49], [48]. The radial ejector has a short flow path compared to the axial configuration, possibly contributing to the lower critical and malfunction pressures at this operating condition.

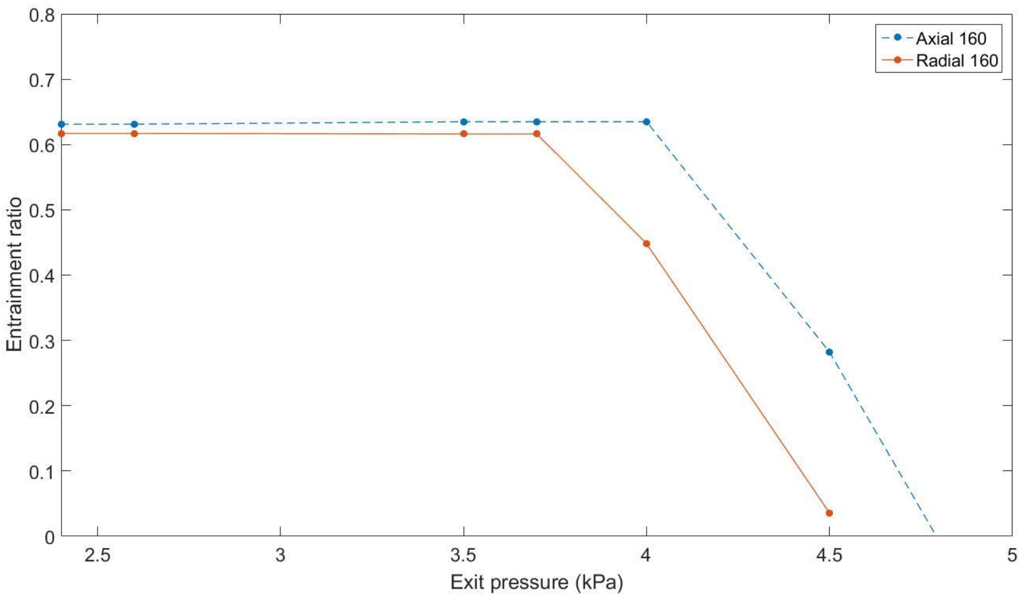

Figure 3-3: Characteristic curves for axial and radial configurations for primary and secondary pressures of 160 and 1.8 kPa respectively.

Figure 3-4 shows the contours of Mach number for the exit pressure of 3.5 kPa. By comparing contours of Mach numbers for exit pressures of 3.5 kPa (Figure 3-4) and 2.5 kPa (Figure 3-2), it is observed that increasing the exit pressure moves the position of the shock structures upstream. This effect is also reported elsewhere [74], [75].

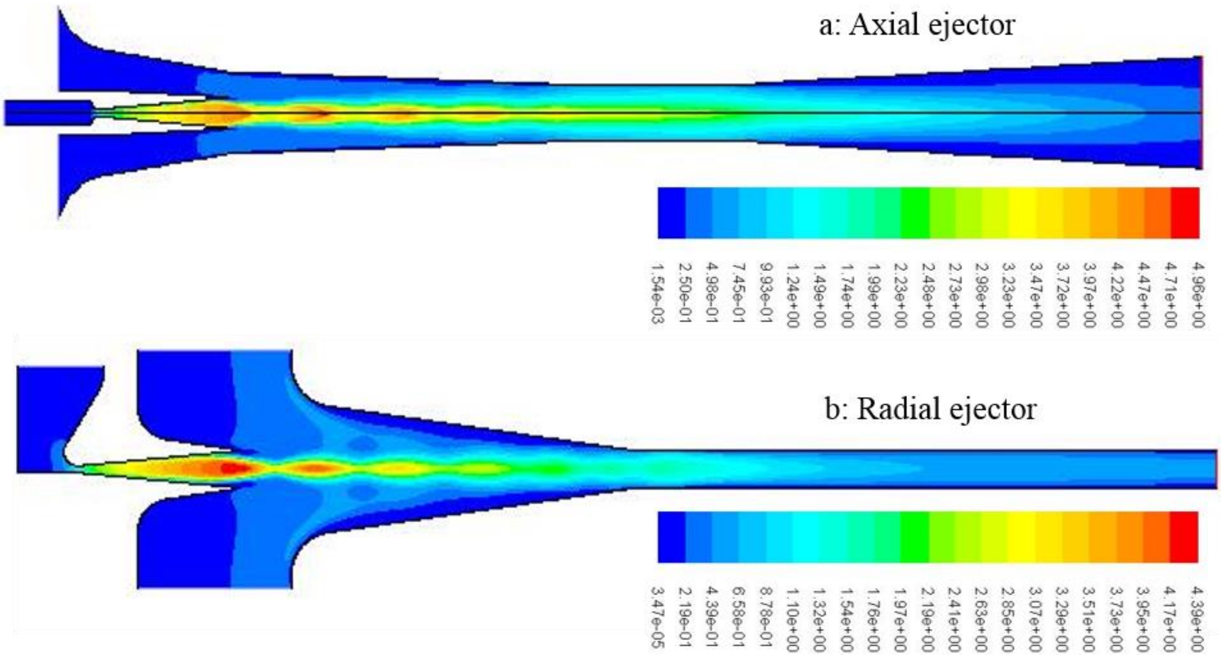

Figure 3-4: Contours of Mach number in the radial and axial configurations for primary pressure of 160 kPa, secondary pressure of 1.8 kPa and exit pressure of 3.5 kPa. The physical scale of the radial ejector illustrated here is approximately 7 times that of the axial ejector shown.

To determine the effect of primary pressure on both ejector configurations, CFD simulations were performed for higher primary pressures of 200 and 250 kPa. Figure 3-5 shows that by increasing primary pressure, both ejector configurations can achieve higher critical pressures. However, the entrainment ratio decreases with increasing primary pressure. One explanation for this effect is that increasing primary pressure leads to an under-expanded condition for the primary jet at the nozzle exit resulting in further expansion of the primary flow downstream of the nozzle, and resulting in a smaller effective flow area available for the secondary stream [75].

At higher primary pressure, the difference between the entrainment ratio for the axial and radial configurations approaches zero. The difference in exit pressure at malfunction also decreases and at higher primary flow pressures, the radial ejector actually shows a slightly better performance.

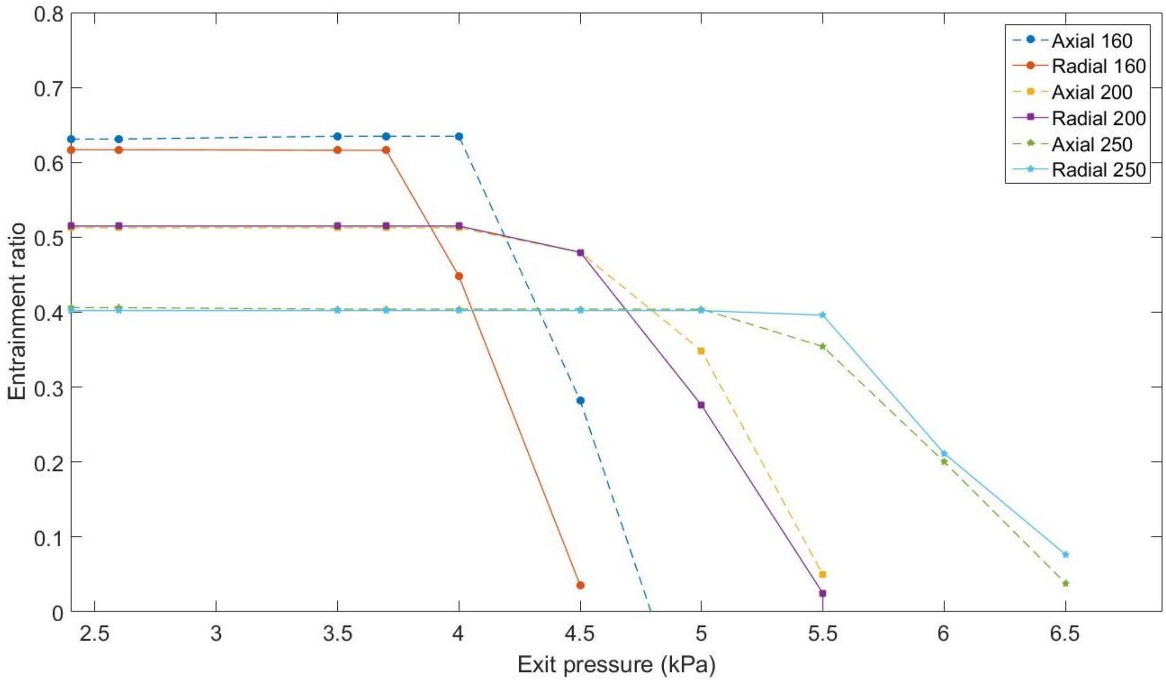

Figure 3-5: Characteristic curves for axial and radial configurations for different primary pressures and for the secondary pressure fixed at 1.8 kPa.

Figure 3-6 shows the contours of Mach number for the primary, secondary and exit pressure of 250, 1.8 and 3.5 kPa, respectively. By comparing contours of Mach number for primary pressures of 160 kPa (Figure 3-2) and 250 kPa (Figure 3-6), it is observed that increasing the primary pressure moves the position of the shock structures downstream. This effect is also mentioned elsewhere [74], [75].

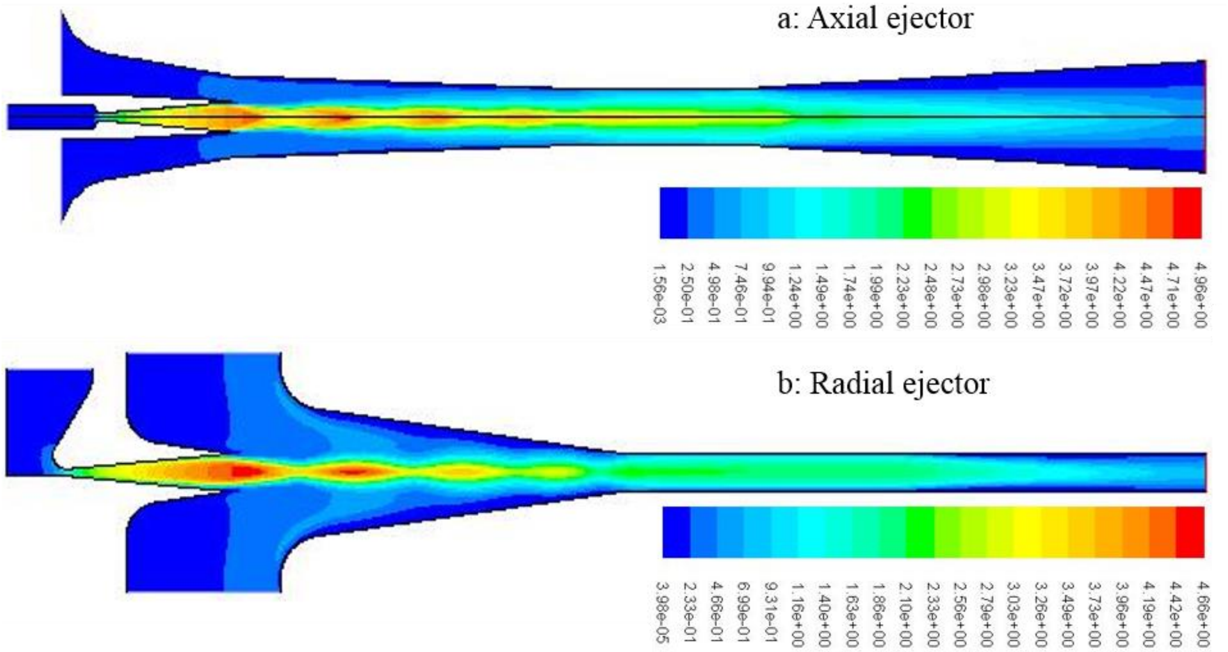

Figure 3-6: Contours of Mach number in the radial and axial configurations for primary pressure of 250 kPa, secondary pressure of 1.8 kPa and back pressure of 3.5 kPa. The physical scale of the radial ejector illustrated here is approximately 7 times that of the axial ejector shown.

Figure 3-7 shows the static wall pressure along the ejector for axial and radial configurations for primary and secondary pressures of 250 and 1.8 kPa respectively and different back pressures. The overall trend in the static pressure distribution is similar. However, there are some differences. The axial configuration shows a gradual reduction in the pressure as the location of the minimum pressure is approached, whereas the radial pattern shows a relatively sharp decrease in the pressure.

By increasing the back pressure in both configurations, the position of the compression moves upstream. In the radial ejector, by increasing back pressure, the static wall pressure on the upper and lower walls become slightly different. It seems the flow inside the radial duct is not completely symmetric across the centre-plane of the duct and these asymmetries are amplified by increased back pressure – compare the different line types in part (b) of Figure 3-7.

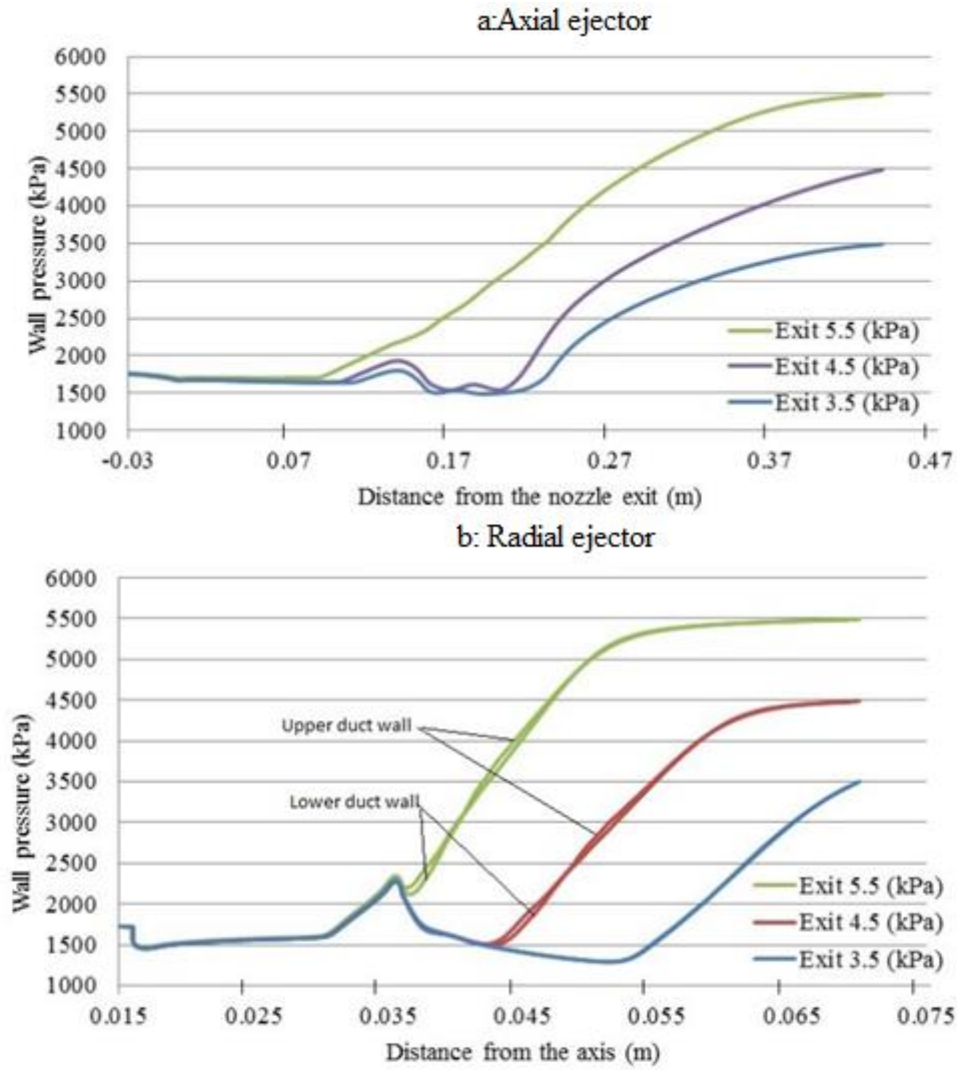

Figure 3-7: Static wall pressure within (a) the axial, and (b) the radial configurations.

3.5 Conclusion

CFD simulations using Ansys Fluent have been performed for a supersonic radial ejector configuration working with air. The radial ejector simulations have been compared with an equivalent, conventional axial configuration. The radial ejector produces similar performance to the axial configuration. For lower primary pressures, the axial configuration shows slightly better performance than the radial configuration. At higher primary pressures, the radial configuration has comparable performance to the axial configuration and at some operating conditions, the radial configuration is actually more effective.

Results from the CFD simulations of the radial ejector configuration are encouraging. To progress the radial ejector concept towards a physical solution, experiments on a prototype configuration are required. Further simulations using validation data from such a prototype would also be warranted in order to confidently use the CFD as a design and optimisation tool for the radial configuration.

The primary appeal of the radial ejector configuration is that it provides convenient access for adjustment of the nozzle and ejector throat sizes with prospects for practical implementation. Because it appears that a radial ejector can achieve similar performance to a conventional axial ejector, the radial concept warrants further work and shows potential for application in systems where varying operating conditions exist.

Chapter 4

CFD Study of a Variable Flow Geometry Radial Ejector

Tuning the flow rates of axisymmetric axial flow ejectors to match required operating conditions is difficult because altering a cylindrical throat size without introducing flow losses from blockage effects is difficult. However, the geometric adjustment of a radial ejector could be made by simply changing the separation of the radial ejector duct walls and/or the separation of the nozzle walls in order to optimize performance over a range of different conditions. The effects of such changes on the performance of a radial ejector have been investigated using a Computational Fluid Dynamic (CFD) analysis with Ansys Fluent software. Axisymmetric CFD models were generated to assess performance for a primary nozzle throat area of 8.792 mm^2 and for ejector throat separations of 2.2 mm, 2.4 mm and 3.0 mm, corresponding to ejector throat areas of 497, 543 and 678 mm^2, respectively. The CFD analysis reveals that changes in ejector performance can be achieved by changing the ejector duct's separation. An increase of 34% in entrainment ratio can be achieved by increasing the ejector throat separation from 2.2 mm to 3.0 mm at fixed primary and secondary pressures of 160 kPa and 1.8 kPa, respectively. If an increase in the ejector critical back pressure is needed, it could be achieved by decreasing the ejector duct separation. An increase in the critical back pressure in excess of 40% can be achieved by decreasing the ejector throat separation from 3.0 mm to 2.2 mm at primary and secondary pressures of 250 and 1.8 kPa, respectively.

4.1 Introduction

Traditionally, ejectors are configured as cylindrical pipes with conical transitions between the pipes of different diameters. Such ejector configurations are well-established and can be integrated with existing pipe-work through the use of standard flanges and fittings. However, the cylindrical pipe arrangement makes it difficult to change the throat size of such ejectors to match the performance of the ejector to the necessary operating condition for the ejector.

Although the radial configuration of [76] was introduced as a simple approach to achieve geometric variability in the ejector, no analysis has yet been reported to demonstrate the effectiveness of the concept. This chapter presents CFD simulations that quantify the sensitivity of radial flow ejector performance to geometry variations that can be achieved by altering the separation of the plates that form the walls of the ejector duct.

4.2 Approach

The design of a radial ejector by adapting axial flow ejector design methods [50], [13] to suit the radial configuration was presented in [76]. The radial ejector described in [76] forms the basis for the present work. Figure 4-1 provides a schematic illustration the ejector primary nozzle and the plates that form the ejector duct showing the separation of the ducts (h). The separation is the minimum distance between the upper and lower ejector plates. By changing the separation, the ejector area is changed.

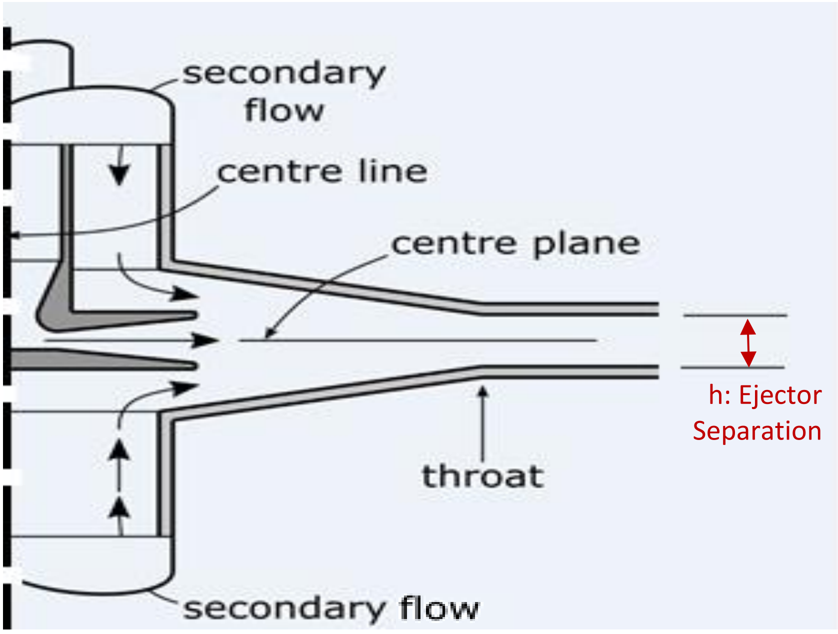

Figure 4-1: The radial ejector duct showing the radial ejector duct separation.

Figure 4-2 shows the radial ejector flow cross sectional areas for ejector duct separations of 2.2, 2.4 and 3.0 mm. The ejector throat areas for separation of 2.2, 2.4 and 3 mm are 497, 543 and 678 mm^2 respectively and the corresponding ejector area ratios are 56.5, 61.8 and 77.

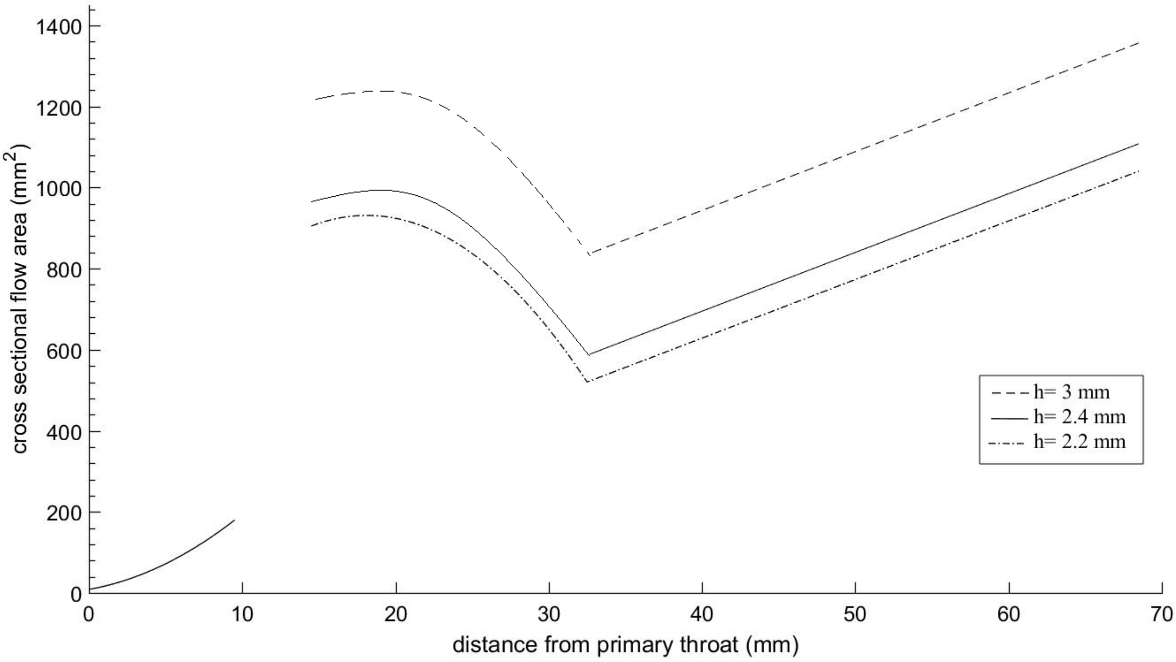

Figure 4-2: Variation of the radial ejector cross-sectional flow area with distance from the primary throat.

Three axisymmetric (two dimensional) CFD models were created for this study and Ansys Fluent 14.5 was used for the simulations. A mesh independence analysis was performed for the model in previous work [76] and based on those results, the total number of elements chosen for the simulations in this study were 51451, 53126 and 59324 for the 2.2, 2.4 and 3.0 mm throat separations respectively. The details of mesh independence analysis and validation strategy has been reported in [76].

The working fluid for the simulations was air, treated as an ideal gas. The primary and secondary inlets were set as 'pressure-inlet' and the ejector exit was set as a 'pressure-outlet'. Primary pressures of 160, 200 and 250 kPa were selected for the motive fluid conditions and the secondary pressures of 1.8, 2.5 and 3.2 kPa were used for the secondary inlet condition. Different outlet pressures ranging from 2 to 7 kPa were applied. The k-ω SST turbulence model has shown consistent results in other ejector simulations [15] and has been used in this study as well.

The density-based implicit solver, which has been verified as a suitable solver for supersonic flow fields [74], [75], has been employed in this study. A second order upwind scheme was selected to discretise the equations to achieve higher accuracy at cell faces [73]. To define convergence of the solution, all residuals for calculations must fall to a specific level [75], which, for the present work was specified as less than 10^{-5}. Essentially the same CFD modelling has been used for the three different separations of the plates that form the ejector duct in the present work: the choice of solver, the turbulence model, the working fluid, the boundary conditions and convergence criteria were the same for all simulations. Therefore, it is expected that simulation results from the three different ejectors will reflect the real flow with similar accuracy to that achieved with the previous study [76].

4.3 Results and Discussion

Figure 4-3 shows the Mach number contours for the three separations of 2.2, 2.4 and 3.0 mm at the primary pressure of 160 kPa, secondary pressure of 1.8 kPa and exit pressure of 2.5 kPa. For all three cases, the expected flow features – such as sonic velocity at the primary nozzle throat and supersonic flow in the divergent part – have been obtain by CFD simulations.

The effects of exit pressure have been evaluated using CFD for the primary and secondary pressure of 160 kPa and 1.8 kPa respectively and different ejector exit pressure values from 1.8 to 5 kPa. The ejector performance in terms of entrainment ratio (ER) is presented in Figure 4-4 for separations of 2.2, 2.4 and 3.0 mm. At this working condition, the maximum entrainment ratio of 0.82 was obtained for a separation of 3.0 mm. Entrainment ratios of 0.67 and 0.61 were obtained for separations of 2.4 and 2.2 mm respectively. By analogy to axial flow ejector cases such as discussed in [75], an explanation for this effect is that a larger effective secondary flow area is available for larger plate separations.

The critical pressure (where the entrainment ratio starts to decrease with increasing exit pressure) and the malfunction pressure (where the entrainment ratio drops to zero) are also affected by the duct separations. The lowest malfunction pressure occurred for a plate separation of 3 mm for this working condition. The critical pressure was increased by about 15 % when the separation was decreased from 3 mm to 2.4 mm. The malfunction pressure was likewise increased by about 7 % when the separation was decreased from 3 mm to 2.4 mm. However, further reductions in the plate separation from 2.4 mm to 2.2 mm did not yield a significant change in either the critical pressure or the malfunction pressure. Previous work has shown that the total length of the ejector plays an important role in the critical and malfunction pressures [50], [49], [48], however, the total length of all three ejectors with different duct separations are the same in the present work.

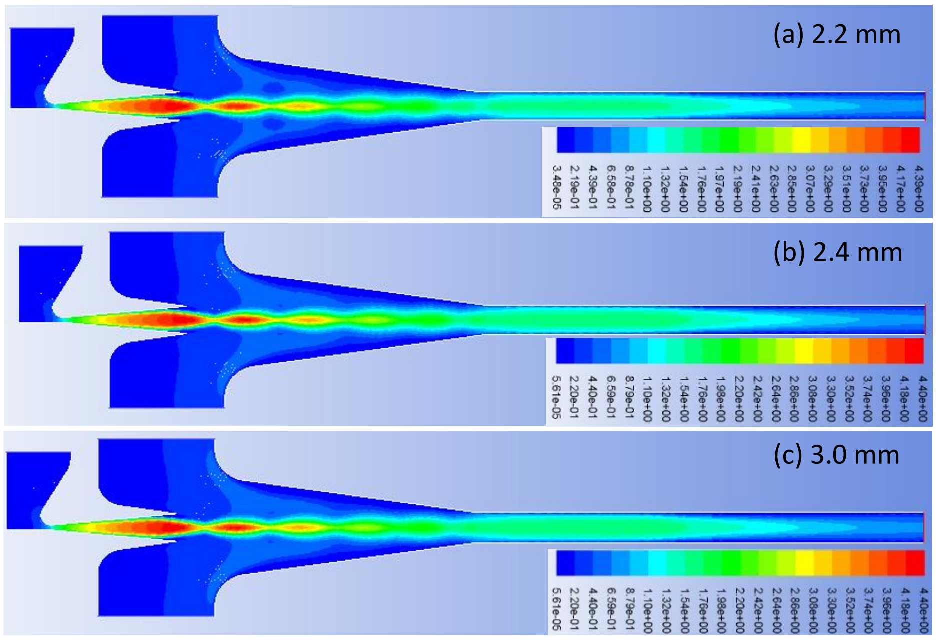

Figure 4-3: Contours of Mach number for primary pressure of 160 kPa, secondary pressure of 1.8 kPa and exit pressure of 2.5 kPa for minimum plate separations of (a) 2.2 mm; (b) 2.4 mm; and (c) 3.0 mm.

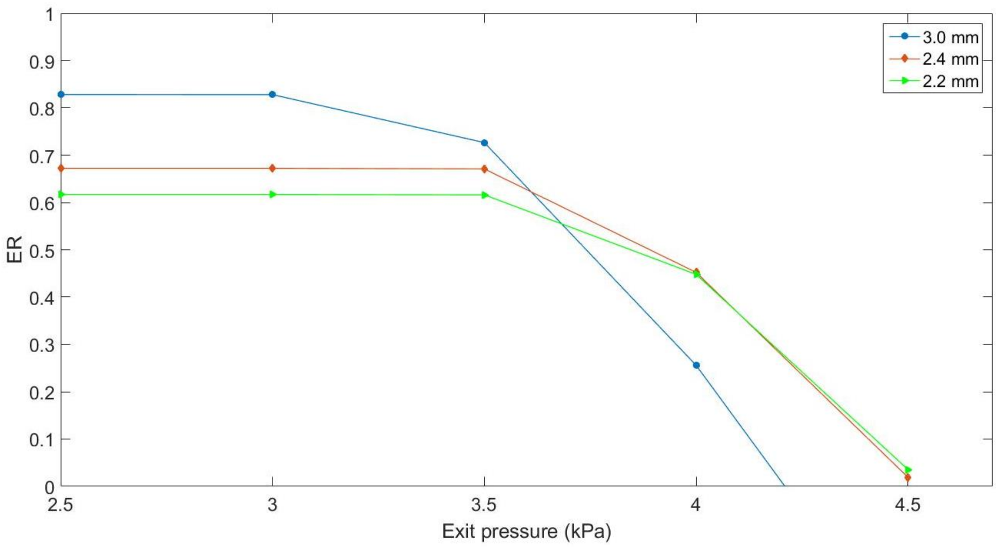

Figure 4-4: Characteristic curves for radial ejector for 2.2, 2.4 and 3mm separations at primary and secondary pressures of 160 and 1.8 kPa respectively.

Figure 4-5 presents the contours of Mach number for the exit pressure of 4.5 kPa. By comparing contours of Mach numbers for exit pressures of 4.5 kPa (Figure 4-5) and 2.5 kPa (Figure 4-3), it is observed that increasing the exit pressure moves the position of the shock structures upstream. This effect is also reported elsewhere [76], [75], [74]. Figure 4-5 show that for the 3 mm separation, asymmetric flow in the ejector occurs with an exit pressure of 4.5 kPa. A similar behaviour is shown for separation of 2.2 mm, but for the intermediate separation of 2.4 mm, the flow is also un-choked but retains a higher degree of symmetry than for the 2.2 and 3.0 mm separation cases.

To find the effect of primary pressure on the radial ejector with different separations, higher primary pressures of 200 and 250 kPa were analysed by CFD model. Figure 4-6 shows the radial ejector entrainment ratios for primary pressures of 200 and 250 kPa. It can be seen that, similar to primary pressure of 160 kPa shown in Figure 4-4, by increasing the ejector duct separation, the entrainment ratio increases. These results show that at the low primary pressure of 160 kPa, increasing the separation has largest effects on the maximum entrainment ratios. At this working condition, by increasing separation from 2.2 to 3 mm, the maximum entrainment ratio increases about 34% while at both higher primary pressures of 200 and 250 kPa the maximum entrainment ratio increase is about 29%. The effects of ejector duct separation on the critical back pressure and malfunction pressure are more significant at the higher primary stream pressures. By decreasing the separation from 3 to 2.4 mm, the critical back pressure increases by approximately 15%, 30%, and 40% for primary stream pressures of 160, 200, and 250 kPa, respectively.

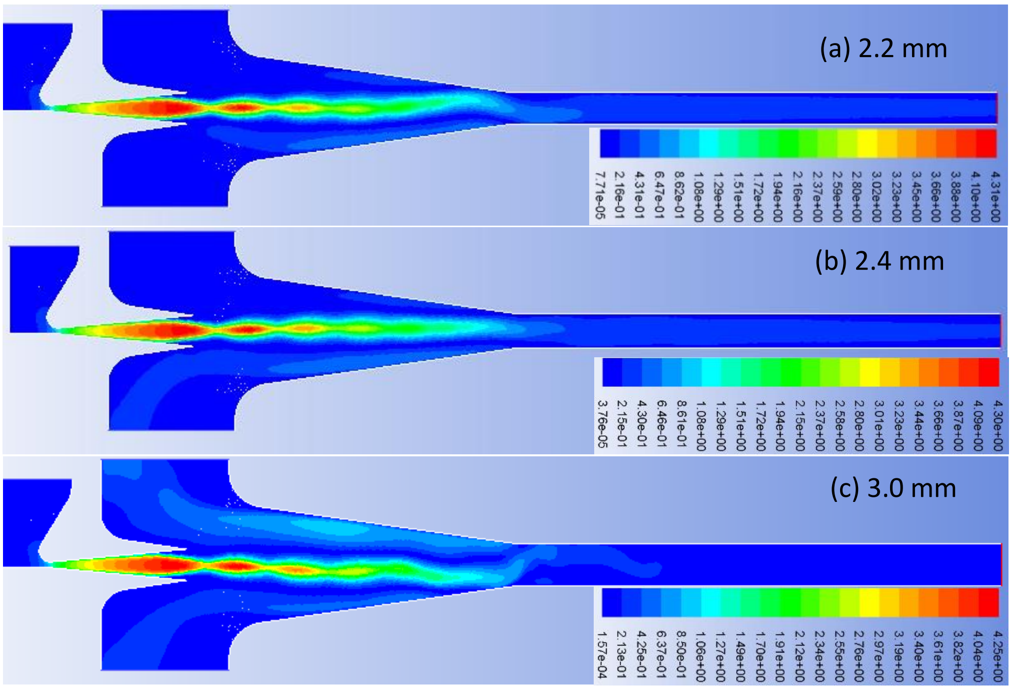

Figure 4-5: Contours of Mach number for primary pressure of 160 kPa, secondary pressure of 1.8 kPa and exit pressure of 4.5 kPa with throat separations of (a) 2.2 mm; (b) 2.4 mm; and (c) 3 mm.

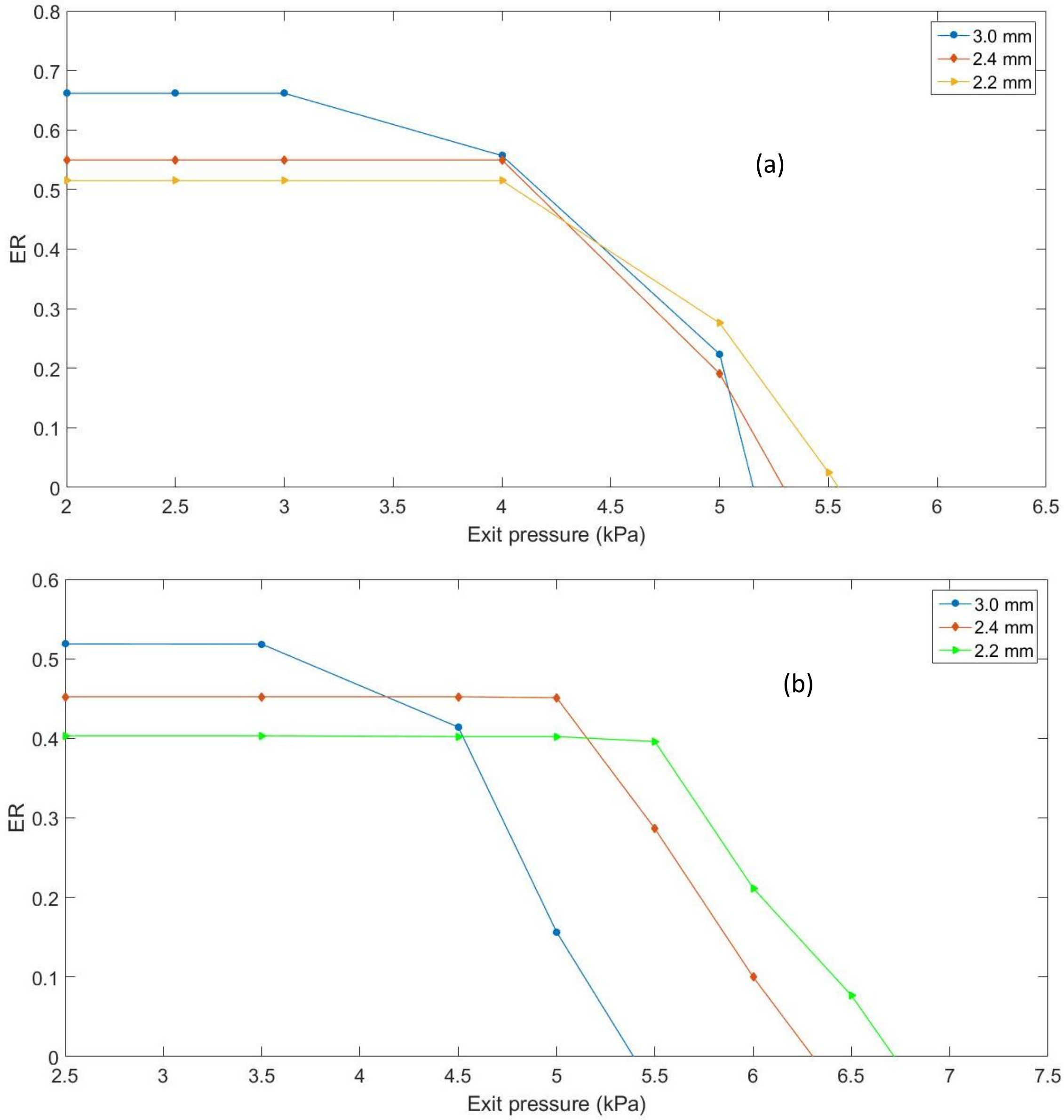

Figure 4-6: Characteristic curves for separations of 2.2, 2.4 and 3 mm for the secondary pressure fixed at 1.8 kPa and for primary pressures of (a) 200 kPa and (b) 250 kPa.

Figure 4-7 shows the static wall pressure along the ejector for separations of 2.2, 2.4 and 3 mm for primary and secondary pressures of 160 and 1.8 kPa respectively and back pressures of 2.5 and 4.0 kPa. The overall trend of the static pressure distribution is similar to the distributions reported by [76]. Higher ejector exit pressures tend to move the location of the pressure rise upstream. At the primary pressure of 160 kPa, by increasing the ejector duct separation, the minimum static pressure along the wall of the ejector decreases and the location of the pressure rise tends to move downstream. For the higher back pressure case of 4 kPa, ejectors with separations of 2.2 and 2.4 experience a pressure rise that is initiated in the mixing section, but by increasing the separation to 3 mm, the location of the pressure rise shifts downstream.

Figure 4-8 shows the static wall pressure along the ejector for separations of 2.2, 2.4 and 3 mm for primary and secondary pressures of 250 and 1.8 kPa respectively and back pressures of 3.5 and 5.5 kPa. As was the case for the 160 kPa primary pressure, increasing the exit pressure in the 250 kPa primary pressure simulations tends to move the location of the pressure rise within the ejector duct upstream. However, in contrast to the results at the primary pressure of 160 kPa, increasing the duct separation in the case of the primary pressure of 250 kPa actually tends to cause the location of the pressure rise within the ejector to move upstream.

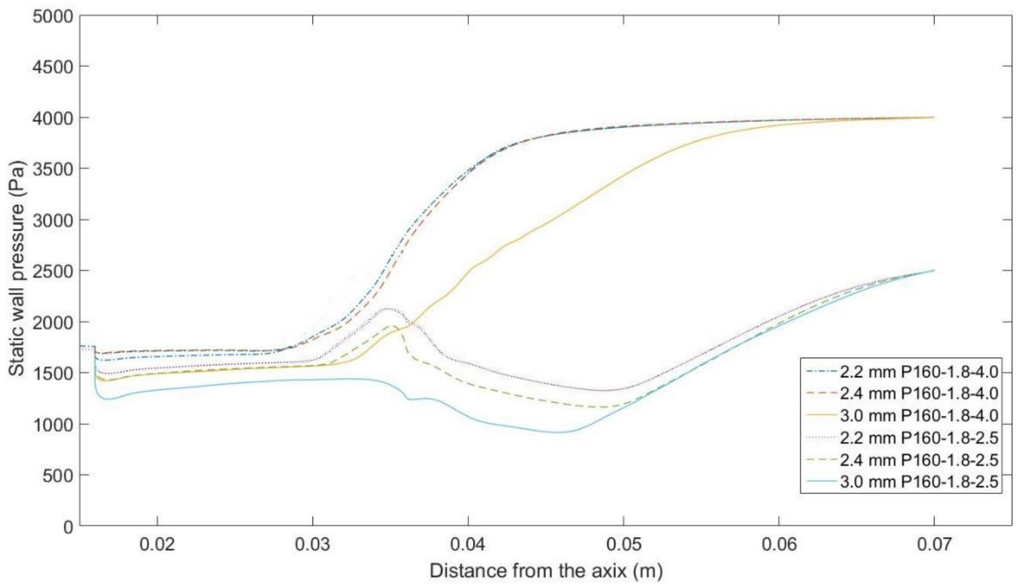

Figure 4-7: Static wall pressure for primary pressure of 160 kPa and exit pressures of 2.5 and 4 kPa.

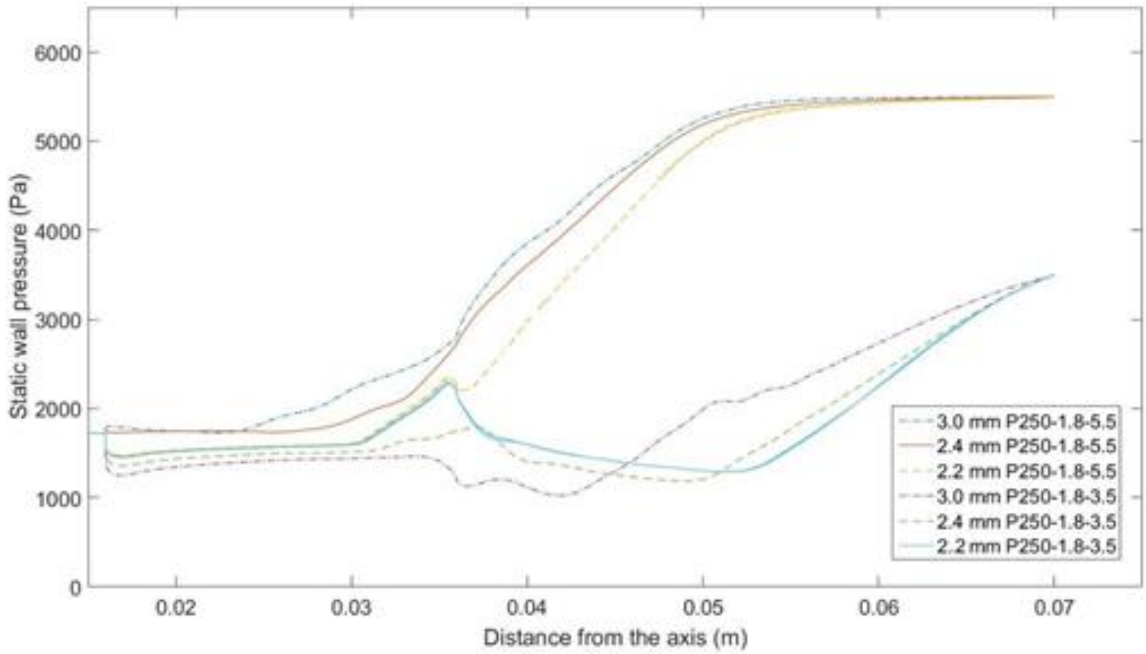

Figure 4-8: Static wall pressure for primary pressure of 250 kPa and exit pressures of 3.5 and 5.5 kPa.

4.4 Conclusion

CFD simulations using Ansys-Fluent have been performed for an adjustable geometry supersonic radial ejector configuration working with air. Three different ejector flow areas were created by changing the separation of the radial ejector ducts; separations of 2.2 mm, 2.4 mm, and 3 mm were simulated. The CFD results reveal that by simply changing the separation of ejector ducts, different ejector performance in terms of entrainment ratio and critical back pressure could be achieved.

Higher entrainment ratios can be achieved by increasing the radial ejector separation. In the current configuration, an entrainment ratio increase of 34% was achieved by increasing the ejector duct separation from 2.2 mm to 3 mm, but increasing the separation typically reduces the critical back pressure that can be achieved. By decreasing the ejector duct separation from 3 mm to 2.2 mm, increases in the critical back pressure of in excess of 40% were achieved at the highest primary pressure condition.

Results from the CFD simulations suggest that a variable area ejector can be achieved through the radial ejector configuration. To progress the variable radial ejector concept towards a physical solution, experiments on a prototype are required. Further simulations using validation data from such a prototype would also be warranted in order to confidently use the CFD as a design and optimization tool for the radial configuration.

Chapter 5

Experimental Evaluation of a New Radial Ejector Design

A radial flow ejector that produces comparable performance to an axial flow ejector potentially offers a broader operating envelope through adjustable throat sizes. Design of a radial ejector was undertaken and the process was informed by empirical axial flow ejector design procedures. Experiments on a prototype configuration have quantified the ejector performance. The prototype radial flow ejector area ratio was 59 and when operating with air in both motive and suction streams, the ejector produced entrainment ratios between 0.95 and 0.24 for expansion ratios between 50 and 139. Critical pressure lift ratios around 1.5 were obtained across this range of working conditions. The entrainment ratio achieved in the prototype radial ejector agreed well with those from a quasi-one-dimensional gas dynamic model that was tuned to match previously published, axial flow ejector data, the average error being less than 10%. However, the pressure lift ratios obtained from the tuned quasi-one-dimensional model overestimate the pressure lift ratios of the prototype. Radial flow ejectors deserve further attention, with more extensive modelling and prototype testing to optimise performance.

5.1 Introduction

Ejectors have many applications including refrigeration and air conditioning. Many industrial applications for pumping take advantage of ejectors' long service life, resistance to wear and ability to pump from low pressures. Ejectors employ a jet of high pressure primary fluid to induce a low pressure secondary flow and to compress the secondary flow to a higher pressure. In the case of gas or vapour ejectors, as the primary flow is expanded through the nozzle, a partial vacuum is created which induces the secondary flow and mixing occurs between the primary and secondary flows downstream of the nozzle [29]. The transfer of momentum from the primary to the secondary flow enables the static pressure of secondary flow in the diffuser to reach a higher value than it had at the secondary inlet [4], [6]. Figure 5-1 presents an axisymmetric ejector schematic showing the general flow directions which are predominantly in the axial direction.

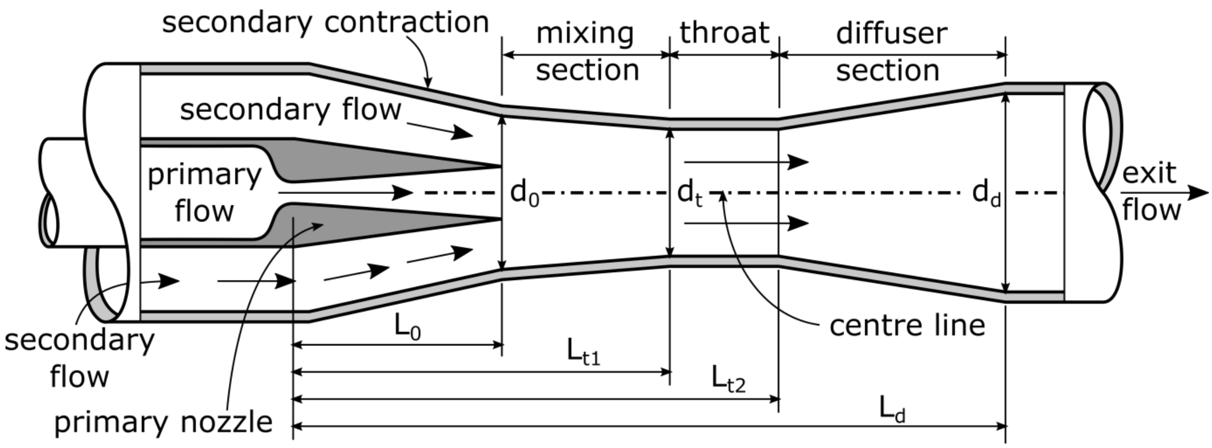

Figure 5-1: Illustration of an axisymmetric ejector with a predominantly axial flow path.

An important area of study in ejector performance improvement is employing unsteady primary flow. The design of, and additions to, the primary nozzle for the purpose of producing unsteady primary flow might improve the system performance [68]. Variability of the nozzle throat cross-sectional area could be a method for generating unsteady primary flow at the nozzle, and using loud speakers [18], and 'novel wall-mounted cavities' [65] are examples of other pulsation systems used for mixing enhancement in ejectors.

The radial flow ejector concept was introduced by Ng and Otis [69] and in their arrangement, disks with an ajustable separation formed the upper and lower boundaries of the diffuser, the primary flow entered the ejector adjacent to the upper disk, and the secondary flow entered adjacent to the lower disk. A spool was used to adjust the relative flow areas available for entry of the primary and secondary streams to the ejector. Since the introductory work of [69], the concept of radial flow ejectors has been revisited, but in the context of pressure exchange devices: a rotary nozzle radial ejector was introduced by Garris et al. [67]. Because of this identified benefit and the positive effect of the oscillatory behaviour of the primary flow, other rotary concepts have also been investigated [66]. The earlier concepts were not successful because of mechanical failure [64] due to very high rotary speed which was about 50000 rpm. Work on the rotary nozzle radial ejector concept exposed many problems with this concept, including mechanical failures, vibration, and a requirment of high precision components resulting in high costs.

The concept for a radial ejector proposed in this paper does not use a rotary nozzle. The proposed ejector does not have rotating parts, so the issue of mechanical failure resulting from high rotary speeds is not relevant. The radial ejector investigated in this paper is also different from the original device of Ng and Otis [69] in that the primary flow enters the ejector through a centrally-positioned nozzle so that the high speed flow does not enter the diffuser adjacent to one of the diffuser disks.

The main difference between traditional ejector designs and the proposed radial ejector is the pattern of fluid flow. In the traditional axial ejector arrangement, the working fluid enters the nozzle and passes through the ejector in an axial direction as illustrated in Figure 5-1; the nozzle and suction chamber, the throat and diffuser are all co-axial in a traditional ejector arrangement. The new radial ejector generates radial flow patterns as illustrated in Figure 5-2: the primary and secondary flows are accelerated principally in the radial direction and deceleration in the diffuser also occurs in the radial direction; the flow is sandwiched between disk-like surfaces that form the primary nozzle and the ejector duct.

Axial flow ejectors typically have primary nozzles and ejector ducts that are circular in cross section which inhibits changes in throat area in a mechanically reliable and aerodynamically efficient manner. The introduction of a contoured centre-body that can be traversed along the axis of the primary nozzle and/or the ejector duct can be used to alter the throat areas in an axial flow ejector but aerodynamic losses will accompany such configurations. In contrast, the radial ejector is a promising solution that enables variability in the throat sizes without introducing large pressure loss, as the geometry change is simply achieved by changing the separation of the nozzle surfaces and/or the duct walls. The work discussed below presents experimental evaluation of a prototype radial ejector.

5.2 Radial Ejector Design

5.2.1 Overall Configuration

The design of the radial ejector followed traditional axial-flow ejector design rules [50], [49], interpreted in the context of the new radial ejector geometry. An axial flow ejector designed by Al-Doori [13] was also used as a benchmark arrangement, and the design targets for the radial flow ejector were chosen to match Al-Doori's system. The general arrangement of the radial ejector is illustrated in Figure 5-2.

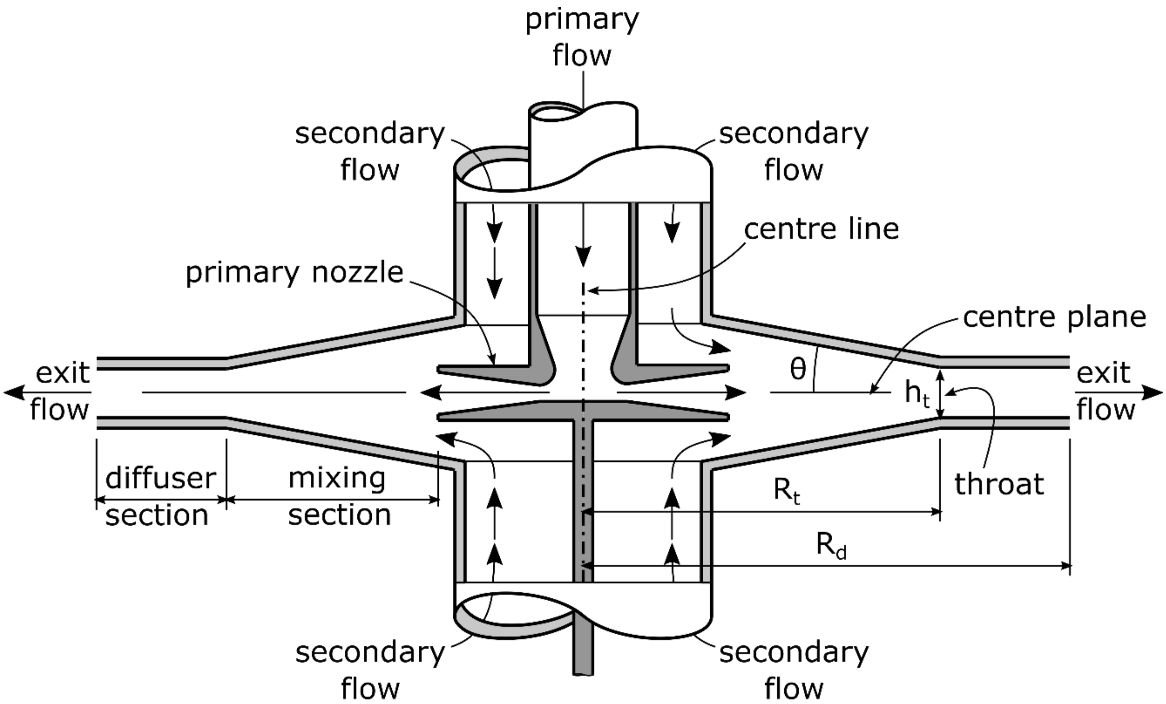

Figure 5-2: Illustration of an ejector with a predominantly radial flow path: the radial ejector.

5.2.2 Supersonic Nozzle

The supersonic nozzle is a critical part of gas or vapour ejector systems, so special consideration has been given to the design of the radial supersonic nozzle. This supersonic nozzle is similar to an axial nozzle in that it has 4 different sections: (1) uniform cross-sectional area inlet; (2) convergent section; (3) throat; and (4) divergent section. Figure 5-3 part (a) shows the radial nozzle cross section and in part (b) the axial nozzle cross section is shown. Figure 5-3 presents the geometric characteristics of the benchmark axial flow supersonic nozzle and the radial flow supersonic nozzle. The discussion that follows describes the design decisions that led to the specifications in Table 5-1.

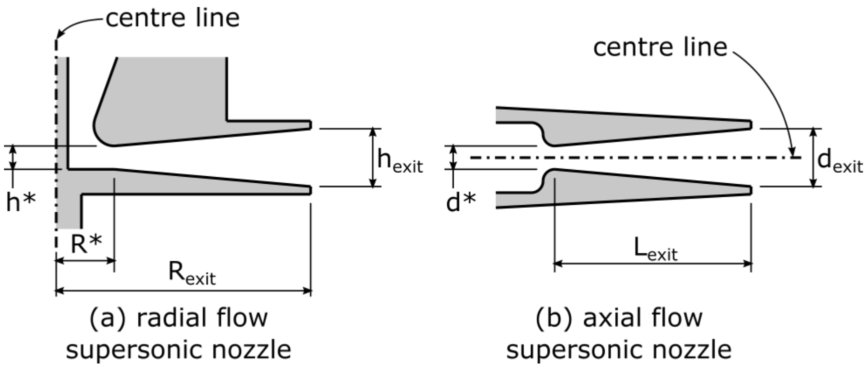

Figure 5-3: Illustration showing cross sections of primary nozzle features in the case of (a) radial flow supersonic nozzle; and (b) axial flow supersonic nozzle.

In supersonic axial nozzles, the length of the uniform cross-sectional area inlet is recommended to be more than 10 times the throat diameter [41]. In the proposed radial configuration, the separation of the nozzle at the throat was specified as 0.4 mm at a radius of 3.5 mm, giving an equivalent axisymmetric throat diameter was 3.35 mm. The length of the uniform cross-sectional area inlet upstream of the subsonic contraction was set to 30 mm, in an effort to accommodate the uniform cross-sectional area inlet requirement, but this length was also limited by fabrication constraints.

For choked primary nozzle operating conditions, the mass flow rate through the supersonic nozzle is essentially proporational to the nozzle throat area [77]. The nozzle throat area of the radial ejector was chosen as 8.8 mm^2, a value that is 9% larger than that of the axial flow benchmark nozzle. A larger throat area was selected for the radial nozzle to accommodate the slightly lower discharge coefficient of the radial nozzle anticipated due to the sharp flow direction changes and the increased surface area in the convergent part of the radial nozzle. Fabrication restrictions based on achievable strength and machinability of the stem of the lower portion of the radial nozzle also constrained the radial supersonic nozzle throat size.

The required nozzle exit Mach number was defined based on the benchmark axial flow nozzle, which itself was designed using traditional ejector design procedures. The exit area of the radial nozzle was chosen as 180 mm^2 which is about 2.4% larger than the axial flow nozzle, and resulted in an area ratio for the radial nozzle of 20.4, whereas the area ratio of the benchmark conical nozzle was 18.1, as indicated in Table 5-1.

Convergent and divergent angles and the nozzle area ratio (A/A^*) have a strong impact on the uniformity of the nozzle exit flow and its Mach number [44], [46]. To improve the uniformity of the flow at the nozzle exit, the divergent angle should be small, but to create the desired nozzle area ratio with low friction losses, a larger angle is required [78]. Therefore, a compromise in the selection of the divergent angle is required. The divergent angle of the radial nozzle was chosen as 5^o which is equal to the axial benchmark. The radial length of the divergent section of radial supersonic nozzle was therefore determined to be 9.5 mm, which is significantly less than the axial benchmark. Figure 5-4 illustrates the variation in cross sectional flow area for the radial and axial ejectors; the cross sectional area variation for the supersonic nozzle in each case follows a very similar profile, although the flow path length of the radial nozzle is much shorter than the axial nozzle.

The difference in supersonic nozzle length, in combination with the other characteristics of the radial nozzle, creates a very low contact area (the 'wetted surface') between the flow and nozzle body in the divergent section, relative to that in the axial supersonic nozzle, as illustrated in

Figure 5-5. The wetted area reported in Table 5-1 and illustrated in Figure 5-5 for both nozzles refers to the area downstream of the nozzle throat. For given flow conditions, a lower wetted area will decrease frictional losses between the flow and the nozzle surface.

Table 5-1: Fundamental dimensions and derived geometric parameters of the axial and radial ejectors

Axial ejector		Radial ejector	
dimensions	values	dimensions	values
d^* (mm)	3.2	R^* (mm)	3.5
L_{exit} (mm)	59.5	h^* (mm)	0.4
d_{exit} (mm)	13.6	R_{exit} (mm)	13
L_0 (mm)	59.5	h_{exit} (mm)	2.2
d_0 (mm)	37	Θ	9^o
L_{t1} (mm)	214.5	R_t (mm)	36
d_t (mm)	25.4	h_t (mm)	2.3
L_{t2} (mm)	289.5	R_d (mm)	72
L_d (mm)	499.5	Valve stem diameter (mm)	1.8
d_d (mm)	50	-	-
Nozzle throat area (mm^2)	8.04	Nozzle throat area (mm^2)	8.8
Nozzle exit area (mm^2)	145	Nozzle exit area (mm^2)	180
Nozzle area ratio	18.1	Nozzle area ratio	20.4
Divergent part length (mm)	59.5	Divergent part length (mm)	9.50
Divergent half angle (degree)	5	Divergent half angle (degree)	5
Nozzle wetted area (mm^2)	1590	Nozzle wetted area (mm^2)	990
Ejector throat area (mm^2)	507	Ejector throat area (mm^2)	520
Ejector Diffuser exit area (mm^2)	1960	Ejector Diffuser exit area (mm^2)	1040
Ejector area ratio	63	Ejector area ratio	59
Ejector flow length	500	Ejector flow length	68.5
Ejector wetted area (mm^2)	92500	Ejector wetted area (mm^2)	31800

5.2.3 Ejector Duct

In an axial ejector configuration, the secondary flow is propelled into an annular space between the ejector body and supersonic nozzle. The secondary stream moves to the mixing chamber and later passes through the diffuser section. Based on the type of mixing chamber (constant area or constant pressure), different mixing chamber profiles can be created [50]. The ejector area ratio, ejector convergent angle, diffuser half angle and lengths of the convergent part, constant area part and diffuser can be selected based on semi-empirical design procedures for axial flow ejectors. This was the approach adopted in the design of benchmark axial ejector [13]. The radial ejector area ratio and the radial ejector throat area were specified as 59 and 520 mm^2 respectively, values that are in close agreement with the corresponding values of 63 and 507 mm^2 respectively for the benchmark axial ejector. Figure 5-4 shows the variation of flow cross sectional area for the radial and axial ejectors, and Figure 5-5 shows variation of wetted area for the axial and radial ejectors.

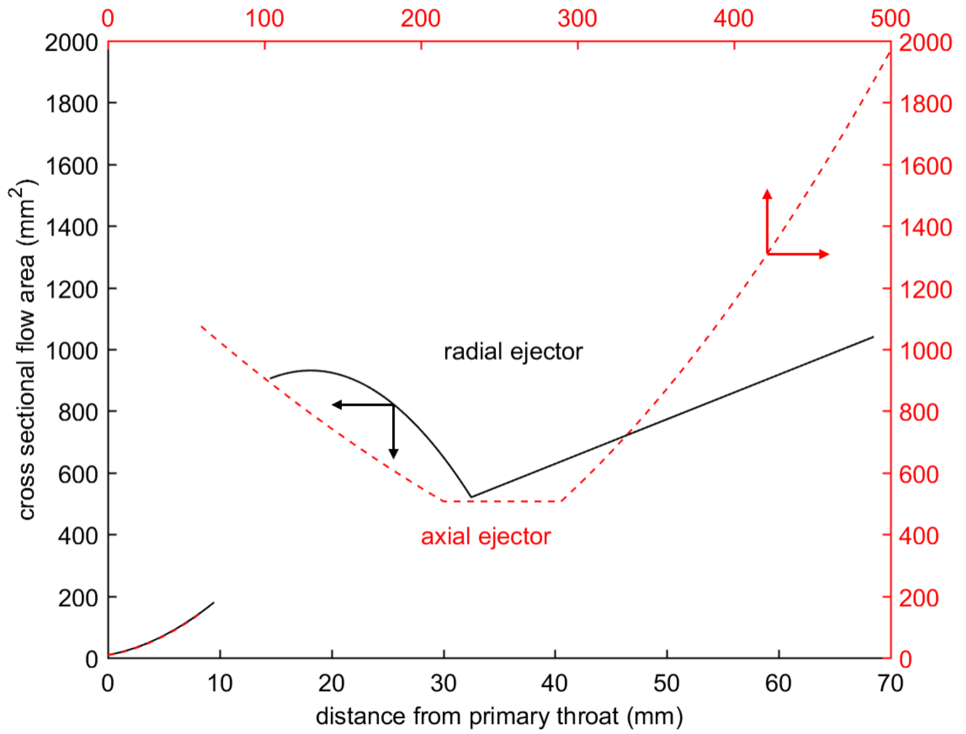

Figure 5-4: Variation of flow cross sectional area for the radial and axial ejectors.

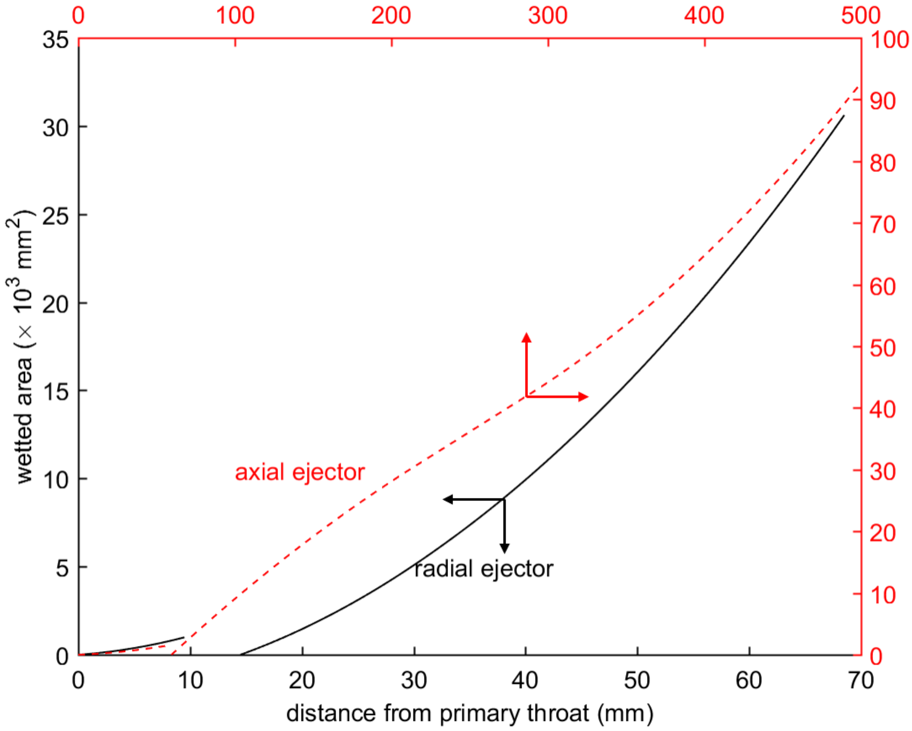

Figure 5-5: Variation of wetted area for the radial and axial ejectors.

The lengths of the mixing chamber, constant area section, and diffuser are suggested in the traditional (semi-empirical) procedures for axisymmetric ejectors based on the ejector throat diameter. For example, it is recommended to choose the length of mixing chamber between 5 and 10 times that of the throat diameter [48], [49], [50]. The benchmark ejector has a mixing chamber length of 9 times of the throat diameter. Other recommendations include: the convergent half angle of the ejector should be between 2^{o} and 10^{o}; the diffuser half angle should be in range of 3^{o} to 4^{o} and no more than 7^{o}; and the area ratio of the ejector outlet and ejector throat should not be more than 5 [50]. In the benchmark ejector, the convergent half angle, the divergent half angle and the ejector exit area ratio were specified as 10^{o}, 3.3^{o} and 4 respectively.

The radial ejector is inherently different from an axial ejector. Therefore, the traditional recommendations could not be adopted directly. For simplicity, the radial ejector diffuser for the present work consisted of two parrallel plates, and thus a length of constant area throat was not generated in the radial ejector, as illustrated in Figure 5-4. The distance between the two parallel plates was chosen to generate a throat area, at a single radial location, approximately the same as the throat area of the reference axisymmetric ejector. The length of mixing chamber was choosen as 10 times the distance between the parrallel plates. To create a convergent contour, a convergent half angle of 9^o was choosen based on the fabrication capability and geometrical arrangement of the secondary inlets and ejector ducts. This positioned the throat of the radial ejector at the a radial location half way between the centre of the radial ejector and its exit. A zero divergence angle was specified in the diffuser of the radial ejector because a higher amount leads to decrease in the diffuser length if the ejector exit area ratio is the design constraint.

5.3 Experiment Hardware

A radial air ejector prototype was constructed in order to investigate the concept's performance. Figure 5-6 shows supply, control and instrumentation on the radial ejector system.

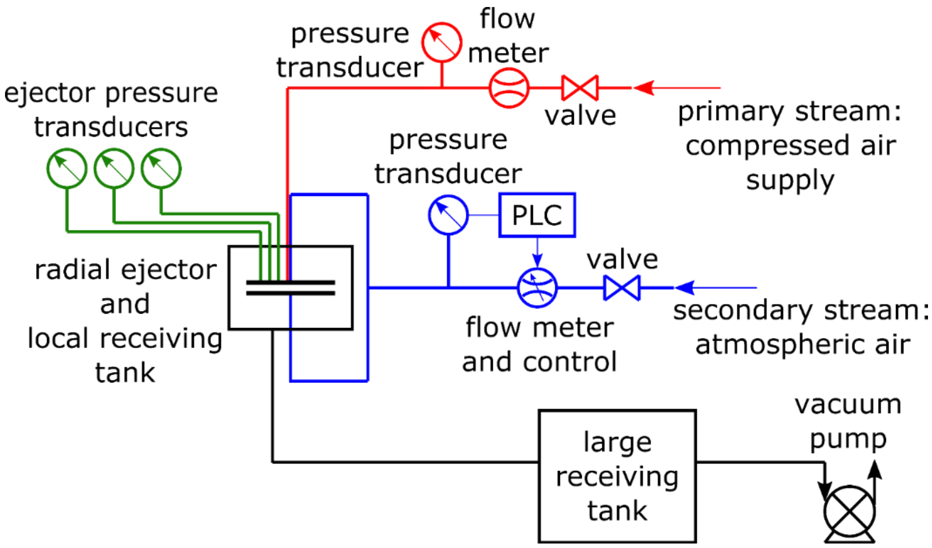

Figure 5-6: Illustration showing supply, control and instrumentation for the primary and secondary streams, and for the mixed stream.

Figure 5-7 depicts the radial air ejector as a sectioned 3D solid model. The compressed air from the motive supply inlet expands in the supersonic radial flow nozzle, induces the secondary flow and passes through the ejector diffuser formed by the duct's parallel surfaces.

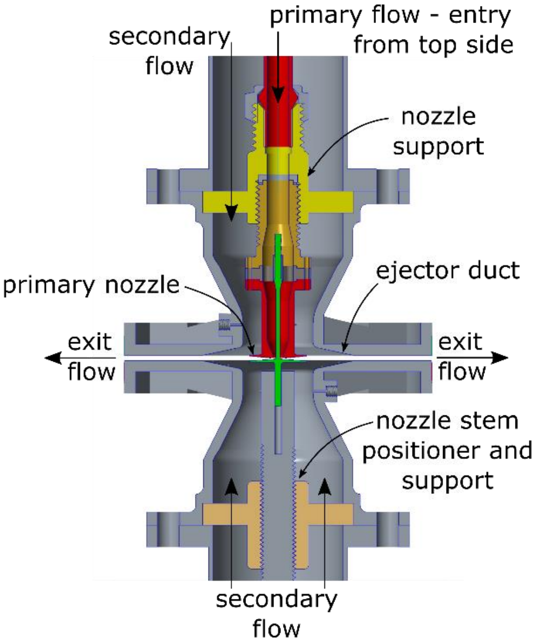

Figure 5-7: Illustration of a sectioned 3D model of the radial ejector developed for the experiments. The position of this part of the apparatus is shown in the dashed circle of Figure 5-8.

Figure 5-8 shows the hardware for delivery of the primary and secondary streams and for the receipt of the mixed stream. The air discharged from the ejector is collected by the local receiving tank and exhausted to a large volume vacuum chamber. Both secondary inlets are connected together and a mass flow controller (Omega FMA-2600A) was used to adjust the secondary air flow rate so that the set point for the pressure of the secondary flow was maintained while the pressure in the local receiving tank increased. Although the FMA-2600A has in-built control capability, it was more convenient to achieve control using an external PLC. The PLC was programmed to drive the Omega flow controller so as to vary the secondary mass flow in such a way that the prescribed secondary pressure was maintained constant as the ejector back pressure increased due to the finite volume of the receiving tank. Another ball valve and a pressure regulator controls the flow rate and pressure of the primary flow. Four pressure transducers (Wika model 10-A) were used in this apparatus, in high and low pressure ranges for the primary stream pressure, the secondary and exit stream pressures, respectively. The pressure transducers were calibrated using a dead weight tester [13]. Signals from all transducers were recorded using a National Instruments Compact Data Acquisition (cDAQ) system. Details of the interfaces via the NI-cDAQ drivers is available in [13]. The mass flow of the primary stream was calibrated separately as a function of the primary pressure with the aid of the mass flow meter (the Omega FMA-2600A device) that was installed in the primary line for this purpose. During the experiments, the one mass flow meter was installed on the secondary stream delivery line to enable direct measurement of the secondary stream flow rate only; the flow rate of the primary stream was deduced from the prior pressure-mass flow calibration.

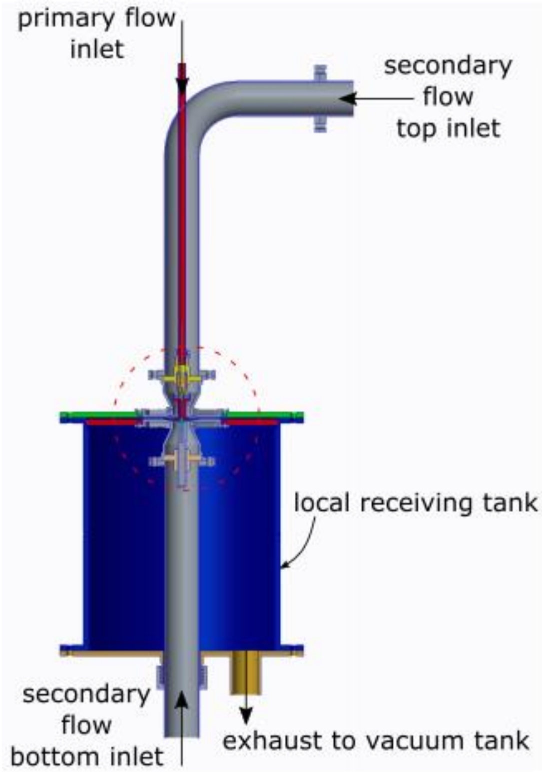

Figure 5-8: Illustration showing hardware for delivery of the primary and secondary streams, and for the receipt of the mixed stream. The dashed circle encloses the detail shown in Figure 5-7.

5.4 Quasi One-Dimensional Gas Dynamic Simulation

Quasi one-dimensional gas dynamic modelling has worked reasonably well for axial ejectors. In this work, a model previously calibrated using data for axial flow ejectors [79] was applied to the simulation of the radial ejector performance. In the model, the primary and secondary streams are assumed to enter a control volume at a matched pressure condition that is defined by the Mach number of the secondary stream. For fully choked operation of the ejector, the Mach number of the secondary stream entering the control volume is specified as unity. Heat transfer and frictional effects between the fluid and the ejector walls are neglected. Furthermore, discharge coefficients and isentropic coefficients that are commonly applied in other ejector models are not used to tune results to the observed ejector performance. Instead, ejector overall performance is defined from the model in terms of the entrainment ratio and the critical pressure lift ratio and these values are compared directly to values achieved by actual ejectors working with air, R141b, and steam, in order to calibrate the model.

The entrainment ratio of the ejector is defined in terms of the ratio of mass flow rates in the secondary and primary streams,

$$\omega = \frac{\dot{m}_2}{\dot{m}_1}$$

The model assumes that complete mixing between the primary and secondary streams is achieved and the critical pressure lift ratio $\frac{p_{crit}}{p_s}$ is then determined by assuming the flow is decelerated to rest by a single normal shock followed by isentropic compression. All relevant equations are reported in [79].

For axial flow ejectors in which the primary nozzle position has been tuned to maximize the entrainment ratio, the model typically underestimates the maximum achievable values of ω according to [79]. However, across the spectrum of ejector sizes, operating conditions and working fluids reported in [79], there is substantial variability in observed ejector entrainment ratios relative to the model. Therefore, to assess the radial ejector performance in the present work, reference entrainment ratio values are taken directly from the model without any calibration adjustment. In the case of the critical pressure, the model always over estimates performance by a substantial margin [79] and an adjustment to the values from the theoretical model according to

$$\frac{\Delta p_{crit}}{p_s} = -4.61 \times 10^{-3} \frac{p_p}{p_s} - 0.397$$

was sufficient to bring the model into agreement with the experimental data from the axial flow ejectors with a representative uncertainty of around $\pm 20\%$.

5.5 Results and Discussion

The primary nozzle performance was evaluated for primary pressures of 160, 200 and 250 kPa. Table 5-2 shows the primary nozzle performance results from the mass flow rate measurements in the experiments. Theoretical mass flow rates through the primary nozzle for the 3 primary nozzle working pressures are also reported in Table 5-2 based on the ideal gas, isentropic flow relationship

$$\dot{m}_{p,theory} = \sqrt{\frac{\gamma}{R}\left(\frac{2}{\gamma+1}\right)^{(\gamma+1)/(\gamma-1)}}\,\frac{p_p}{\sqrt{T_p}}A^*$$

and for the application of this equation, values for air are taken as $\gamma = 1.4$ and $R = 287$ J/kgK, and the nozzle throat was $A^* = 8.8$ mm^2, corresponding to a cylindrical throat area with a radius of 3.5 mm and a height of 0.4 mm. In each case, the primary pressures p_p were taken as the stagnation values as reported in Table 5-2 and the temperature T_p was taken as 27 °C, also corresponding to the ambient condition during the experiments.

Table 5-2: Primary nozzle mass flow characteristics

p_p (kPa)	$\dot{m}_{p,experiment}$ (g/s)	$\dot{m}_{p,theory}$ (g/s)
160	3.84	3.286
200	4.78	4.107
250	5.97	5.134

As it can be seen from Table 5-2, the actual mass flow rate of the primary nozzle is about 16.5% larger than the theoretical estimates, implying a discharge coefficient larger than unity. Assembly of the prototype radial flow ejector posed a number of challenges and the uncertainty in achieving the target dimension of $h^* = 0.4$ mm separation on the primary nozzle throat was estimated to be around ±30%. Therefore it seems likely that the actual separation of the primary nozzle disks during the experiments was at least 16.5% larger than the design value, giving a best estimate for the throat dimension of $h^* = 0.47$ mm.

The prototype radial ejector performance was evaluated in terms of entrainment ratio and the critical pressure lift ratio achieved relative to the results from the quasi one-dimensional gas dynamic model. Measurements were performed for a primary pressure of $p_p = 200$ kPa, secondary pressures p_s of 1.8, 2.5 and 3.2 kPa, and a variety of diffuser exit pressures p_d in each case. Illustrative results are presented in Figure 5-9 showing that the radial ejector has performance characteristics similar to axisymmetric ejectors in that a critical diffuser exit pressure p_{crit} (denoted with the open symbol) can be defined in for each operating condition. For diffuser exit pressures lower than p_{crit}, the ejector operates in a choked mode with the entrainment ratio maintaining its maximum value ω_{max}, largely independent of the diffuser exit pressure. For diffuser exit pressures higher than p_{crit}, the entrainment ratio decreases with increasing diffuser exit pressure. For the three operating conditions illustrated in Figure 5-9, the performance curves are slightly rounded in the vicinity of p_{crit} so the critical point in each case has been defined by the intersection of the two straight lines that have been fitted to the data. Values of p_{crit} obtained in this manner are presented in Table 5-3 along with the other relevant ejector operating parameters.

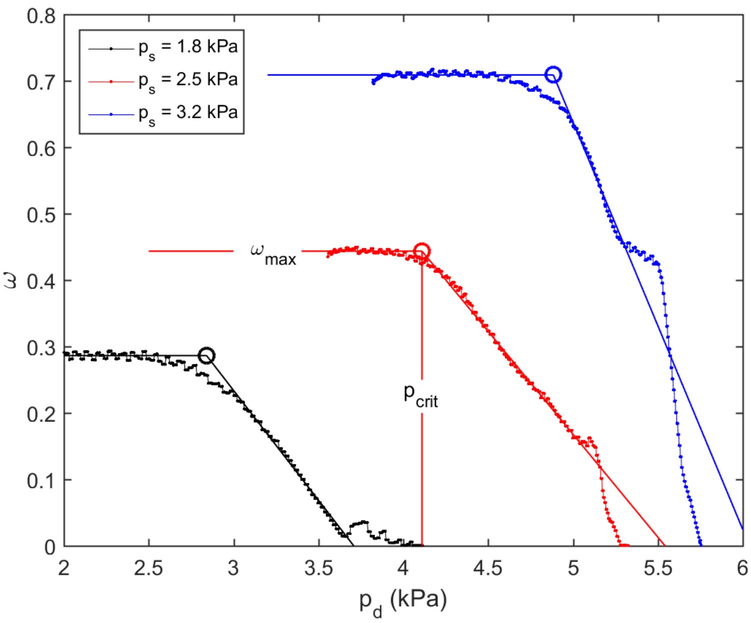

Figure 5-9: Experimental data showing the variation of entrainment ratio with ejector exit pressure for a primary pressure of 200 kPa and secondary pressures of 1.8, 2.5, and 3.2 kPa

Table 5-3: Experimental results from the radial ejector

p_p (kPa)	p_s (kPa)	p_{crit} (kPa)	$\frac{p_p}{p_s}$	$\frac{p_{crit}}{p_s}$	ω_{max}
160	1.8	2.72	88.9	1.51	0.37
200	1.8	2.84	111.1	1.58	0.286
250	1.8	2.87	138.9	1.59	0.24
160	2.5	3.75	64.0	1.50	0.61
200	2.5	4.11	80.0	1.64	0.444
250	2.5	3.90	100.0	1.56	0.33
160	3.2	4.55	50.0	1.42	0.95
200	3.2	4.88	62.5	1.53	0.709
250	3.2	5.49	78.1	1.72	0.55

The variation of the radial ejector entrainment ratio with the expansion ratio p_p/p_s from the experiments and the quasi one-dimensional gas dynamic model is illustrated in Figure 5-10. The error bars presented with the data in Figure 5-10 are representative of the uncertainties associated with the measurement of the primary and secondary pressures, and the measurement of primary and secondary mass flow rates. The estimated uncertainty in the entrainment ratio ω and $\frac{p_p}{p_s}$ are ±3% and ±2% respectively. For the gas dynamic model simulations, the primary nozzle throat size was specified as $h^* = 0.47$ mm, the value deduced from mass flow rate calibrations of the primary nozzle. Estimated uncertainties in the ejector throat size give $h_t = 2.3 \pm 0.6$ mm or a relative uncertainty in the throat height or area of about ±26%. The trend and the magnitude of the entrainment ratio data for the radial ejector agrees well with the simulations from the gas dynamic model. The discrepancy between the simulation entrainment ratio and the experiments is less than 10%, which is a relatively small margin within the context of the observed variability in the axial flow ejector data [80], and the uncertainty in the ejector throat dimension.

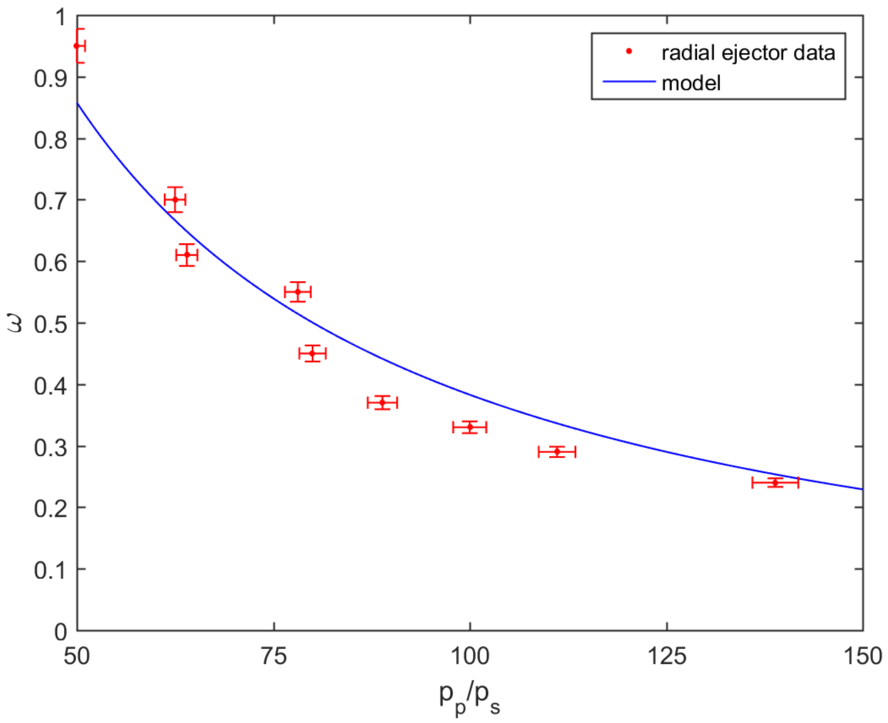

Figure 5-10: Variation of radial ejector entrainment ratio with the expansion ratio – comparison of experimental data and gas dynamic model.

The critical pressure ratio data for the radial ejector are compared to the results from the calibrated gas dynamic model in Figure 5-11. The error bars presented in Figure 5-11 represent the uncertainties associated with measuring primary, secondary and exit pressures. The critical pressures achieved in the prototype radial ejector are significantly lower than the simulations from the calibrated model, even when the uncertainties in the model results due to the uncertainties in the ejector area ratio of around $\pm 26\%$ are taken into account, as shown in Figure 5-11. The critical pressure lift ratio data p_{crit}/p_s presented in Figure 5-11 show very little variation with the expansion ratio p_p/p_s, whereas the calibrated model demonstrates significant sensitivity to the expansion ratio. There appears to be some additional loss process operating in the case of the prototype radial ejector that is not accommodated by the calibrated axial flow ejector model.

As illustrated in Figure 5-4, the radial ejector prototype has a very short flow path length, relative to the reference axial flow ejector. The effect of the ejector length was investigated by [80] using numerical simulations and departures from the optimum length caused a significant decrease in the critical back pressure achieved by the ejector, although the entrainment ratio was largely unaffected. Sufficient opportunity for mixing between primary and secondary streams is needed for the primary stream to impart momentum to the secondary stream prior to deceleration in the diffuser, otherwise, recovery of the dynamic pressure in the diffuser is compromised. Although the radial ejector flow path length is relatively short, it was anticipated that the radial ejector design did provide sufficient opportunity for mixing, based on estimates of the contact area between the primary and secondary streams. In the case of the benchmark axial flow ejector, the contact area between the primary and secondary streams was estimated as 6630 mm^2, based on the surface area of a cylinder equal in diameter to the primary nozzle exit having a length from the primary nozzle exit to the start of the ejector throat. In the case of the radial ejector, the contact area was slightly larger, estimated as 7080 mm^2, based on the area of two disks from the primary nozzle exit to the ejector throat. A more precise assessment of mixing efficiency in the radial flow ejector is necessary.

The other major contributor to the pressure lift performance in the ejector is the rate of pressure rise in the diffuser. For axial flow ejectors, small diffuser half-angles are recommended to minimize the adverse pressure gradient which tends to separate the diffuser boundary layers. For a given momentum flux in subsonic flow, the value of $\frac{1}{A}\frac{dA}{dx}$ is indicative of the magnitude of the pressure gradient. In the case of the benchmark axial flow ejector, at the start of the diffuser $\frac{1}{A}\frac{dA}{dx} = 9.27$ m^{-1} whereas the corresponding value at the start of the diffuser in the radial flow ejector is 27.8 m^{-1}. Thus the adverse pressure gradient in the present radial flow diffuser may exceed reasonable limits for optimal pressure recovery. The diffuser in the present radial flow ejector currently consists of two parallel disks, so to reduce the adverse pressure gradient in future, it will be necessary to have a profile in which the separation of the disks reduces with increasing radius.

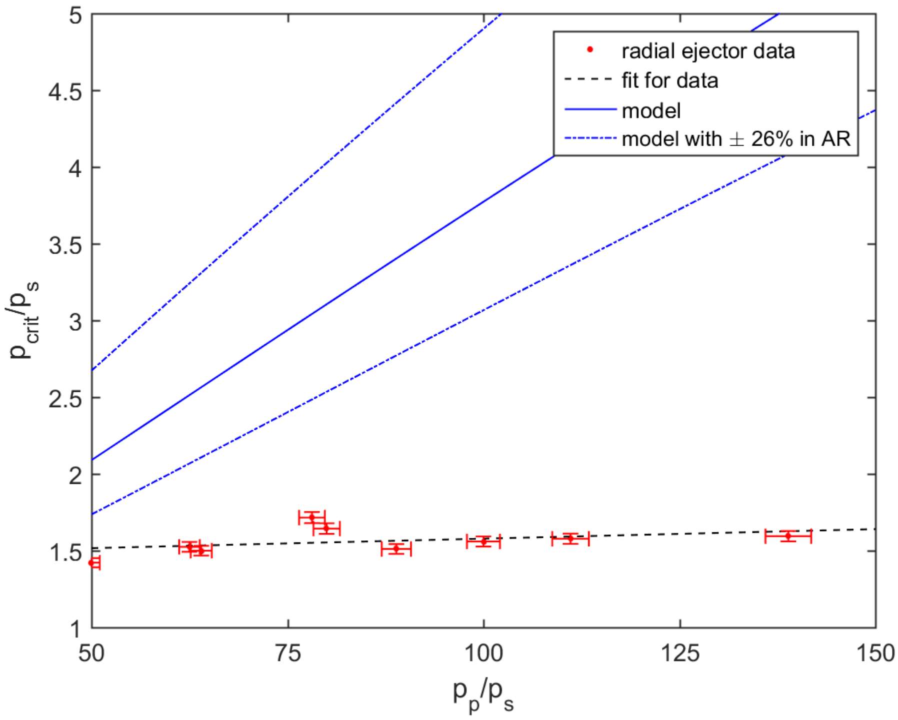

Figure 5-11: Variation of radial ejector critical back pressure with the expansion ratio – comparison of experimental data and gas dynamic model.

5.6 Conclusion

In this study, a new radial ejector was designed and experiments were conducted to investigate the performance of the prototype. Measurements were performed for primary pressures of 160, 200, and 250 kPa and secondary pressures of 1.8, 2.5 and 3.2 kPa. Values of entrainment ratio and critical pressure lift ratio achieved in the radial ejector prototype were compared to expected values for a conventional, axial flow ejector with the same area ratios derived from a calibration quasi one-dimensional model. The entrainment ratio values achieved in the radial ejector were in good agreement with the model. However, the critical pressure lift ratios achieved in the radial ejector were lower than would be expected for an axial flow ejector having the same area ratios as the radial ejector. Candidate explanations for the short-fall in critical pressure lift performance of the radial ejector include possible departure of the ejector duct separation from the nominal design value, the relatively short flow path of the radial ejector, and the relatively high adverse pressure gradient in the radial flow diffuser. Further analysis is required for definitive explanations. Nevertheless, the concept has demonstrated sufficient potential to warrant further attention.

Chapter 6

Experimental Investigation of Radial Ejector Performance

A prototype radial flow ejector has been designed and constructed to operate with air and experiments have been conducted at three different primary pressures of 160, 200 and 250 kPa and three secondary pressures of 1.8, 2.5 and 3.2 kPa. A range of exit pressures were applied to the ejector, and ejector performance and local ejector wall pressures were measured. The maximum entrainment ratio achieved was 0.98 for an expansion ratio of 50 at primary pressures of 160 kPa and secondary pressure of 3.2 kPa, and the pressure lift ratio of 1.42 was achieved at this condition. Trends observed in the measurements of entrainment ratio for the radial ejector configuration are generally consistent with those for axial flow ejectors: for a constant secondary pressure, increasing the primary pressure leads to a decrease in the entrainment ratio and an increase in the lift ratio, and for a constant primary pressure, increasing the secondary pressure leads to an increase in both the entrainment ratio and critical exit pressure but the pressure lift ratio decreases. Similarly, trends observed in the measurements of wall pressure for the radial ejector configuration are generally consistent with those for axial flow ejectors. The distribution of static pressure in the mixing region (upstream of the ejector throat) is largely unaffected by changes in the ejector exit pressures in the critical mode of ejector operation. Secondary stream Mach numbers of around 0.7 in the ejector throat are deduced from an isentropic flow calculation for the ejector operating in the critical mode. For ejector operation in the subcritical mode, wall pressures in the throat and at locations upstream of the throat increase, leading to a peak in pressure prior to the final pressure increase in the diffuser.

6.1 Introduction

In some ejector applications, variability in the primary flow operating conditions and the required ejector exit pressure make it difficult for a fixed geometry ejector to successfully operate. One such example occurs with solar-assisted heat pumping that operates with reduced effectiveness at off-design conditions as the solar input changes and/or the ambient temperature changes [40]. Changes in ejector performance arising from variation in working conditions and the advantages of adjustability in the geometry for another ejector-based system were discussed by [39]. In the work of [16], by changing the nozzle throat size or by using different nozzle area ratios, the possibility of successfully operating at different boiler or condenser temperature was demonstrated. Although different approaches to performance and efficiency improvement have been employed in the literature [15], the need for a mechanically-convenient solution for adjustment of the ejector throat size that is achieved without compromising ejector performance is evident.

A movable cone attached to a cylinder positioned downstream of the primary nozzle was used by [35] to adjust the size of the ejector throat and the primary nozzle throat. The cone-cylinder arrangement was inserted into the ejector from the downstream end and longitudinal adjustment to its position was also achieved from the downstream end of the ejector. This method demonstrates a mechanically-convenient approach for changing the ejector and nozzle throat sizes, however the cone-cylinder shape was positioned in the centre of the primary nozzle which therefore blocked the passage of the high speed flow into the ejector throat. The losses associated with the deflection and blockage of the primary flow by the cone-cylinder were not reported in the work [35]. Ejector nozzles with pintle adjustment from upstream of the primary nozzle throat have been investigated by other researchers [17], [8] and [36] and this configuration avoids the high speed flow deflection and blockage that occurs with the arrangement of [35]. However, pintle adjustment from upsteam of the primary nozzle cannot alter the ejector thoat size and hence such adjustable ejectors cannot meet the target of a fully-variable geometry ejector.

It may be possible to relax the requirements for variability in ejector throat size for ejectors if on-design ejector performance could be enhanced to the extent that off-design performance is still satisfactory. Establishing oscillations in primary pressure may achieve increases in ejector performance under some working conditions [18], [19]. An ejector concept drawing on flow pulsation methods is that of the radial ejector with rotating components which was suggested by [67], [81], [74]. Application of rotary nozzles or other ejector components has also been studied in the literature [66], [64]. However, the majority of rotary concepts have not progressed beyond the prototype stage due to mechanical failures and limitations associated with experimental validation [64], [68].

In the radial ejector configuration both nozzle and ejector throat areas can be conveniently adjusted. The proposed radial ejector configuration [76] has some similarities with an earlier radial arrangement [69]; the principle point of differentiation between the arrangements is the location at which the primary flow which enters the duct. In the case of the earlier arrangement, the primary flow enters adjacent to one of the duct surfaces, but in the new configuration, the primary flow enters the duct aligned with the central plane.

Computational simulations suggest that new radial ejector concept is viable and should be capable of achieving similar performance to that of axial ejectors [76]. Further CFD analysis by [82] demonstrated that an increase in the ejector throat size achieved by increasing the separation between the ejector plates should induce an increase in the entrainment ratio during operation. A successful prototype of the new radial ejector concept has been experimentally investigated and compared with a quasi one-dimensional model in Chapter 5. The results demonstrated that the radial ejector entrainment ratio was within 10% of the model with a standard deviation of about 11%, but the critical back pressure was significantly lower than simulated by the model. It was speculated that part of under-performance of the radial ejector is related to the shape of the radial ejector with relatively high adverse pressure gradients in the diffuser of the ejector.

To provide further insight into the flow within the prototype radial ejector, this following work analyses static wall pressure measurement at different primary, secondary and exit conditions.

6.2 Methodology

The radial ejector evaluated in this work is illustrated in Figure 6-1 and it consists of two shaped discs forming the ejector duct, and two shaped discs forming the primary nozzle. Both the primary flow and secondary flow have a predominantly radial flow pattern; the flow enters the components from near the axis of the ejector and then spreads radially, ultimately being collected in a large pipe enclosing the ejector assembly. The primary flow passing out of the nozzle induces the secondary flow from both sides of the ejector duct. Static pressures were measured on the upper side of the duct along different radial lines and at the radial locations shown in Figure 6-1. The arrangement illustrated allowed for more closely spaced wall pressure measurements than could be achieved if the pressure tappings were placed in one radial line. The symmetry of the radial ejector suggets that the pressure at a specified radial distances should be independent of the angular postion at which it is measured.

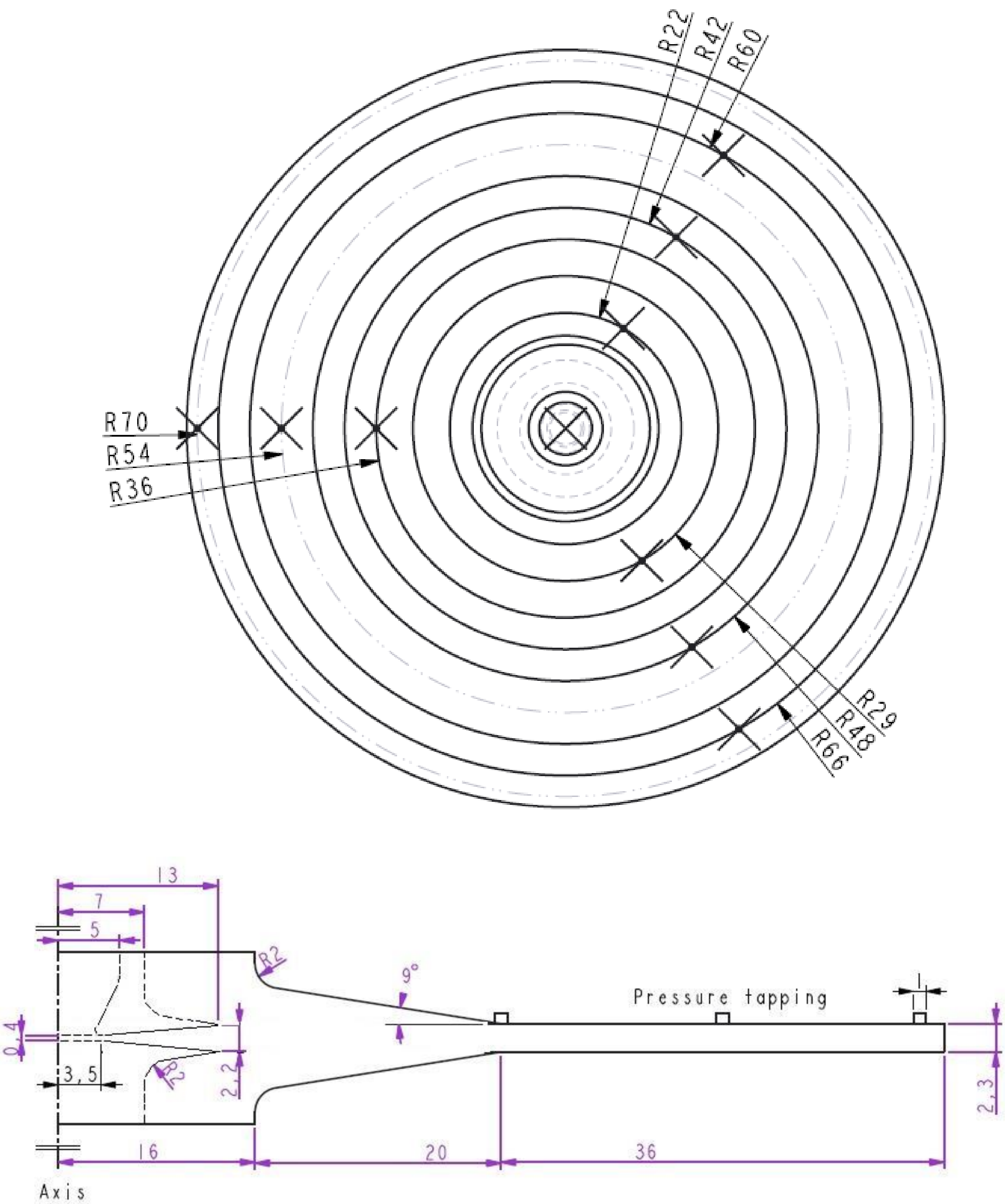

Figure 6-1: Sketch showing dimensions and pressure measurement locations on the radial ejector.

The experimental arrangement details are presented in Chapter 5. Eleven Wika 10-A transducers were used to measure wall pressure on the ejector duct at the locations shown in Figure 6-1 and each of these transducers was connected to the duct via flexible tubing with an inner diameter of 1.0 mm. Three other similar transducers were used in the secondary stream piping system, and another Wika transducer, but with a higher pressure range, was employed to measure the primary pressure. Details of the pressure transducers and their calibration method has been reported by [13].

The operating pressures used in the experiments were: primary pressures of 160, 200 and 250 kPa, secondary pressures of 1.8, 2.5 and 3.2 kPa and a range of exit pressures between 1.8 and almost 7 kPa. The temperature of the air used in the experiments was approximately 20 ºC, reflecting the fact that the compressed air in the primary reservoir had been stagnant for a sufficient period to cool to the ambient temperature, and that the secondary air flow was drawn from laboratory air at the ambient temperature.

Based on the manufacturer's data, the accuracy of the low and high-pressure range transducers is 0.5%. Considering the calibration of the transducers, the noise of the electrical and data acquisition systems and the repeatability of the measurements, the uncertainty of the primary, secondary and exit pressure is estimated to be ±1.5%. For measuring the secondary mass flow, the mass flow meter has an accuracy of 0.5%. Considering the calibration, repeatability and system noise, the uncertainty of the mass flow measurements is estimated to be ±2.5% for the primary stream, and ±1.5% for the secondary stream. As the entrainment ratio is calculated from the ratio of secondary and primary mass flow rates, the uncertainty in the entrainment ratio is estimated to be ±4%.

An illustrative performance curve showing the variation of the radial ejector entrainment ratio with back pressure is presented in Figure 6-2 for a primary pressures of 200 kPa and a secondary pressure of 1.8 kPa. The radial ejector has similar characteristics to conventional axial flow path ejectors in that the radial flow ejector operates in a choked mode with the entrainment ratio close to the maximum entrainment ratio ω_{max} for diffuser exit pressures lower than some critical value, p_{crit}. If the diffuser exit pressure is increased beyond p_{crit} a decrease in the entrainment ratio results. A critical diffuser exit pressure p_{crit} was identified from the experimental data for each operating condition by first fitting a straight line to entrainment ratio results at diffuser exit pressures substantially higher than p_{crit}. This fitted line representing the decline of entrainment ratio for pressures in excess of p_{crit} was then extrapolated back to a horizontal line representing the value of ω_{max} as illustrated in Figure 6-2. The intersection of these two lines is interpreted as specifying the critical pressure p_{crit} for each operating condition. The ejector performance actually declines gradually as the exit pressure approaches p_{crit}: in practice a sudden decline in the entrainment ratio is not initiated precisely at this pressure. Nevertheless, defining the critical pressure in this manner provides a consistent basis for assessment of the radial ejector performance and for comparison with other ejectors.

The ejector characteristic curve is modelled in the bilinear form with the intersection at p_{crit} being defined as the critical point can be divided into critical, subcritical and malfunction modes as has been done elsewhere [9], [10]. If the diffuser exit pressure is less than critical pressure, in the bilinear model the entrainment ratio ω_{max} remains constant and increasing exit pressure does not have any effect on the entrainment ratio. As the exit pressure increases beyond the critical pressure, according to the bilinear model the entrainment ratio decreases linearly with increasing exit pressure and reaches zero at a pressure defined as the malfunction pressure p_{mal}. Any increase beyond the malfunction pressure causes back flow into the secondary inlet resulting in no useful function from the ejector. Modest departures from the bilinear model for ejector operation are observed in Figure 6-2 for the prototype radial flow ejector considered in the present work, in the vicinity of p_{crit} and p_{mal}: there is actually a gradual transition between the critical and subcritical modes, and some entrainment does occur for pressures higher than p_{mal}.

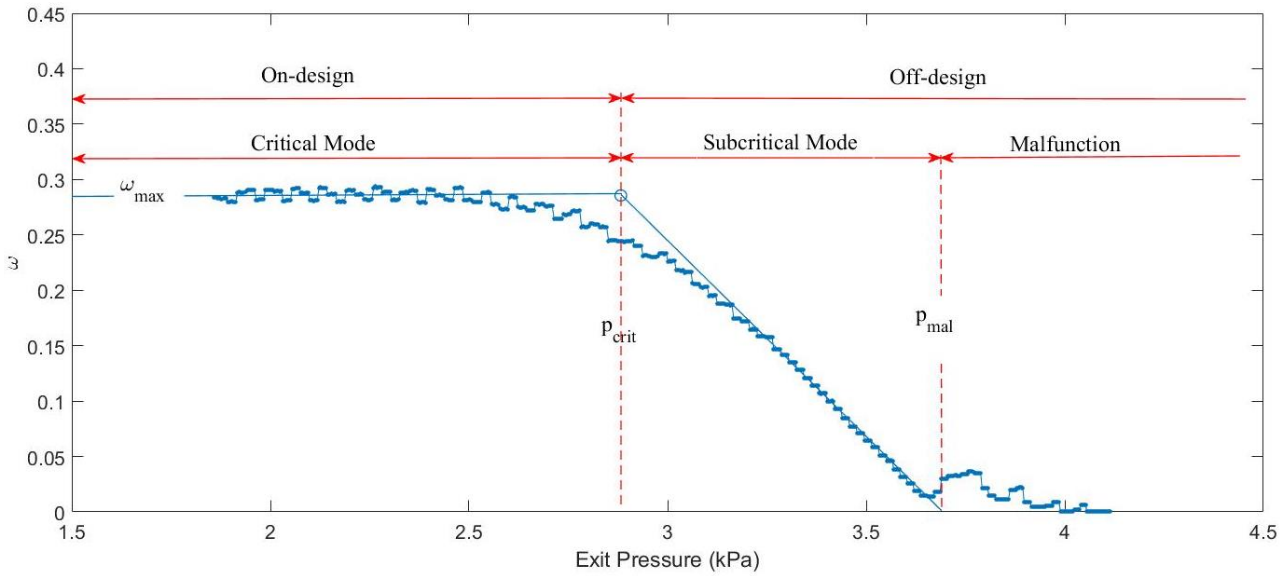

Figure 6-2: Entrainment ratio variation with exit pressure for primary pressure 200 kPa and secondary pressures of 1.8 kPa

6.3 Results and Discussion

To evaluate the prototype radial ejector performance, mass flow rates were measured for primary pressures of 160, 200 and 250 kPa, secondary pressures of 1.8, 2.5 and 3.2 kPa, and different exit pressures. Table 6-1 presents a summary of results obtained from the experiments.

Table 6-1: Experimental values of mass flow rates, entrainment ratio and critical back pressure.

Primary pressure (kPa)	Secondary pressure (kPa)	Expansion ratio	Primary mass flow rate (g/s)	Secondary mass flow rate (g/s)	Entrainment ratio	Critical exit pressure (kPa)
160±2.40	1.8±0.027	88.9±2.67	3.88±0.097	1.4356±0.022	0.37±0.015	2.72±0.041
160±2.40	2.5±0.037	64.0±1.92	3.87±0.097	2.3607±0.035	0.61±0.024	3.75±0.056
160±2.40	3.2±0.048	50.0±1.50	3.83±0.096	3.6385±0.055	0.95±0.038	4.55±0.068
200±3.00	1.8±0.027	111.1±3.33	4.78±0.120	1.3862±0.021	0.29±0.012	2.84±0.043
200±3.00	2.5±0.037	80.0±2.40	4.82±0.121	2.169±0.033	0.45±0.018	4.11±0.062
200±3.00	3.2±0.048	62.5±1.87	4.75±0.119	3.325±0.050	0.70±0.028	4.88±0.073
250±3.75	1.8±0.027	138.9±4.17	5.97±0.149	1.4328±0.021	0.24±0.010	2.87±0.043
250±3.75	2.5±0.037	100.0±3.00	5.99±0.150	1.9767±0.030	0.33±0.013	3.90±0.059
250±3.75	3.2±0.048	78.1±2.34	6.02±0.151	3.311±0.050	0.55±0.022	5.49±0.082

Figure 6-3 presents the prototype radial ejector characteristic curves for all of the operating conditions and shows that these curves for the radial ejector have similar trends to axial ejectors that can be observed in many recent works: at a fixed secondary pressure, increasing in the primary pressure reduces the maximum entrainment ratio but increases the critical back pressure. The subcritical mode of the radial ejector has a slightly different trend in some working conditions compared to typical axial ejector performance curves presented in the literature in that the rate at which the entrainment ratio decreases with increasing exit pressure is not particularly constant in the case of the radial ejector. An audible change in noise generated within the ejector was found to accompany the changes in the slope of the entrainment ratio curve in the subcritical region, suggesting that the features may be related to some form of oscillatory flow behaviour.

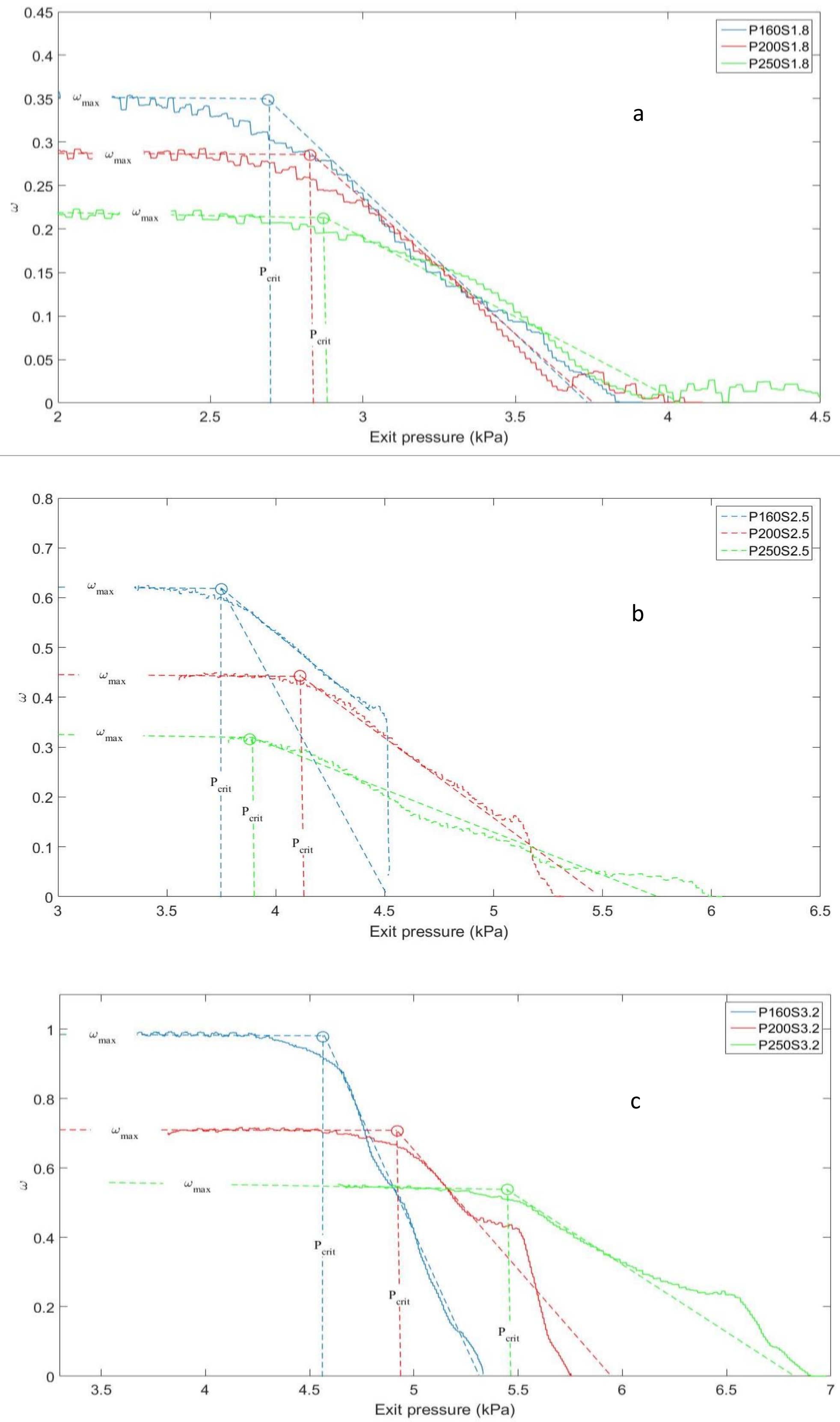

Figure 6-3: Entrainment ratio versus exit pressure at primary pressures 160, 200 and 250 kPa and constant secondary pressure of: (a) 1.8 kPa; (b) 2.5 kPa; and (c) 3.2 kPa.

Figure 6-4 presents the relationship between entrainment ratio and critical exit pressures obtained from the radial ejector characteristic curves. The fitted line for each secondary pressure is shown in this figure in the dashed form. The ejector only works under this fitted line for each secondary pressure [83]. For fixed values of secondary pressure, increasing the primary pressure caused a decrease in entrainment ratio and an increase in critical exit pressure in all cases except for the secondary pressure of 2.5 kPa when increasing the primary pressure from 200 kPa to 250 kPa. It can be seen that by increasing the secondary pressure, higher entrainment ratio and critical back pressure are achieved. This figure clearly shows that the radial ejector performance is significantly influenced by operating conditions.

The dashed contour map shown in Figure 6-4 represents corresponding data calculated from quasi one-dimensional model presented in Chapter 5, and based on the experimentally measured values for the primary mass flow rate. Comparing the experimental map contour and the map contour from the quasi one-dimensional model shows that the radial ejector is significantly underperforming in terms of critical back pressure. By increasing primary pressure from 200 to 250 kPa, it is expected that the critical back pressure significantly increases but at secondary pressures of 1.8 and 2.5 kPa, this simulated increase did not occur in the experiments.

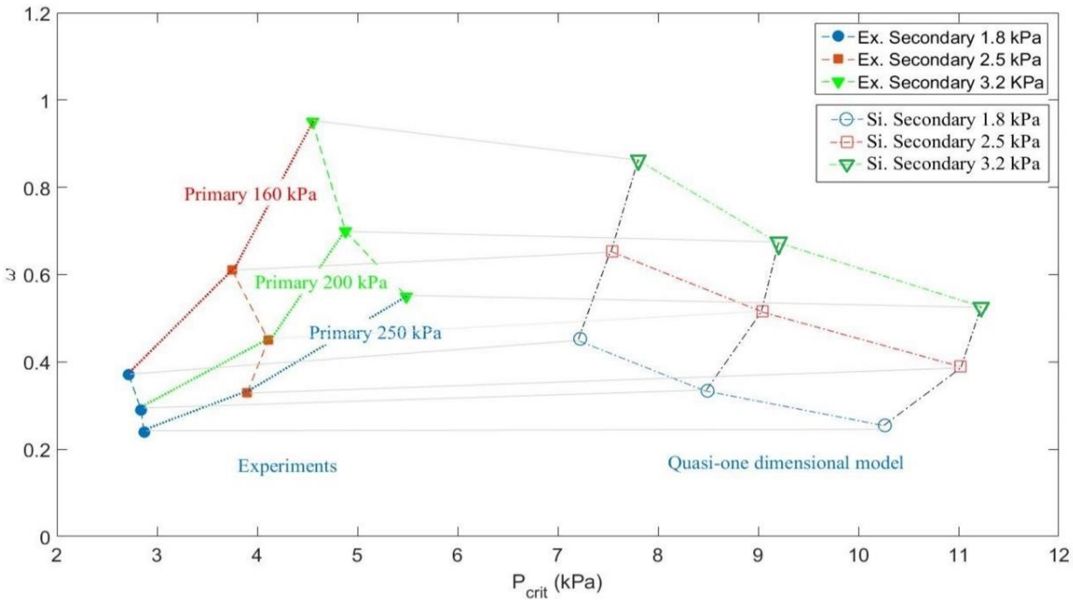

Figure 6-4: Entrainment ratio versus critical back pressure over the range of conditions tested.

Figure 6-5 to Figure 6-7 show the wall pressure results from the experiments at the different working conditions. Static pressure results for exit pressure values above p_{crit} (corresponding to the subcritical mode) are shown in dashed lines, and for exit pressure values below p_{crit} (corresponding to the critical mode) results are shown in the solid lines. The location of the physical throat of the ejector is also shown in all figures, and the choked secondary stream static pressure for each case is indicated by a horizontal line. The choked secondary stream static pressure was determinded from the secondary stream stagnation pressure (either 1.8 kPa, 2.5 kPa, or 3.2 kPa) and the isentropic equation

$$\frac{p_0}{p} = \left(1 + \frac{\gamma - 1}{2} M^2\right)^{\frac{\gamma}{\gamma - 1}}$$

with $M = 1$, and the ratio of specific heats $\gamma = 1.4$.

The measurements at the physical throat show that the wall pressure for the secondary pressure of 1.8 kPa is between 1.25 and 1.30 kPa for the different primary pressures, when the ejector is operating in the critical mode. For the secondary pressure of 2.5 kPa, corresponding throat pressure data for choked ejector operation show the wall pressure is between 1.75 and 1.87 kPa, and for the secondary pressure of 3.2 kPa, the throat wall pressure is between 2.25 and 2.30 kPa for different primary pressures. Using the isentropic pressure relationship for the secondary flow, the secondary stream Mach number at the physical throat of the ejector operating in the critical mode is estimated to be 0.70 to 0.74 for the secondary pressure of 1.8 kPa, and 0.66 to 0.73 for secondary pressure of 2.5 kPa, and 0.70 to 0.73 for secondary pressure of 3.2 kPa. Thus, for critical ejector operating conditions, the Mach number of the secondary stream at the throat, assuming isentropic acceleration, is approximately 0.7. Therefore, the secondary stream is not choked through an isentropic acceleration process at the physical throat of the ejector in any case.

Figure 6-5 to Figure 6-7 demonstrate that for radial ejector operation in the critical mode with exit pressures substantially lower than p_{crit}, the lowest wall pressures occur at locations between

50 and 60 mm from the axis of the ejector. By increasing the ejector exit pressure, the ejector operating mode transitions from critical to sub-critical and the location of the minimum wall pressure within the radial ejector moves upstream. The further increase in exit pressure within the sub-critical operating mode leads to the development of an initial pressure rise at the ejector throat which then occurs further upstream in the mixing chamber as the malfunction pressure is approached. The location of the compression process inside axial ejectors varies with the exit pressure and secondary pressure: higher exit pressures cause the location of the compression process inside the ejector to move upstream while higher secondary pressure moves the position of the compression process downstream [74], [75]. Such trends are also apparent in the radial ejector results presented in Figure 6-5 to Figure 6-7. Prior to testing the radial ejector, it was anticipated that the minimum wall pressure of the radial ejector operating in the critical mode would be located somewhere in the mixing chamber or around the physical throat, however, the measurements indicate the minimum wall pressure in the critical mode occurs well downstream of the throat.

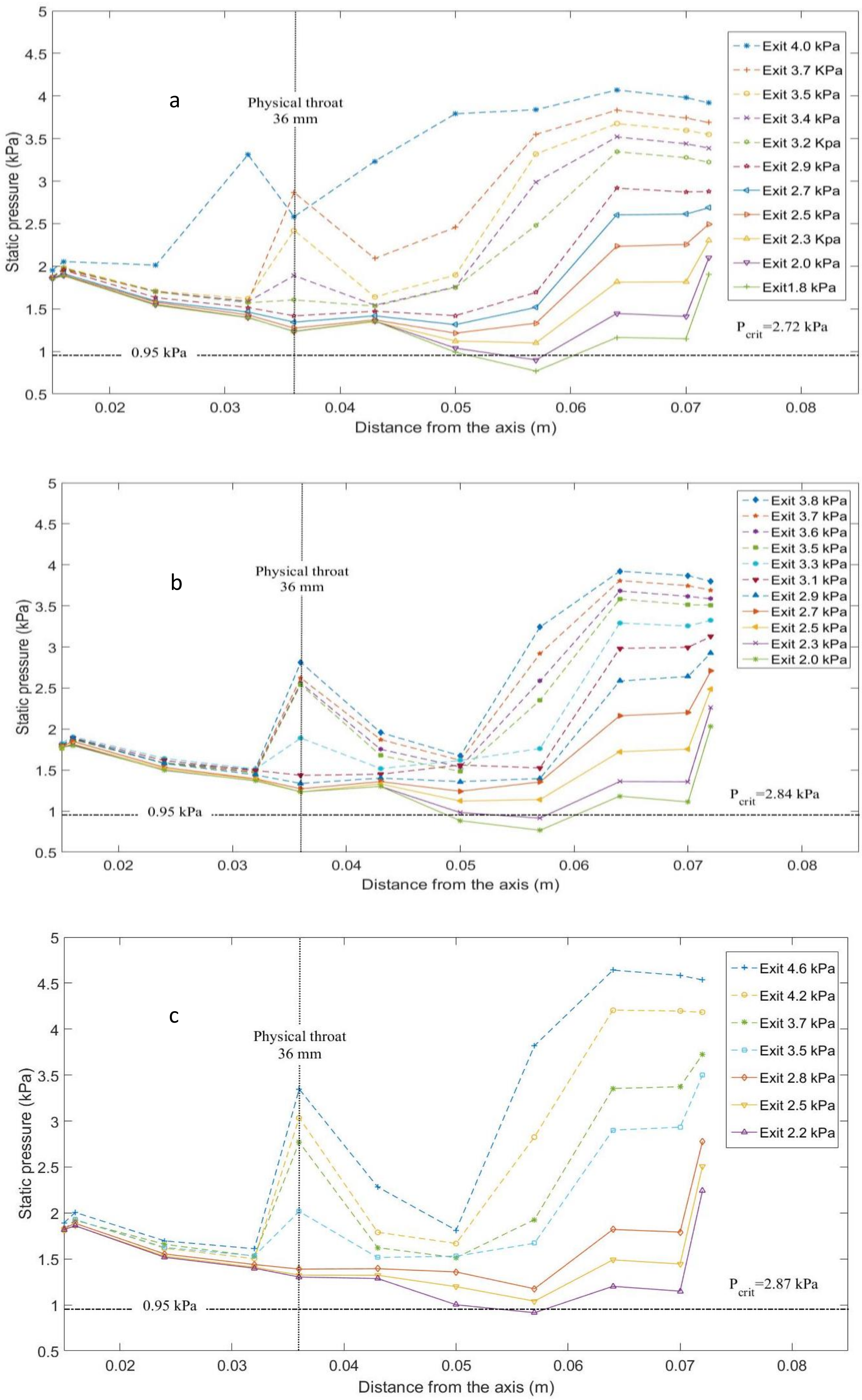

Figure 6-5: Static wall pressure along the radial ejector for secondary pressure of 1.8 kPa and various exit pressures and: (a) primary pressure of 160 kPa; (b) primary pressure of 200 kPa; and (c) primary pressure of 250 kPa.

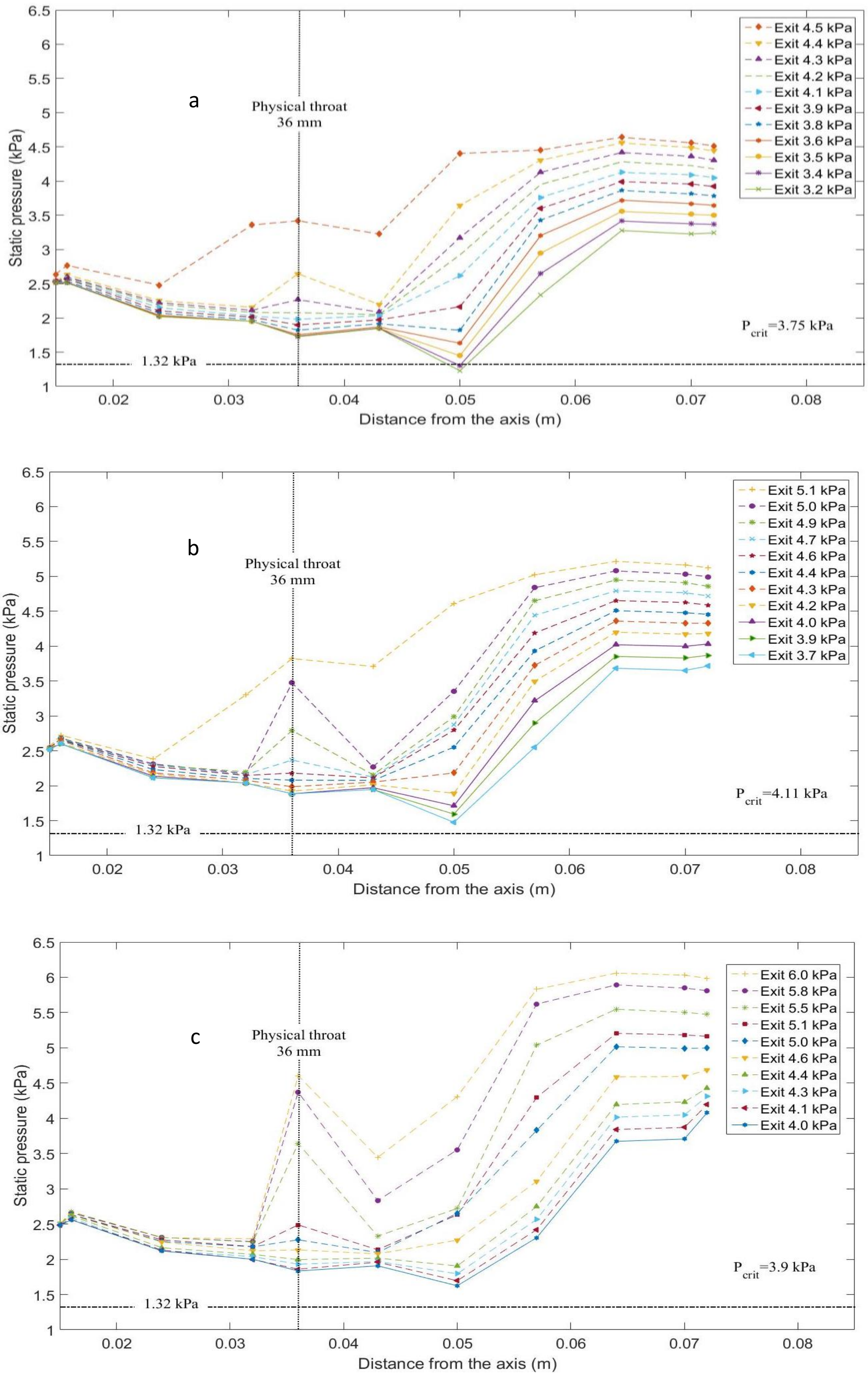

Figure 6-6: Static wall pressure along the radial ejector for secondary pressure of 2.5 kPa and various exit pressures and: (a) primary pressure of 160 kPa; (b) primary pressure of 200 kPa; and (c) primary pressure of 250 kPa.

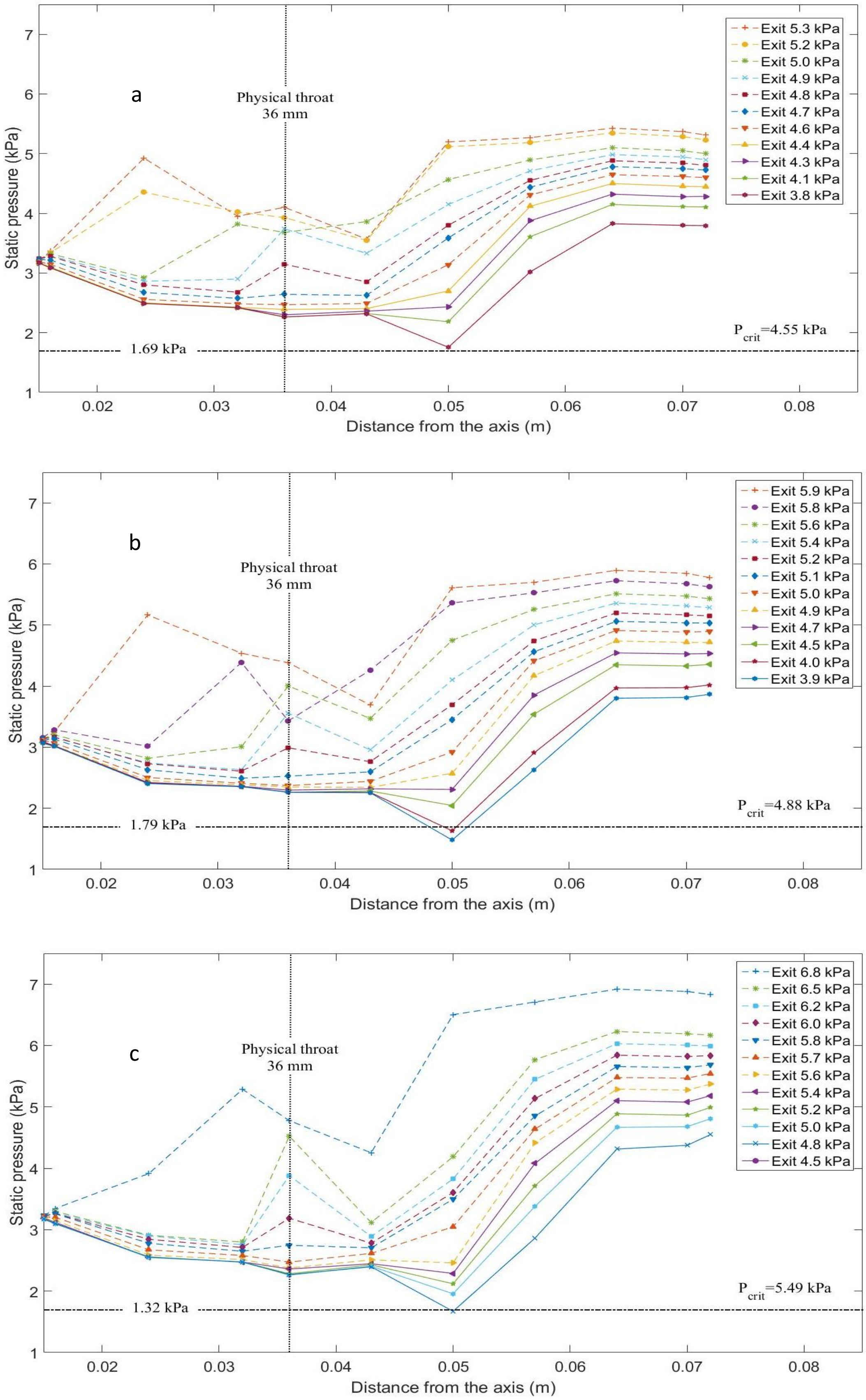

Figure 6-7: Static wall pressure along the radial ejector for secondary pressure of 3.2 kPa and various exit pressures and: (a) primary pressure of 160 kPa; (b) primary pressure of 200 kPa; and (c) primary pressure of 250 kPa.

As shown in Figure 6-5 to Figure 6-7, the wall pressure increases that occur in the region of the physical throat are generated in cases where the ejector exit pressure is at about the point that the critical pressure is reached. Further increases in the exit pressure beyond the critical pressure causes an increase in the severity of pressure rise in the vicinity of the throat. When the flow static pressure rises above the secondary inlet pressure and there has been insufficient mixing with the primary flow, then recirculation / flow separation will occur. For cases of sub-critical ejector operation where there is a peak wall pressure in the vicinity of the throat, the drop in wall pressure after the throat implies that the flow re-accelerates as it enters the diffuser. A second wall pressure rise does occur, this time in the diffuser, implying a final deceleration of the flow prior to leaving the diffuser. The key to reaching higher values of critical back pressure is perhaps the elimination of the appearance of the flow separation in the region ahead of the throat.

Figure 6-8 shows the variation of wall pressure at the physical throat of the ejector with ejector exit pressure, for primary pressures of 160, 200 and 250 kPa and secondary pressures of 1.8, 2.5 and 3.2 kPa. Critical pressures for each combination of primary and secondary pressures are marked on Figure 6-8 as the vertical lines. The major feature in the wall pressure at this location is that for exit pressures lower than the critical pressure, the wall pressure remains almost constant, being independent of the changes in the ejector exit pressure. However, a rapid increase in the pressure at the throat occurs with modest increases in the exit pressure, once the critical pressure is exceeded.

For a constant primary pressure, the local wall pressure at the throat is related to the secondary pressure and exit pressure, as illustrated in Figure 6-8. Higher secondary pressure leads to higher local wall pressure at the measured position. When the primary pressure is held constant, the primary mass flow of the supersonic nozzle remains constant, independent of secondary and exit pressures for this range of operating conditions. Higher secondary pressure leads to more secondary mass flow into the ejector, so the pressure inside the ejector increases. Higher secondary pressure also aids the radial ejector to continue working at higher exit pressures. For a given secondary pressure, the local wall pressure remains almost independent of changes in the primary pressure for lower secondary pressures of 1.8 and 2.5 kPa. For the secondary pressure of 3.2 kPa, increases in the primary pressure lead to slight increases in the local wall pressure at the throat. Increasing the primary pressure also aids the ejector to work at higher exit pressures.

The local wall pressure in the throat region of the prototype radial ejector is similar in many respects to the throat pressures observed in axial ejectors where the local wall pressure remain almost constant for exit pressures less than the critical exit pressure. At exit pressures close to the critical pressure, the local static wall pressure rises gradually [25], [7] in the case of axial flow ejectors, and a similar effect is observed in the case of the radial ejector, Figure 6-8. Once the exit pressure exceeds the critical pressure, the pressure at the throat increases more rapidly with the exit pressure, but further into the subcritical mode of the radial ejector, the rate of rise of wall pressure at the ejector throat often reduces before a very rapid pressure rises occurs, bringing the throat pressure up to the exit pressure, at which point ejector malfunction is reached. Such variations in the wall pressure at the throat reflect the observed variations in entrainment ratio with increasing exit pressure as presented in Figure 6-3: in the subcritical mode, the entrainment ratio generally reduces with increasing exit pressure but it is not a monotonic reduction. In the subcritical mode, the observed variations in the rate at which entrainment ratio decreases and the rate at which the throat pressure increases could be related to some form of oscillatory flow behaviour, because an audible tone accompanied ejector operation within these regions of the subcritical mode.

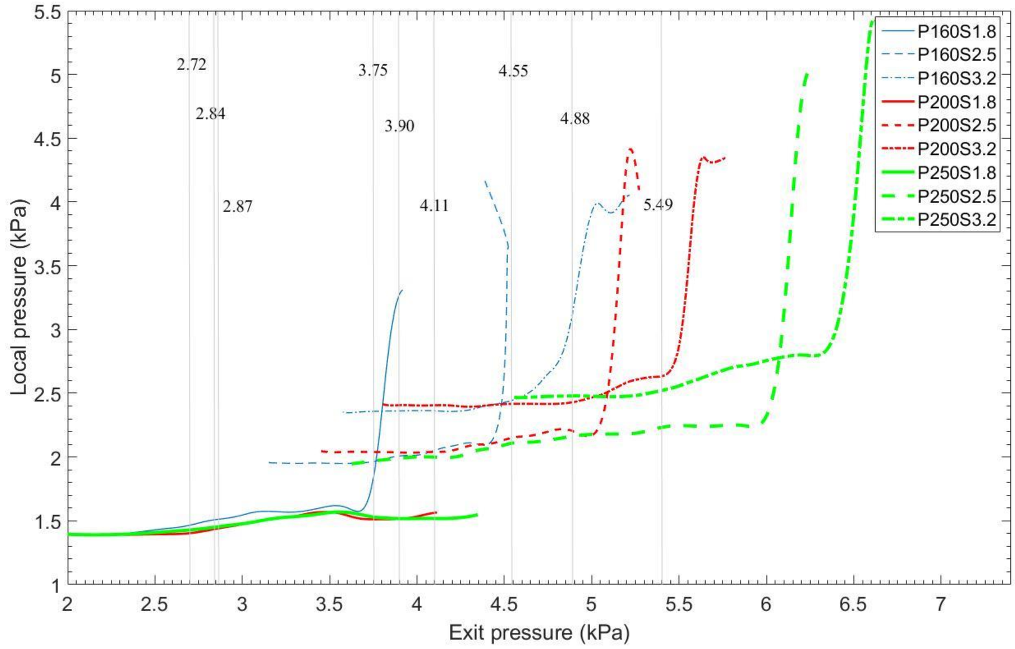

Figure 6-8: Local wall pressure changes at the physical throat of the ejector versus exit pressure for primary pressures of 160, 200 and 250 kPa and secondary pressures of 1.8, 2.5 and 3.2 kPa.

6.4 Conclusion

In this study, the performance of a prototype radial ejector operating with air as the working fluid at different conditions was experimentally investigated. The characteristic curves and measurements of local ejector wall pressures were analysed for primary pressures of 160, 200 and 250 kPa and secondary pressures of 1.8, 2.5 and 3.2 kPa. The effects of different primary and secondary pressure on the radial ejector performance is consistent with expectations for conventional, axial flow ejector performance. Increasing the primary flow pressure leads to a decrease in the entrainment ratio and an increase in the pressure lift ratio. Increasing the secondary flow pressure leads to an increase in both the entrainment ratio and the critical exit pressure. The overall minimum and maximum entrainment ratios achieved were 0.24 and 0.98 for corresponding expansion ratios of 139 and 50 respectively. The overall minimum and maximum lift ratios achieved were 1.42 and 1.72 for corresponding expansion ratios of 50 and 100. Higher pressure lift ratio is achieved with higher expansion ratios.

Wall pressure measurements demonstrate that the location of the compression process inside axial ejectors varies with the exit pressure and secondary pressure. Higher exit pressure moves the location of the compression process upstream while higher secondary pressure moves the compression process downstream. At exit pressures much lower than the critical pressure, the wall pressure reaches a mimimum value close to the isentropic choking static pressure for the secondary stream, and this occurs at a location well downstream of the physical throat of the ejector. For the radial ejector operating in the critical mode, the measured static pressure at the physical throat of the ejector is always higher than the value corresponding to isentropic choking of the secondary stream. When operating in the critical mode, the Mach number in the unmixed portion of the secondary stream at the ejector throat is calculated to be around 0.7, based on the measured static pressure.

When the ejector exit pressure increases and approaches the critical pressure, the static pressure at the physical throat of the ejector gradually increases. With further increases in exit pressure, the ejector enters the subcritical mode and the throat pressure increases more rapidly with exit pressure, and a point is reached where the measured throat pressure exceeds the secondary inlet pressure. At this point it is likely that a region of separated flow will have formed near the throat. In the subcritical operating mode, the rate of entrainment ratio decrease with increasing exit pressure is not particularly constant compared to typical axial ejector performance curves. The same is true for the rate of change on the wall pressure at the throat of the ejector in the subcritical mode: the rate of change of throat pressure is not constant with increases in exit pressure. An audible noise was detected within the radial ejector at conditions where the changes in the slope of the entrainment ratio curve and the throat static pressure were observed, so it is speculated that some form of oscillatory flow might be responsible for these features.

Chapter 7

CFD Simulation of Radial Flow Air Ejector Experiments

Radial ejectors employ a radial flow path facilitating options for variable geometry. Computational Fluid Dynamic (CFD) analysis of a radial ejector is performed using a two dimensional (axisymmetric) model, and the simulated performance is compared with experimental measurements of entrainment ratio, critical exit pressure, and wall pressure data from a prototype ejector. Results from the k-epsilon standard turbulence model demonstrate that the simulated entrainment ratio and the critical pressure are in reasonable agreement with the experimental results with an average discrepancy between the simulations and the physical data being less than 16% for the entrainment ratio and critical pressure across the variety of working conditions. However, there are systematic differences between the measurements and the computational simulations: the k-epsilon standard model underestimates the entrainment ratio at expansion ratios less than 78, and overestimates the entrainment ratio at higher expansion ratios. The k-epsilon standard model also underestimates the critical back pressure at low expansion ratios and at higher expansion ratios, the discrepancy between the k-epsilon standard model and experimental data approaches zero. There are also significant discrepancies between simulations obtained using the k-epsilon standard and k-omega SST model: the k-omega SST model significantly overestimates both entrainment ratio and critical back pressure at all conditions. Comparisions between the simulations and measurements of the pressure on the ejector wall demonstrate that the k-omega SST model provides a pressure distribution that reflects the physical results more accurately than the k-epsilon standard model. However, in the critical mode of ejector operation, both the k-omega SST and k-epsilon standard models simulate a pressure peak in the throat region that is not observed in the experimental data. Efforts to improve the simulated ejector performance through altered duct shape were largely uncessessful, but did demonstrate that performance of the radial ejector is likely to be very sensitive to duct shape. Therefore, good prospects remain for optimising radial ejector performance through CFD simulation.

7.1 Introduction

Adjustment of the physical throat size of a nozzle or ejector can be achieved in an axisymmetric, axial flow arrangement by introducing blockage in the flow path and many papers have considered such flow blockage features on the centreline [37], [38], [39], [8], [40]. However, the major drawback resulting from such methods in axial ejectors is the loss of total pressure that arises due the blockage of the high speed primary stream.

In the work of [76] the radial flow ejector concept was investigated through a CFD study using the k-omega SST turbulence model; the results suggested that the radial ejector has comparable performance to an equivalent axial configuration with essentially the same primary nozzle throat and ejector throat size. Over the reported working conditions, the simulated radial ejector entrainment ratio was less than 2% smaller than the simulated axial ejector results. The simulated critical exit pressure for the radial ejector was about 10% lower than that of the axial ejector for relatively low primary pressure conditions, but at higher primary pressures, the difference in simulated critical exit pressures for the radial and axial ejector configurations approached zero. Further CFD analysis using the k-omega SST turbulence model was performed in [82] to assess the performance of this concept over a range of working conditions when the ejector throat size was altered. An increase of up to 34% in the entrainment ratio was simulated when the separation of radial ejector duct's surfaces was increased by up to 0.8 mm. If increasing the ejector critical exit pressure, a decrease in the ejector duct separation could be applicable, and according to the simulations, about a 40% increase in the critical exit pressure can be achieved by decreasing the ejector throat separation from 3.0 mm to 2.2 mm at a primary and secondary pressure of 250 and 1.8 kPa, respectively. Experimental results from a prototype of this radial ejector concept have also been compared with results from a quasi one-dimensional gas dynamic model tuned to match published data on high-performance, axial ejectors (Chapter 5) and the results show that the physical entrainment ratio of the radial ejector was in good agreement with values from the quasi one-dimensional gas dynamic model, but that the critical exit pressure for the radial ejector prototype was significantly lower than the model results. Therefore, the CFD simulations performed using the k-omega SST model on this radial ejector configuration have over-estimated the critical back pressures across the different working conditions.

Although research such as [26], [30], [70] has reported that CFD analysis can simulate axisymmetric axial ejector performance with acceptable accuracy [71] showing an average discrepency with experiments of less than 10% [17], [26], larger discrepencies have also been reported [17] where the simulated entrainment ratio was not within 20% of experimental data. The production of CFD simulations of variable fidelity might result from the inadequacies in the turbulence modelling; the a priori identification of the most appropriate turbulence model not being compeletly understood [30]. In this study, a k-epsilon standard turbulence model (as implemented within Ansys Fluent was employed to simulate the radial ejector performance in terms of its entrainment ratio and critical back pressure. The results from these simulations are compared to experimental data on the prototype radial ejector reported in Chapter 6 and other simulations performed using the k-omega SST turbulence model in an effort to identify a satisfactory simulation strategy for probing the radial ejector performance. Possible departures of the nozzle plates separation or the ejector ducts separation from the designed values, other radial ejector geometric limitations, and high adverse pressure gradients in the ejector have previously been identified as potential reasons for underperformance of the radial ejector relative to theoretical expectations. The present work investigates the contribution that such features have on the apparent radial ejector performance shortfall through the computational simulations.

7.2 Methodology

7.2.1 Hardware

A schematic diagram of the radial ejector system is shown in Figure 5-6. The system consists of: two plates forming the radial ejector duct; the radial supersonic nozzle assembly; two secondary inlet pipes, one from either side of the ejector; the primary inlet pipe connecting the compressed air source feeding the primary nozzle; the local receiving tank for collecting the outlet flow and exhausting it to a large vacuum chamber. Measurement and control systems were also required to operate the experiment. For further details of the arrangement of the hardware, refer to Chapters 5 and 6.

Figure 6-1 shows the key dimensions and geometry of the radial ejector. The radial ejector has a nominal throat separation of 0.4 mm giving a nozzle throat area of 8.8 mm^2 and a nozzle exit area of 180 mm^2, giving a nozzle area ratio of 20.4. The ejector itself has a nominal throat separation of 2.3 mm giving a physical throat area of 520 mm^2, and an ejector area ratio of 59. The experiments were performed for primary pressures p_p of 160, 200 and 250 kPa and secondary pressures p_s of 1.8, 2.5 and 3.2 kPa, and a variety of exit pressures p_d in each case; computational simulations were performed matching these pressure boundary conditions.

Illustrative performance curves showing the variation of the radial ejector entrainment ratio with exit pressure from the experiments are presented in Figure 7-1 for primary pressures of 200 kPa. The radial ejector has similar characteristics to convential axial flow path ejectors in that the radial flow ejector operates in a choked mode with a maximum entrainment ratio ω_{max} for diffuser exit pressures lower than some critical value, p_{crit}. If the diffuser exit pressure is increased beyond p_{crit} a decrease in the entrainment ratio results. A critical diffuser exit pressure p_{crit} was identified from the experimental data for each operating condition by first fitting a straight line to entrainment ratio results at diffuser exit pressures substantially higher than p_{crit}. This fitted line representing the decline of entrainment ratio for pressures in excess of p_{crit} was then extrapolated back to a horizontal line representing the value of ω_{max} as illustrated in Figure 7-1. The intersection of these two lines is interpreted as specifying the critical pressure p_{crit} for each operating condition.

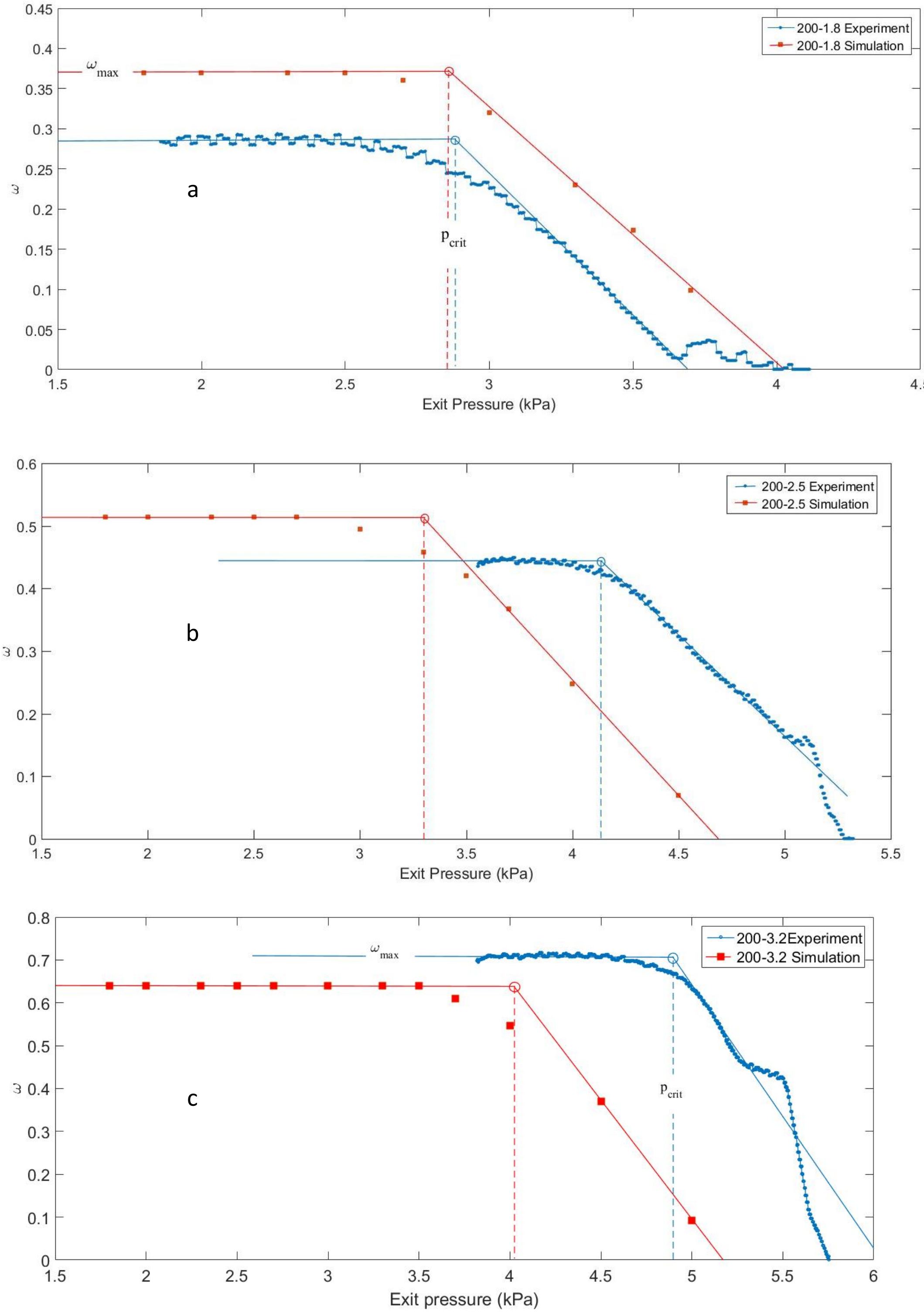

Figure 7-1: Entrainment ratio variation with back pressure for primary pressure 200 kPa and secondary pressures of: (a) 1.8 kPa; (b) 2.5 kPa; and and (c) 3.2 kPa.

7.2.2 Simulation

The computational simulation technique involved specification of the computational domain and boundary conditions, and the solution of the algebraic, finite volume forms of the relevant compressible flow equations using Ansys Fluent 16.1. All dimensions of the computational domain were taken from the physical model of the radial ejector as shown in Figure 6-1. The computational domain was specified as 2D axisymetric. The computational domain was meshed using Ansys Mesh software. The standard k-epsilon turbulence model was employed for the majority of the simulations, and for comparison, results from the k-omega SST model presented in [76] and [82] were used along with additional k-omega SST simulations performed where needed. The density-based implicit solver was used and this solver has been proven to be a suitable solver for supersonic flow fields, [74] and [75].

Air was specified as the flow medium and the primary and seconday in-flow boundaries were set as pressure-inlets. The ejector exit was specified as a pressure-outlet. Primary pressures of 160, 200 and 250 kPa were simulated in combination with secondary pressures of 1.8, 2.5 and 3.2 kPa giving a total of 9 simulated primary-secondary stream operating conditions corresponding to the physical conditions in the experiments. The stagnation temperature of the air entering the ejector through the primary and secondary inlets was specified as 27 °C corresponding to the conditions in the experiments. For each of the primary and secondary stream operating conditions, different outlet pressures ranging from approximately 2 kPa to 7 kPa were applied to emulate the conditions encountered in the physical experiments. The simulations were run as steady analyses even though the experiment for each combination of primary and secondary pressure had a gradually increasing outlet pressure. The relatively slow rate of change of the outlet pressure encountered in the experiments is assumed to allow the information obtained at any specifc outlet pressure to be the equivalent of that which would be obtained at a steady state condition. The solver was set to the second order upwind scheme. For the final solution to be considered converged, two criteria needed to be satisfied:

1- the difference of the mass flow rate at the inlets and outlet were less than 10^{-6} kg/s, amounting to a maximum error of 0.0244% in the mass flow rate across the simulated range of operating conditions.

2- All residuals for caclculations must fall to less than 10^{-5}.

A mesh independence analysis was performed. Different mesh sizes consisting of between 15000 and 80000 elements were produced. A uniform fine mesh with maximum face size of 0.08 mm was initially applied to the flow domain shown in Figure 7-2a and then, to accurately simulate boundary layers, 10 inflation layers were adopted close to the walls. The sizes of the cells nearest to the ejector walls are characterised in terms of the dimensionless parameter, y^+ and for the mesh with 51451 elements and the ejector operating condition of primary, secondary and exit pressures of 200, 1.8 and 3.5 kPa respectively, the values of y^+ are shown in Figure 7-2b. The sublayer should be resolved with reasonable accuracy in this case because the y^+ values do not exceed 1.

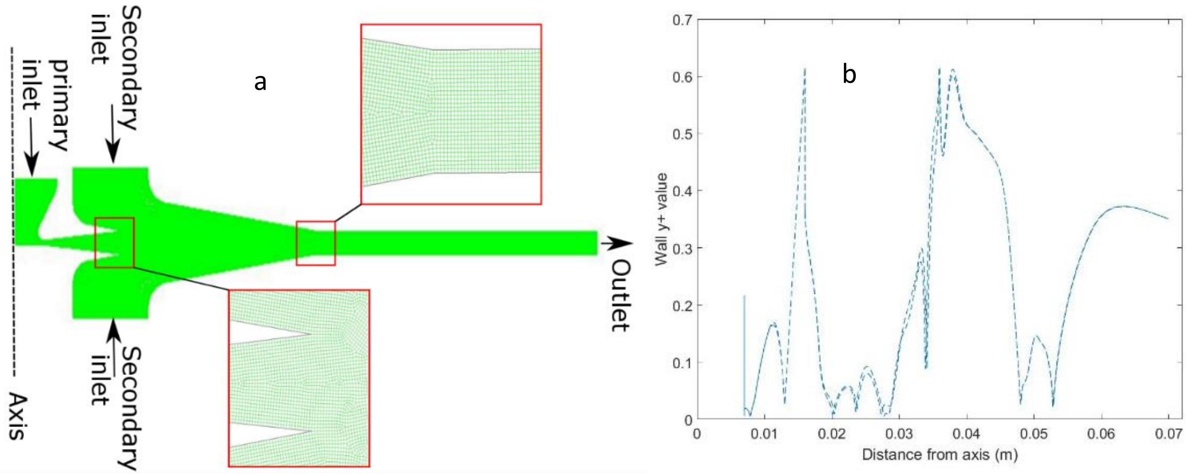

Figure 7-2: Mesh arrangement for the radial ejector: (a) uniform mesh arrangement with no inflation layers illustrating the level of refinement in the majority of the flow domain for the case of 44701 elements; (b) wall y^+ values for 51451 mesh elements and for primary, seconday and exit pressures of 200, 1.8 and 3.5 kPa.

Figure 7-3 shows the variation of entrianment ratio with the number of mesh elements for: (a) a choked ejector operating condition (diffuser exit pressure was less than p_{crit}) with primary pressure 200 kPa, secondary pressure 3.1 kPa and exit pressure of 3.0 kPa; and (b) an unchoked ejector operating condition (diffuser exit pressure was greater than p_{crit}) with primary pressure 200 kPa, secondary 1.8 kPa and exit pressure 3.5 kPa. Results in Figure 7-3 demonstrate monotonic convergence in the entrainment ratios for meshes with element numbers greater than 33888 for both choked and unchoked ejector operation, apart from the point identified in part (a) of the figure. Entrainment ratio results obtained from simulations with the 51451 mesh elements were compared to the equivalent results with the finer mesh, and based on these comparisons, the choked ejector (maximum) entrainment ratio determined from the 51451 mesh is estimated to be within ±0.5% of the fully grid-independent solution. Therefore the domain with 51451 mesh elements was primarily used for the subsequent simulations described herein because of the reduced time to convergence it provided relative to the 79979 mesh element simulations.

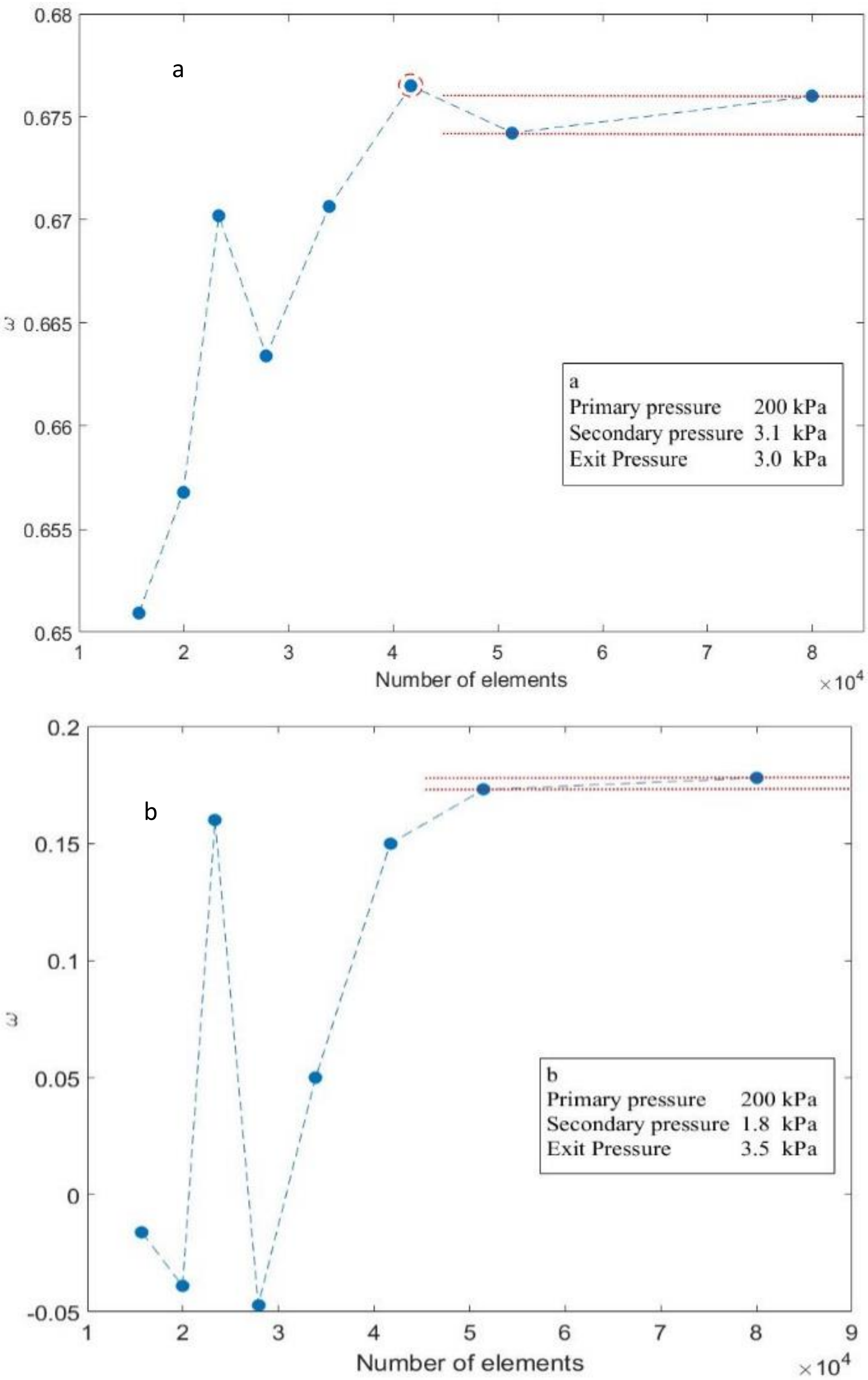

Figure 7-3: Variation of entrainment ratio with number of mesh elements for: (a) typical choked conditions; and (b) typical unchoked conditions.

Figure 7-4 shows the variation of the centre-plane static pressure with distance from the axis of the radial ejector for secondary and exit pressures of 200, 1.8 and 3.5 kPa respectively, which corresponds to an unchoked operating condition. The lower resolution simulations (33888 mesh elements and lower) indicate that the increase in the centre-plane static pressures occurs somewhat upstream of the static pressure increase in the case of the higher resolution simulations (41701 mesh elements and higher). The initial region of the centre-plane static pressure variation shown in this figure is dominated by primary nozzle flow, but at regions away from the ejector centre-plane, mixing between the primary and seconday streams occurs and the region is therefore labelled as the "mixing section", the zone corresponding to the converging inlet of the ejector. On this converging inlet, regions of separated flow are established on either side of the primary flow, and this flow separation effect dictates the position of the centre-plane static pressure rise observed in Figure 7-4 upstream of the "diffuser section" of the ejector. A larger zone of separated flow was simulated when the number of mesh elements used was 33888 and lower. Simulations reported in the remainder of this paper were performed using 51451 elements which is demonstrated to be a large enough number for convergence of the entrainment ratio in both choked, and unchoked operating conditions, as illustrated in Figure 7-3, and for convergence in the simulation of critical flow features such as flow separation in the case of unchoked ejector opereation as illustrated in Figure 7-4.

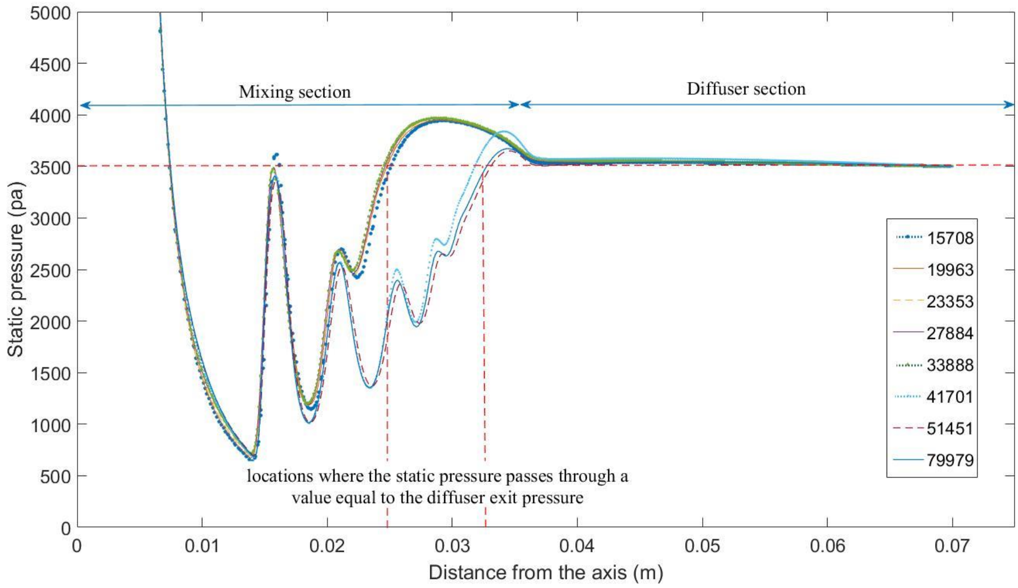

Figure 7-4: Variation of centerline static pressure along the ejector for different mesh elements for the unchoked ejector operating condtions of primary 200 kPa, secondary 1.8 kPa and exit 3.5 kPa pressures.

Simulated mass flow rates through the primary nozzle for the 3 primary nozzle working pressures are reported in Table 7-1, and in order to establish a simulated value for the nozzle discharge coefficient, the ideal value for the mass flow rate was calculated using

$$\dot{m}_{p,ideal} = \sqrt{\frac{\gamma}{R}\left(\frac{2}{\gamma+1}\right)^{(\gamma+1)/(\gamma-1)}}\,\frac{p_p}{\sqrt{T_p}}A^*$$

For the calculation of the ideal mass flow rate, air is considered as an ideal gas with $\gamma = 1.4$ and $R = 287$ J/kgK, and the nozzle throat $A^* = 8.8$ mm^2, corresponding to a cylindrical throat area with a radius of 3.5 mm and a height of 0.4 mm, as illustrated in Figure 6-1. In each case, the primary pressures p_p were taken as the stagnation values used in the simulations and the temperature T_p was taken as 27 °C, also corresponding to the stagnation condition used in the simulations. Values for the ideal mass flow rate through the primary nozzle are also reported in Table 7-1. The discharge coefficient for the nozzle C_d from simulations was then determined by dividing the simulated primary nozzle mass flow rate by the calculated ideal mass flow rate, and for each operating condition, the discharge coefficient was determined to be approximately $C_d = 0.88$, as illustrated in Table 7-1.

Simulated entrainment ratio results vary with the ejector exit pressure in a similar manner to the experiments as illustrated in Figure 7-1. Therefore a similar analysis as that used for the experimental data was applied to the simulated results: (1) straight lines were fitted to the simulated entrainment ratio results for ejector exit pressures somewhat higher than the critical value; (2) horizontal straight lines were fitted to the simulated entrainment ratio results for ejector exit pressures somewhat lower than the critical value; and (3) the intersection of the two lines defined the critical point for the simulated ejector performance.

Table 7-1: Primary nozzle mass flow characteristics

	Experiment	Simulation		
p_p (kPa)	$\dot{m}_p$ (g/s)	$\dot{m}_p$ (g/s)	$\dot{m}_{p,ideal}$ (g/s)	C_d
160	3.84	2.901	3.286	0.883
200	4.78	3.623	4.107	0.882
250	5.97	4.531	5.134	0.883

7.3 Results and Discussion

7.3.1 Entrainment Ratio and Critical Pressure

Table 7-2 presents entrainment ratio and critical pressure results obtained from the experiments and computational simulations using the methods described in Section 7.2. Results showing the comparison of experimental data and simulated values of entrainment ratio and critical pressure are also presented in a graphical form in Figure 7-5.

Table 7-2: Experimental and simulated values of entrainment ratio and critical back pressure

Primary pressure (kPa)	Secondary pressure (kPa)	Expansion ratio	Entrainment ratio		Critical back pressure (kPa)	
			Experiment	Simulation	Experiment	Simulation
160	1.8	88.9	0.37±0.015	0.41±0.002	2.72±0.041	2.25±0.056
160	2.5	64.0	0.61±0.024	0.55±0.003	3.75±0.056	3.15±0.079
160	3.2	50.0	0.95±0.038	0.67±0.003	4.55±0.068	3.75±0.094
200	1.8	111.1	0.29±0.012	0.38±0.002	2.84±0.043	2.85±0.071
200	2.5	80.0	0.45±0.018	0.51±0.003	4.11±0.062	3.21±0.080
200	3.2	62.5	0.70±0.028	0.64±0.003	4.88±0.073	3.65±0.091
250	1.8	138.9	0.24±0.010	0.36±0.002	2.87±0.043	3.05±0.076
250	2.5	100.0	0.33±0.013	0.45±0.002	3.90±0.059	3.44±0.086
250	3.2	78.1	0.55±0.022	0.57±0.003	5.49±0.082	4.45±0.111

From Figure 7-5 it can be seen that simulated entrainment ratio results are mostly within ±16% of the experimental measurements except for the low ($\omega < 0.35$) and high ($\omega > 0.9$) entrainment ratio cases. The simulations of the critical back pressures are, on average, also within 16% of the experimental results, but the simulations tend to underestimate the critical back pressure achieved in the experiments by about this amount. A superficial assessment based on such quantification suggests that the simulations using the k-epsilon standard turbulence model offers an adequate model for the ejector performace because, in the literature, discrepencies between ejector experimental results and computational simulations of up to 20% [8], 25% [86], 30% [25] and even more than 50% in some working conditions [17] have been reported by for different axial flow ejector arrangements. However, the results in Figure 7-5 illustrate systematic departutres of the simulated entrainment ratio from the experimental results, so the computational model is not entirely satisfactory. In the work of Hemidi et al. [26], CFD results very close to experimental data were obtained, the results matching to within 10%, and Hemidi et. al. suggested the success in their case might be partially associated with the very high precision in the test bench setup. Departures in the experimental appartus from nominal dimensions can certainly lead to disagreement between the simulations and experimental results. In the case of the radial ejector, the nozzle and ejector throat dimensions are relatively small and the complex assembly process exposes the prototype used in the experiments to potential variation from the design dimensions.

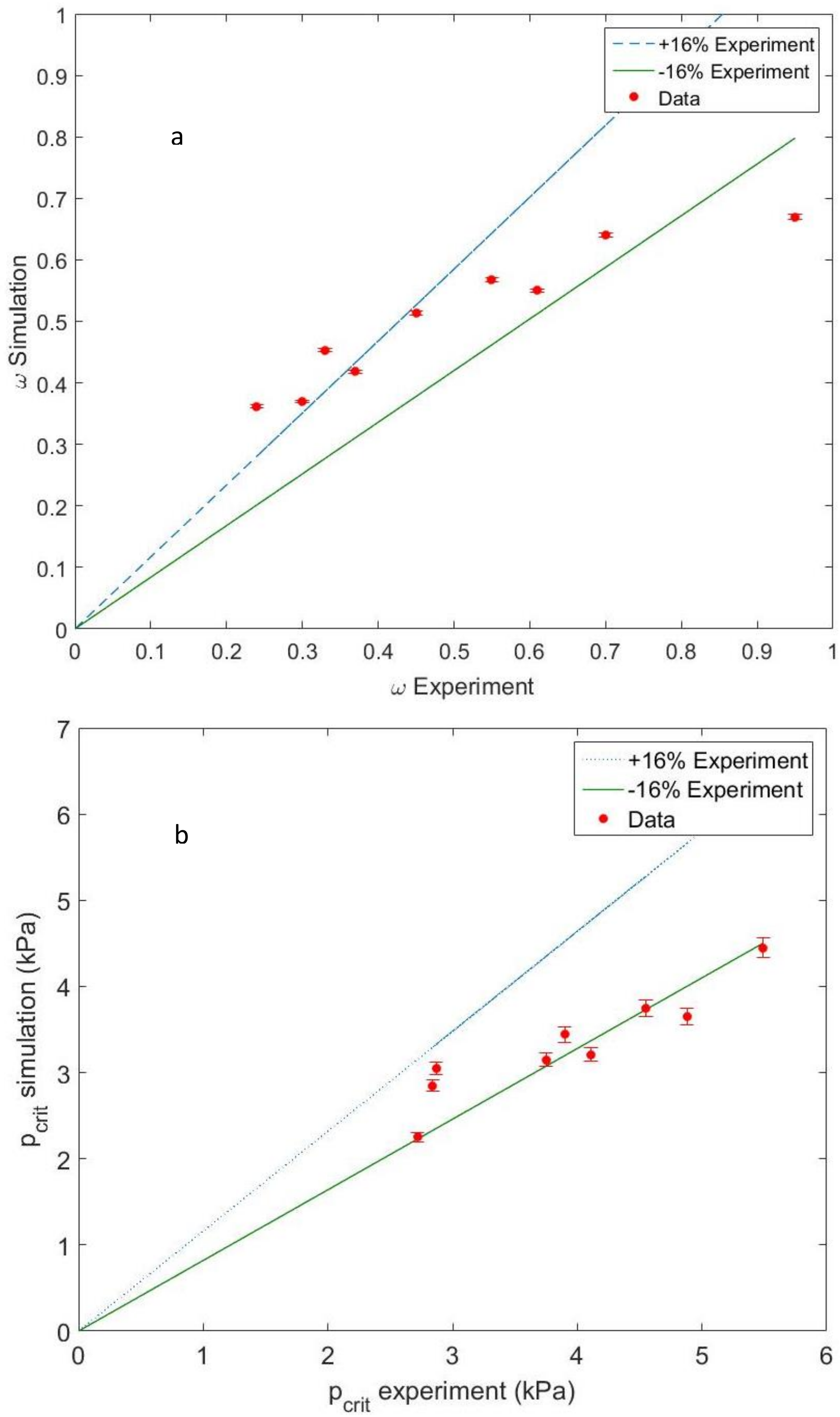

Figure 7-5: Graphical comparison of experimental and computational results for: (a) entrainment ratio; and (b) critical back pressure.

A significant contribution to the uncertainty in the CFD simulations arises from the precision with which the primary nozzle and ejector duct could be assembled. Possible departure of the primary nozzle throat separation from the nominal design value is gauged by referring to the mass flow rates in Table 7-1 where it is observed that on average, the experimental data are approximately 16.5% larger than the simulated values. The nozzle throat separation h^* is therefore likely to be larger than the nominal value of 0.4 mm which was used in the simulations by +16.5% or about +0.066 mm (details in Chapter 5). No such gauge for assessing the actual assembled separation of the ejector throat exists, but based on estimates of assembly precision, flexibility of the 3D printed duct, and potential loading on the duct during assembly and when in operation, the uncertainty in the ejector throat height h_t is estimated to be ±0.6 mm, which amounts to a relative uncertainty of ±26%.

Based on the quasi one-dimensional gas-dynamic analysis reported in chapter 5 and for expansion ratios between 50 and 150, when a 16.5% increase in the nominal nozzle throat area occurs: (1) a decrease in the entrainment ratio by about 18% is anticipated; and (2) an increase in the critical back pressure by about 14% is expected. If a decrease in the CFD-simulated entrainment ratio of about 18% also occurs when the larger nozzle throat size is used, then the simulation results presented in Figure 7-5a will be in better overall agreement with the experiments, but there will still be a systematic difference between the simulations and the experimental results. In a similar manner, if an increase in the CFD-simulated entrainment ratio of about 14% also occurs when the larger nozzle throat size is used, then the simulation results presented in Figure 7-5b will be in better overall agreement with the experiments, but there will still be a systematic difference between the simulations and the experimental results.

In the work of [82], by increasing the ejector duct separation from 2.2 mm to 3 mm which represents an area increase of about 36%, the entrainment ratio increased by 34%, and the the critical back pressure decreased by about 15%. Assuming a linear relationship between the ejector duct separation and both the entrainment ratio and critical back pressure, a 26% increase in the ejector duct separation from the nominal dimension would cause an increase in the entrainment ratio of around 25%, and about 10% decrease in the critical back pressure.

One source of uncertainty in the CFD arises because of the possible deviation of the radial ejector components location from their designed location. For example, the nozzle could have been installed in a position that differs from the designed location. The radial nozzle might deviate from the specified location in different ways including any combination of the following:

- Offset of the nozzle centre plane from the ejector duct centre plane.
- Offset of the nozzle vertical centre line from the ejector vertical centre line.
- Angular deviation of the nozzle centre plane from the ejector duct centre plane.
- Angular deviation of the nozzle vertical centre line from the ejector vertical centre line.

These possible deviations in the assembly of the radial ejector could lead to blockage of the supersonic flow passing the nozzle or non-parallel flow of the primary and secondary streams. To minimize the impact of these possible deviations, the nozzle was supported from both sides of the ejector. The effect of these possible deviations has not been simulated. Further studies are needed to assess the effect of these deviations in the radial ejector performance and flow behaviour.

7.3.2 Comparison of k-epsilon and k-omega SST Models

Figure 7-6 presents the variations of entrainment ratio and critical pressure for the k-epsilon standard and k-omega SST models compared to experimental results (not considering possible departures of nozzle or ejector throat separations) at the different expansion ratios p_p/p_s. The results show that the k-omega SST model overestimates both the entrainment ratios and critical back pressures. The k-epsilon standard model also overestimates the entrainment ratio at expansion ratios of more than 78, but underestimates the entrainment ratio at lower values. The discrepancy between the simulations of the entrainment ratio from the k-omega SST model and the entrainment ratio from the experiments increases with increasing expansion ratio. The k-epsilon standard model underestimates the critical back pressure at low expansion ratios, but with increasing expansion ratio, the discrepancy between the k-epsilon standard model and the experimental data approaches zero while the discrepancy increases for the k-omega standard model with increasing expansion ratio.

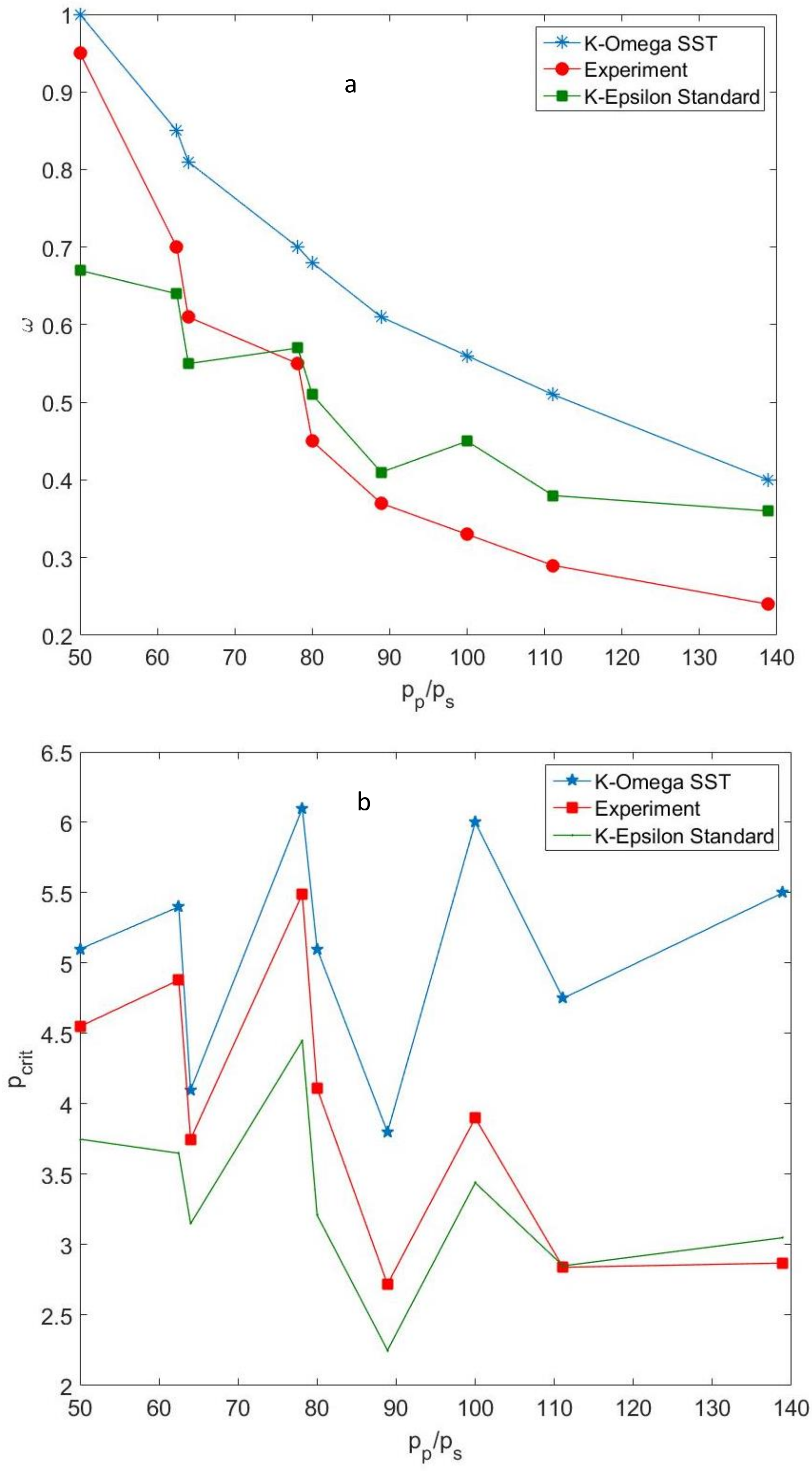

Figure 7-6: Comparison of k-epsilon with k-omega SST ejector simulations: (a) entrainment ratio; and (b) critical back pressure.

7.3.3 Simulations of Mach Number and Static Pressure

Figure 7-7 shows the simulated Mach number contours from the radial ejector for primary pressure of 200 kPa, secondary pressure of 1.8 kPa and two different values for the exit pressure: 2 kPa and 4 kPa. These cases have been selected for consideration because at these values of primary and secondary pressure, the simulated critical back pressure closely matches the experimental value, as illustrated in Figure 7-7a, although the simulated maximum entrainment ratio exceeds the experimental value by approximately 30%, as indicated by the values presented in Table 7-2. The critical back pressure in this condition is 2.84 kPa, so the case where the back pressure is 2 kPa corresponds to a situation where the ejector is operating in the choked mode, and for the back pressure of 4 kPa, the ejector is operating in an unchoked mode. In fact, the back pressure of 4 kPa corresponds to the malfunction pressure, where simulated entrainment of the secondary stream has fallen to zero, as illustrated in Figure 7-7a.

High pressure primary flow enters the radial nozzle relatively close to the axis and the air is accelerated, reaching Mach 1 at the nozzle throat. Supersonic flow is achieved in the diverging part of the nozzle and a sequence of oblique wave structures form at the nozzle lip and these wave structures process the primary flow, adjusting its pressure and flow direction to achieve compatibility with the entrained secondary flow. The maximum Mach number of the flow leaving the nozzle reaches about 4.25 and this maximum Mach number is not significantly affected by different back pressures. By increasing the back pressure from 2 kPa to 4 kPa, the maximum Mach number deceased from 4.2679 to 4.2540. Similar Mach number results have previously been obtained by [76], [75], [3] for axial ejectors.

In typical axial flow ejectors, by increasing the back pressure, the location of the compression process inside ejectors moves upstream, but by increasing the secondary pressure, the position of the compression process moves downstream [74], [75]. Simulations of the prototype radial ejector display a slightly different behavior. As it can be seen from Figure 7-7a, at the low exit pressure of 2 kPa, a zone with a Mach number more than 1 exist at the start of the diffuser section, but at the higher exit pressure of 4 kPa (as illustrated in Figure 7-7b), this zone no longer exists, suggesting an upstream movement in the compression effect. However, on inspection of the static pressure on the centre-plane of the radial ejector shown in Figure 7-8, it is observed that the position of the compression process has moved upstream very little in changing from the back pressure of 2 kPa to the back pressure of 4 kPa.

Figure 7-8 illustrates that the centre-plane static pressure fluctuates with a decaying magnitude within the core flow of the primary nozzle within the mixing chamber section, a feature that is shared with typical axial flow ejectors. For relatively low ejector exit pressures, the fluctuating centre line static pressure in axial ejectors typically approaches an almost constant value near the start of the constant area section, or just prior to the appearance of a second series of shocks which compress the supersonic portion of the mixing ejector flow towards the required diffuser exit pressure. Such behavior has been reported by [87] for an axial ejector that is equivalent to the radial ejector reported in this paper in terms of throat sizes. With increases in the back pressure of typical axial flow ejectors, the point at which the pressure starts to rise shifts upstream [74]. Furthermore, in typical axial flow ejectors operating at low back pressures, almost the entire secondary flow will accelerate to sonic conditions by the start of the diffuser. The present radial ejector has no constant area section similar to the axial ejectors, and by increasing the back pressure, the static pressure rises in the mixing section. There is no significant zone within the simulated radial ejector with an almost constant static pressure prior to the compression process either in the choked or in the unchoked operating conditions. Although the radial ejector clearly displays a constant entrainment ratio effect for back pressures less than the critical value, it seems that complete acceleration of the secondary flow to sonic conditions is not acheivable with the current radial ejector arrangement.

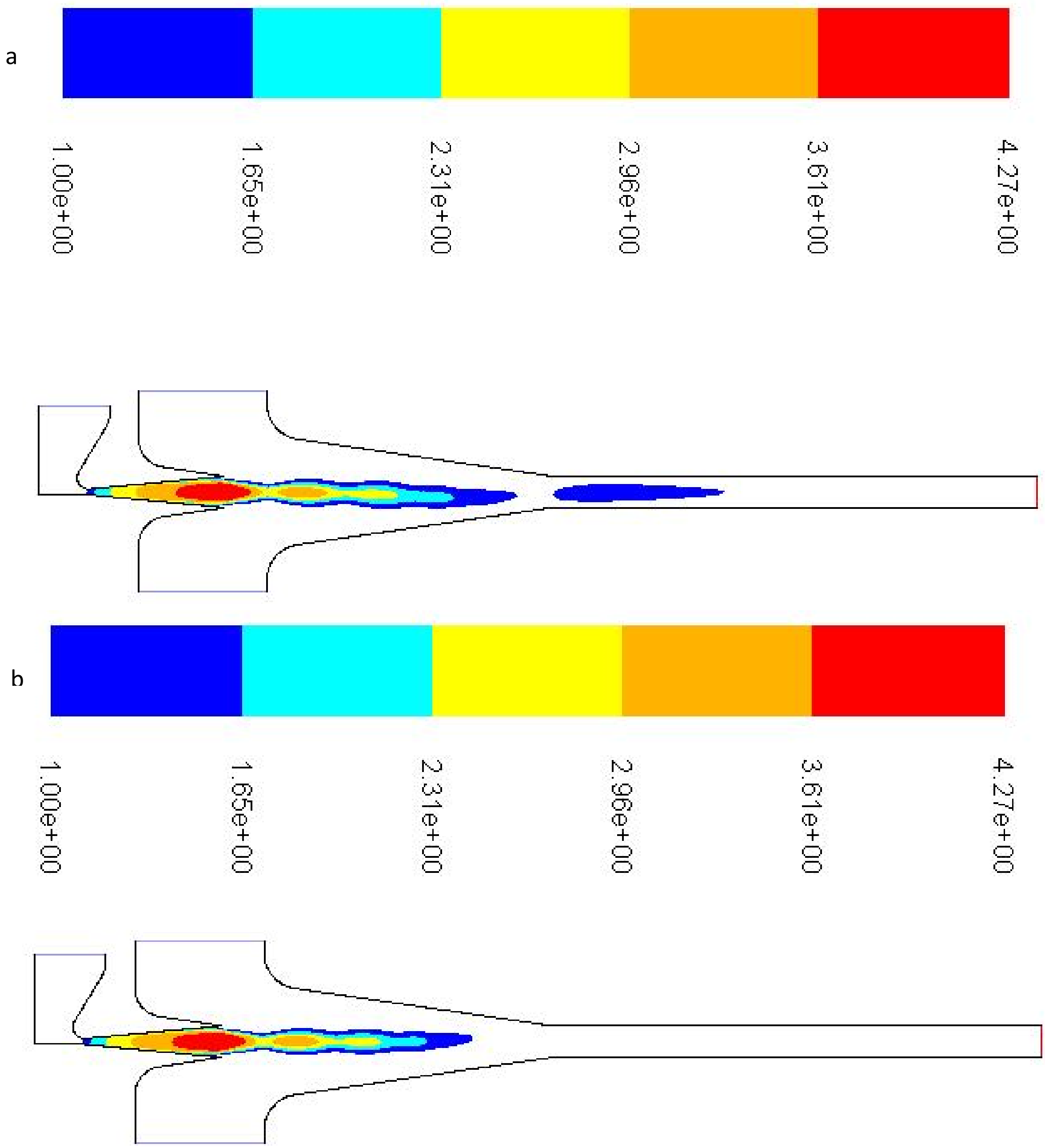

Figure 7-7: Mach number contours for primary pressure of 200 kPa, secondary pressures of 1.8 kPa and back pressures of: (a) 2 kPa and (b) 4 kPa.

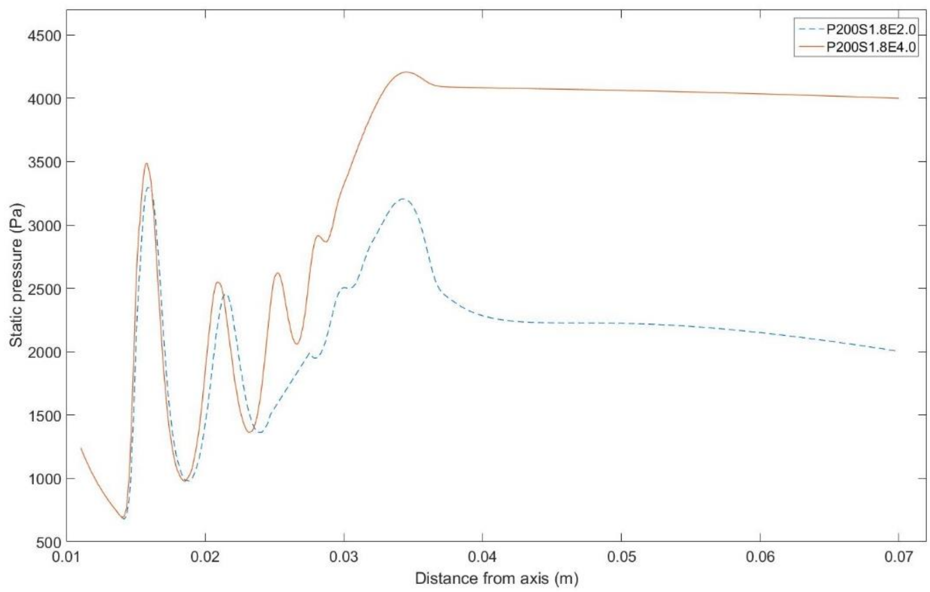

Figure 7-8: Centre-plane static pressure for primary pressure of 200 kPa, secondary pressure of 1.8 kPa and for two cases with different diffuser exit pressures of 2 and 4 kPa.

7.3.4 Wall Pressures: Experiments and Simulations

A comparison of the radial ejector wall pressure for the k-epsilon standard, k-omega SST and experiments is shown in Figure 7-9. The simulated wall pressure of the radial ejector using the k-omega SST model has been reported by [76]. Experimental data demonstrates different characteristics for the different modes of ejector operation: (1) for exit pressures lower than the critical pressure, the ejector is working in the critical mode and the wall pressure reaches a minimum value downstream of the ejector throat; (2) for exit pressures in the vicinity of the critical pressure, the ejector is working in the transition from the critical to subcritical modes and the minimum wall pressure occurs in the vicinty of the throat; and (3) for exit pressures in excess of the critical pressure, a peak in the static pressure occurs at the throat or upstream of the throat but the final rise towards the exit pressure value occurs further downstream, in the diffuser (Chapter 6). As can be seen in Figure 7-9, neither of the turbulence models adequately simulate the wall pressure within the radial ejector. Both models simulate a high pressure zone around the physical throat, even when the ejector is operating in the critical mode which is an effect that is not apparent in the physical data. In fact, the k-epsilon model simulates a peak in the static pressure around the physical throat or in the mixing chamber at all working conditions and this peak value is significantly higher than the exit pressure. Although the k-omega SST model also simulates a throat pressure rise in the critical mode which is not observed in the experiments (Figure 7-9a), the magnitude of the simulated peak in the case of the subcritical mode is slightly lower than the magnitude observed in the experiments (Figure 7-9b). On balance, the k-omega SST model provides simulated wall pressures that are in better agreement with the experimental data.

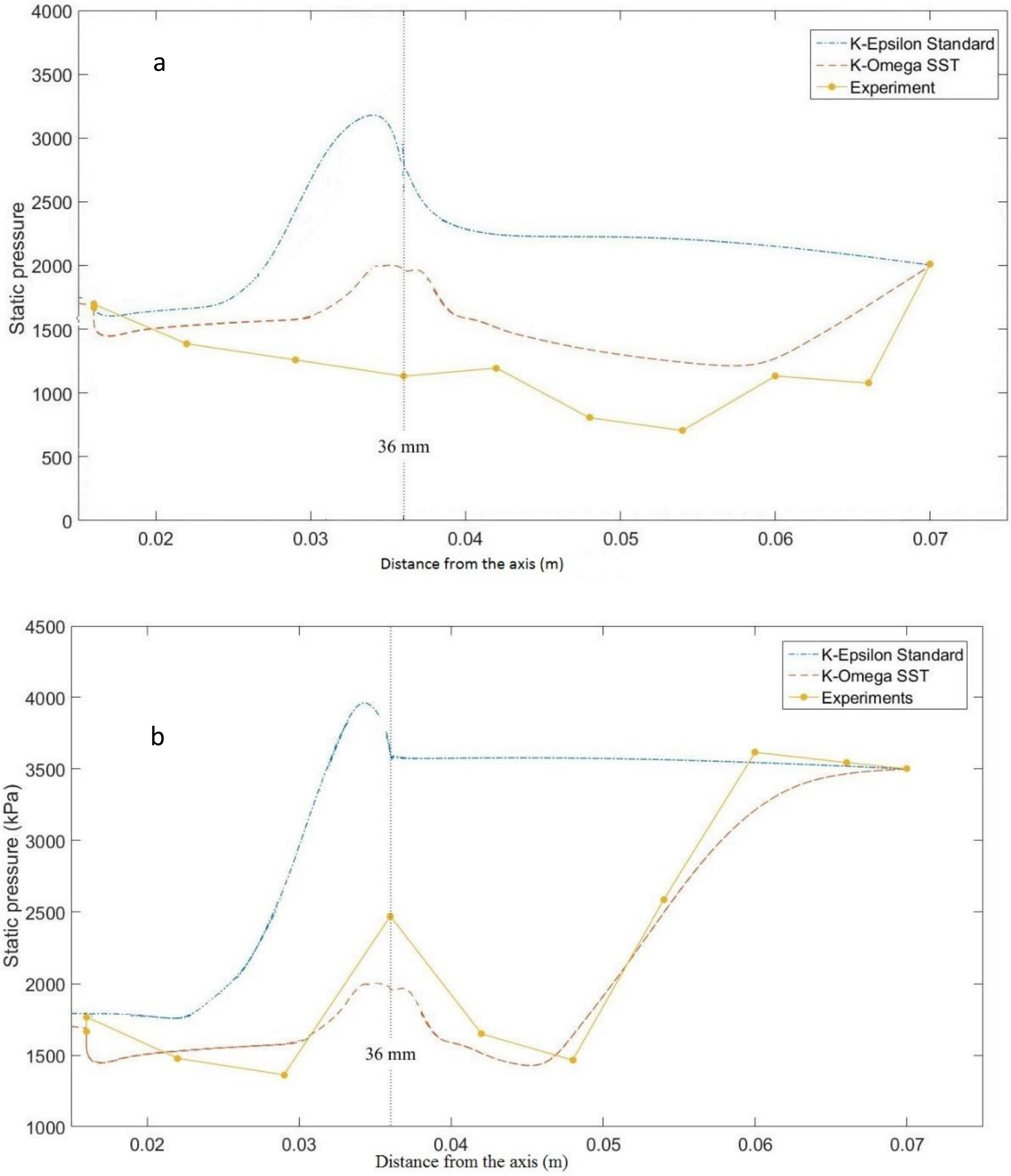

Figure 7-9: Static wall pressure along the radial ejector for primary and secondary pressures of 200 and 1.8 kPa respectively: (a) exit pressure of 2 kPa; (b) exit pressure of 3.5 kPa.

7.3.5 Recirculation in the Mixing Zone

The centre-plane static pressure simulations in Figure 7-8 indicate that lower static pressures are registerd at the exit of the diffuser than are achieved at locations slightly upstream of the physical throat of the ejector, which occurs at a radius of 36 mm (Figure 6-1). Thus, the flow in the ejector is re-accelerating in the diffuser after the throat station has been reached. Such an effect is not observed in typical axial flow ejectors, and arises in the present simulations of this particular radial flow ejector due to flow separation in the mixing region. Figure 7-10 presents the simulated stream functions of the flow inside the radial ejector for primary, secondary and exit pressures of 200, 1.8 and 2 kPa respectively for the radial ejector (in part a of this figure) and a slightly modified profile of the radial ejector (in part b of this figure). For the modified profile, the sharp transition from the contraction half-angle of 9º to the parallel portion of the duct was replaced by a smooth profile in the vicinity of the throat in an effort to reduce the magnitude of the region of separated flow. Simulations of the revised profile ejector indicated that the maximum entrainment ratio increases by 4.2 % for the primary and secondary pressures of 200 and 1.8 kPa respectively, but this configuration also had an ejector throat area that was larger than the usual configuration by 50 %. In the work of [82], by increasing the ejector thoat size by 36%, the entrainment ratio inceased 29% at this operating condition. It seems that increasing the duct separaton is more effective than just increasing the ejector throat area for achieving higher entrainment ratios. However, no increase was registered in the critical back pressure in the modified version at primary and secondary pressures of 200 and 1.8 kPa respectively. According to the simulations, the modification changes the position of the recirculation zone, and reduces the asymmetric flow behaviour.

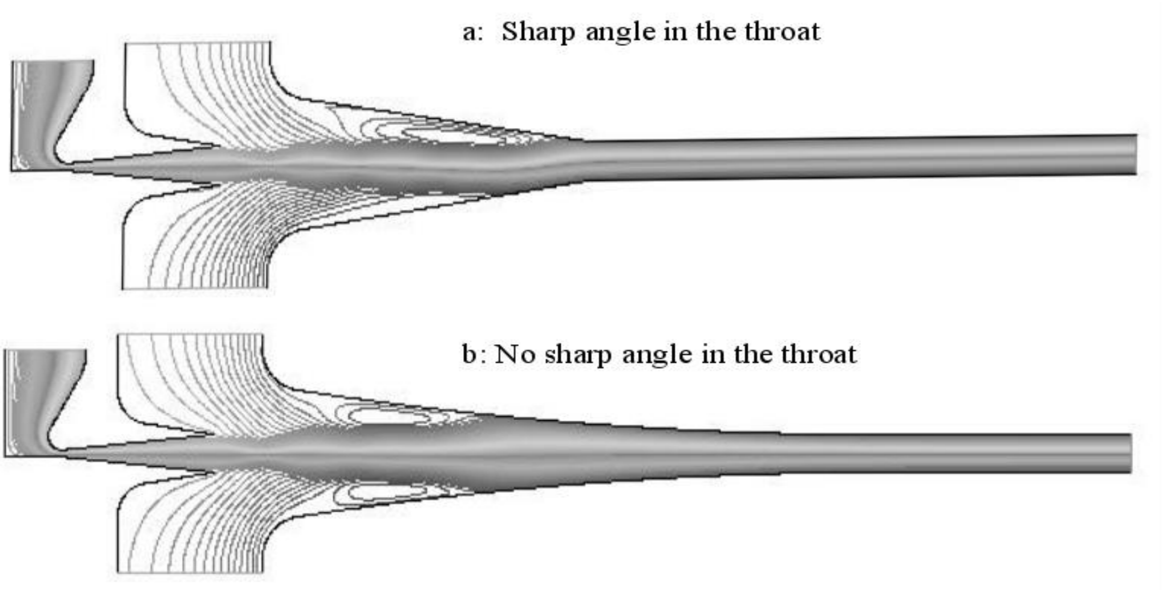

Figure 7-10: Stream functions inside the radial ejector for primary, secondary and exit pressures of 200, 1.8 and 2 kPa respectively for (a) the prototype radial ejector; (b) a modified radial ejector with a smooth shape transition in the throat region.

CFD results shows that there is a flow separation in the mixing chamber. One reason for this separation may be that the radial ejector duct is not contracting sufficiently fast to keep the flow cross sectional area decreasing. In the prototype radial ejector, there is actually a slight maximum in the apparent flow cross sectional area at around 1500 mm^2 at the start of mixing chamber (refer to Chapter 5). To create a more rapid reduction in the cross sectional area of the ejector duct near the start to avoid an apparent area increase, a new flow cross sectional area profile is suggested in Figure 7-11. Additional features intended to improve the radial ejector performance include: (1) a variation in duct separation and associated area variation that should generate lower adverse pressure gradients in the diffuser; and (2) a constant area zone in the throat region.

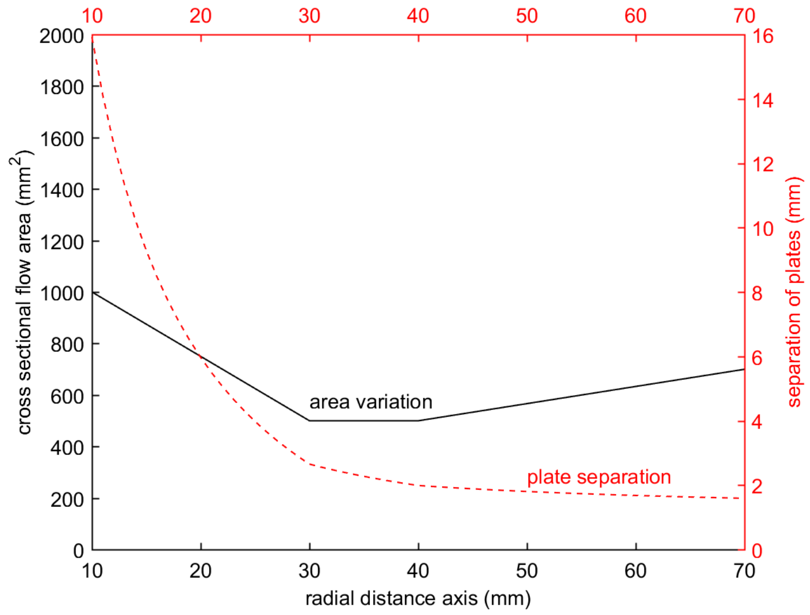

Figure 7-11: Proposed variation of flow cross sectional area and corresponding plate separation for improved radial ejector performance.

Figure 7-12 shows the modified radial ejector flow path based on the suggested area variation shown in Figure 7-11. CFD simulation for this area variation has been conducted using the k-epsilon standard turbulence model. CFD results at primary, secondary and exit pressures of 200, 1.8 and 2 kPa respectively that correspond to a double choked condition in the original prototype configuration with an entrainment ratio of 0.38, show that for the modified configuration, the entrianment ratio decreases to 0.13. The critical pressure is not also improved with this modified configuration; the prototype radial ejector worked in a single choked mode for an exit pressure of 3.5 kPa, but reverse flow existed for this modified configuration at 3.5 kPa exit pressure. This modified version has the same throat area as the prototype radial ejector, but the separation of the ejector duct at the exit of the diffuser decreased from 2.2 mm to about 1.8 mm. As can be seen from Figure 7-12, the separation zone still exist in the mixing chamber. This initial attempt at improving the variation of the flow cross sectional area has not been successful. Further computational simulation work is required to optimise the variation of flow cross sectional area in the radial flow diffuser.

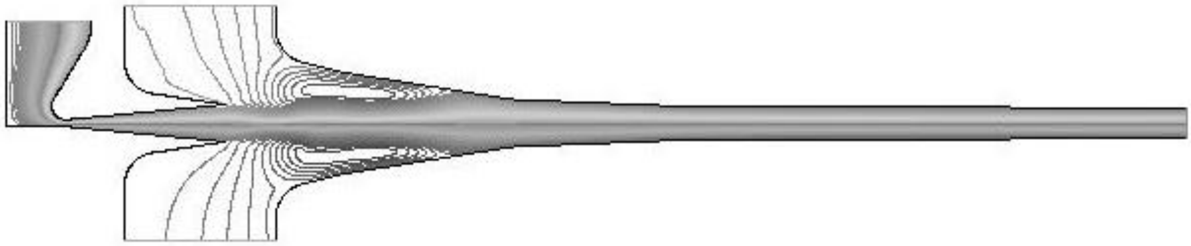

Figure 7-12: The modified radial ejector flow path and stream functions inside the radial ejector for primary, secondary and exit pressures of 200, 1.8 and 2 kPa respectively.

7.4 Conclusion

CFD simulations using Ansys Fluent have been performed for a radial ejector configuration working with air, and the results assessed against experimental data. The CFD simulations using the k-epsilon standard model predicts the ejector performance reasonably well. In terms of the entrainment ratio, the CFD simulations based on k-epsilon standard turbulence model agree with the data from the experiments to withinabout 16% except for entrainment ratios lower than 0.35 and higher than 0.9, where differences are larger. The k-epsilon standard CFD simulations also give critical pressures that agree with data from the experiments with an average discrepancy of less than 16%. However, the comparisions with the experimental data demonstrate that the discrepancies in the simulations are systematic in both the entrainment ratio and critical back pressure. Significant differences also exist between the k-epsilon standard and k-omega SST turbulence model in simulating the entrainment ratio and critical back pressure: the k-omega SST turbulence model over estimates entrainment ratio and critical back pressure at all working conditions. The k-epsilon standard model also overestimates the entrainment ratio at expansion ratios more than 78, but underestimates the entrainment ratio at lower values. The k-epsilon standard turbulence model under estimates critical back pressure at low expansion ratios and by increasing the expansion ratio, the discrepancy approaches zero.

Both k-epsilon and k-omega turbulence models simulate a peak in static pressure around the physical throat of the ejector when operating in both critical and subcritical modes. However, in the experiments, such a peak in pressure only occurs in when the ejector is operating in the subcritical mode. Neither model accurately simulates the distribution of wall pressure in the radial ejector, though on balance, the k-omega model offers better overall agreement with experimental data.

The simulated flow in the radial ejector reaccelerated in the diffuser after the throat position has been reached. Such an effect is not observed in typical axial flow ejectors and arises in the present simulations of this particular radial flow ejector due flow separation in the mixing region. Although the reacceleration effect is not observed in the static pressure measurements for the ejector operating in the critical mode, it is apparent in the static pressure measurements for the subcritical mode. Reducing the size of the recirculation zone in the mixing region was targeted for performance improvement from the radial ejector. Replacing the sharp transition from the mixing region into the ejector throat with a smooth profile in the vicinity of the throat was first simulated, and this modification reduced the size of the region of separated flow and slightly increased the entrainment ratio, but had no positive effect on the critical pressure. Designing the plate separation to more accurately reflect the flow area available in an axial flow ejector through the addition of a constant area throat and a reduced rate of area increase in the diffuser was then tested with the CFD simulation. A significant reduction in both the entrainment ratio and critical pressure was simulated with these modifications. Clearly the shape of the radial ejector plays a strong role in its performance, and it is conceivable that the tuning the nozzle shape to the ejector duct shape could also be important. Further CFD simulation work to optimise the radial ejector configuration is warranted.

Chapter 8

Conclusion

8.1 Summary

For optimum performance of fixed geometry ejectors, a narrow range of operating conditions need to exist. To extend this range by any appreciable amount, adjustability in the nozzle throat area, together with ejector throat area is necessary. Mechanically achievable approaches to employing adjustability in conventional axial ejectors have drawbacks including significant increases in total pressure losses for devices positioned in the high speed flow and physical limitations to the magnitude of dimension change in throat areas.

The inherent form of axial ejectors with circular cross sections impedes the effective, efficient and practical application of variable geometry. A new configuration with a predominantly radial flow was identified to provide the capacity to readily adjust both the primary nozzle and the ejector throat areas without increasing losses due to blockage in the flow. The primary supply expands in the supersonic radial flow nozzle; this expanding disk of primary flow entrains the secondary flow from the inlets positioned on either side of the expanding primary flow.

In this study, the radial flow ejector concept was investigated through experiments and computational simulations using Ansys-Fluent software based on k-epsilon and k-omega turbulence models. Comparisons with a theoretical quasi-one-dimensional gas dynamic model and conventional ejector performance were evaluated. Based on a design optimisation process, a prototype radial ejector was fabricated and evaluated against the performance predicted in the design phase. To simplify fabrication by accommodating materials with restricted operating temperatures, the design has been based on using air as the working fluid and operates as an open system.

8.2 Radial Ejector Design

The pattern of fluid flow is the main difference between the radial ejector and traditional ejector designs. In the traditional axial ejector arrangement, the direction of flow entering the nozzle and passing through the ejector is predominantly axial. The radial ejector operates with a predominantly radial flow pattern. The radial ejector nozzle and ejector duct are both formed from two disk-like surfaces sandwiching the ejector flows. The primary, secondary and exit flows are accelerated or decelerated primarily in the radial direction.

The design of the radial ejector followed traditional axial-flow ejector 'design rules' interpreted in the context of the new radial ejector geometry, in combination with information from CFD simulation. An axial flow ejector with its experimental and simulation data was used as a benchmark; the design targets for the radial flow ejector were chosen to match this axial ejector performance. The radial ejector had a nominal throat separation of 0.4 mm giving a nozzle throat area of 8.8 mm^2 and a nozzle exit area of 180 mm^2, giving a nozzle area ratio of 20.4. The ejector itself has a nominal throat separation of 2.3 mm giving a physical throat area of 520 mm^2, and an ejector area ratio of 59.

8.3 Radial Ejector Performance Evaluation

Experiments and simulation were undertaken to evaluate the radial ejector performance in terms of entrainment ratio and critical exit pressure. Based on a preliminary CFD analysis using the k-omega SST turbulence model, the radial ejector produced similar performance to an equivalent axial configuration. The radial ejector prototype was evaluated experimentally at primary pressures of 160, 200, and 250 kPa and secondary pressures of 1.8, 2.5 and 3.2 kPa. A quasi one-dimensional model was also configured to predict the values of entrainment ratio and critical pressure lift ratio of the radial ejector prototype. The radial ejector entrainment ratio values were in good agreement with the models. However, the radial ejector critical pressure lift ratios were lower than would be expected for an axial flow ejector having the same area ratios as the radial ejector.

8.4 Effect of Primary and Secondary Pressures

Radial ejector performance at three different primary pressures of 160, 200 and 250 kPa was experimentally and numerically investigated. The effects of different primary pressures on the radial ejector performance is consistent with expectations for conventional, axial flow ejector performance. While the entrainment ratio decreased with increases in the primary flow pressure, the pressure lift ratio increased.

Radial ejector performance at three different secondary pressures of 1.8, 2.5 and 3.5 kPa was experimentally and numerically investigated. Both the entrainment ratio and the critical exit pressure increased with increases in the secondary flow pressure, again consistent with expectations based on existing knowledge of conventional, axial flow ejectors. The overall minimum and maximum entrainment ratios achieved were 0.24 and 0.98 for corresponding expansion ratios of 139 and 50 respectively. The overall minimum and maximum lift ratios achieved were 1.42 and 1.72 for corresponding expansion ratios of 50 and 100. Higher pressure lift ratio is achieved with higher expansion ratios.

8.5 Static Pressure in the Radial Ejector

Experimental results show that the location of the compression process inside the radial ejector varies with the secondary and exit pressures. The location of the compression process is moved upstream by increasing the exit pressure. By inceasing the secondary pressure, the compression process location is moved downstream. When the radial ejector is working in the critical mode but with an exit pressure substantially below the critical value, the wall pressure reaches a value close to the secondary stream isentropic choking static pressure at a location that is well downsteam of the physical throat of the ejctor duct. For all exit pressures, the measured static pressure at the physical throat of the radial ejector is always higher than the value corresponding to isentropic choking of the secondary stream. Based on the measured static pressures, the calculated Mach number of the secondary stream at the ejector throat was approximately 0.7 over the range of conditions tested.

For exit pressures close to the critical pressure, the static pressure at the physical throat gradually increased with increasing exit pressure. With further increases in exit pressure, the throat pressure increased more rapidly, and a point was reached where the measured throat pressure exceeded the secondary inlet pressure. This point might be a sign of flow separation. In the subcritical operating mode, the rate of entrainment ratio decrease and the rate of change on the wall pressure at the physical throat with increasing exit pressure is not particularly constant compared to typical axial ejector performance curves. Some form of oscillatory flow might be responsible for these features as an audible noise was detected within the radial ejector at conditions where the changes in the slope of the entrainment ratio curve and the throat static pressure were observed.

8.6 Geometric Adjustability in the Radial Ejector

To investigate the adjustability in the radial ejector, CFD simulations using Ansys-Fluent were performed. By changing the separation of the radial ejector ducts from 2.2 mm to 2.4 mm and 3 mm, three ejector throat areas simulated. The CFD results reveal that adjusting the separation of the radial ejector ducts was effective in achieving different ejector performance in terms of entrainment ratio and critical exit pressure. The following results were achieved from adjustment in the radial ejector geometry in the simulation:

- Increasing the radial ejector duct separation achieved higher entrainment ratios. An entrainment ratio increase of 34% was achieved by increasing the ejector duct separation from 2.2 mm to 3 mm.
- Increasing the separation typically reduces the critical exit pressure that can be achieved.
- Decreasing the ejector duct separation from 3 mm to 2.2 mm increases in the critical exit pressure by more than 40% at the highest primary pressure condition.

8.7 Radial Ejector Simulations

The CFD simulations were performed using the k-epsilon standard and k-omega SST models using Ansys Fluent working with air. Based on the experimental data and CFD simulation, the following conclusions were made:

- The k-epsilon standard CFD simulations predict entrainment ratio and critical pressures with an average discrepancy of less than 16% in most of the operating conditions.
- The comparisons of the experimental data and the k-epsilon standard model demonstrate that the discrepancies are systematic in both the entrainment ratio and critical exit pressure.
- Systematic discrepancies are also observed with the k-omega SST turbulence model which over estimates entrainment ratio and critical exit pressure at all working conditions.
- Significant differences also exist between the k-epsilon standard and k-omega SST turbulence models in simulating the entrainment ratio and critical exit pressure.
- Both k-epsilon and k-omega turbulence models simulate a peak in static pressure around the physical throat of the ejector when operating in both critical and subcritical modes. However, in the experiments, such a peak in pressure only occurs when the ejector is operating in the subcritical mode.

- Neither k-epsilon standard nor k-omega SST model accurately simulates the distribution of wall pressure in the radial ejector, as measured in the prototype experiments.
- The k-omega model offers better overall agreement with experimental data compared to k-epsilon model results.

8.8 Areas for Future Research

The radial ejector developments in this work demonstrate that entrainment ratios matching those of conventional ejectors can be achieved in a radial configuration with adjustable geometry that does not induce additional blockage losses. However, further radial ejector optimization effort is required to increase the critical exit pressures to those that can be achieved in conventional ejectors.

As the radial ejector configuration is in the preliminary stage of development, more experiments and simulation is required to improve its performance. Work to date warrants considerable effort to identify the flow features contributing to the various characteristics of performance, both holistically and specially to the characteristics of various unique feature of the configuration. The following recommendations for future investigations are made:

- Improvement of the nozzle and the radial ejector flow area profiles to reduce the pressure losses in the ejector.
- Investigation into the adjustability in the radial nozzle and its effects on the radial ejector performance.
- Experimental investigation on the adjustability options in the radial ejector.
- Investigation into the radial ejector lift ratio underperformance, the reasons for this and how to improve it.
- Study of new design methods for radial ejector as the conventional approaches employed traditionally for axial ejectors are not fully applicable.

- Optimisation of the CFD models to improve the reliability of simulation used in analysing the radial ejector flow features. Regarding the effects of the walls in the radial ejector, it is recommended to study the radial ejector using other turbulence models.
- The radial ejector configuration may be capable of more readily achieving and controlling oscillatory primary flow than has been shown in axial ejectors. Investigation into employing oscillatory behaviour in the radial ejector flow is recommended.

References

[1] W. Gosney, Principle of refrigeration, Cambridge: Cambridge University Press, 1982.

[2] I. W. Eames, “The jet-pump ccle- A low cost refrigerator option powered by waste heat,” *Heat Recovery System & CHP,* vol. 15, no. 8, pp. 711-721, 1995.

[3] V. Chandra and M. R. Ahmed, “Experimental and computational studies on a steam jet refrigeration system with constant area and variable area ejectors,” *Energy Conversion and Management,* pp. 377-386, 2014.

[4] S. Gurulingam, A. Kalaisselvane and N. Alagumurthy, “Performance improvement of forced draught jet ejector using constant rate momentum change method,” *International Journal of Engineering and Advanced Technology,* vol. 1, no. 2, pp. 149-151, 2012.

[5] W. J. Hong, K. Alhussan, H. Zhang and C. A. J. Garris, “A novel thermally driven rotor-vane/pressure-exchange ejector refrigeration system with environmental benefits and energy efficiency,” *Energy,* vol. 29, pp. 2331-2345, 2004.

[6] H. El-Dessouky, H. Ettouney, I. Alatiqi and G. Al-Nuwaibit, “Evaluation of steam jet ejectors,” *Chemical Engineering and Processing* , vol. 41, pp. 551-561, 2002.

[7] A. Meyer, P. M. S. Lebre and A. C. Oliveeira, “Steam jet ejector cooling powered by waste or solar heat,” *Renewable Energy,* vol. 34, pp. 297-306, 2013.

[8] S. Varga, P. M. S. Lebre and A. C. Oliveire, “CFD study of a variable area ratio ejector using R600a and R152a refrigerants,” *International Journal of Referigeration,* vol. 36, pp. 157-165, 2013.

[9] F. Mazzelli, A. B. Little, S. Garimella and Y. Bartosiewicz, “Computational and experimental analysis of supersonic air ejector: Turbulence modeling and assessment of 3D effects,” *International Journal of Heat and Fluid Flow,* vol. 56, pp. 305-316, 2015.

[10] B. J. Huang, J. M. Chang, C. P. Wang and V. A. Petrenko, “A 1-D analysis of ejector performance,” *International Journal of Refrigeration* , vol. 22, pp. 354-364, 1999.

[11] A. Arbel, A. Shklyar, D. Hershgal, M. Barak and M. Sokolov, “Ejector Irreversibility Characteristics,” *Journal of Fluids Engineering,* vol. 125, pp. 121-129, 2033.

[12] B. Djebedjian, S. Abdalla and M. A. Rayan, “Parametric investigation of boost jet pump performance,” in *Proceddings of FEDSM*, Boston, 2000.

[13] G. F. L. Al-Doori, “Investigation of Refrigeration System Steam Ejector Performance Through Experiments and Computational Simulations,” PhD Thesis, University of Southern Queensland, Toowoomba, 2013.

[14] X. CHen, S. Omer, M. Worall and S. Riffat, “Recent developements in ejector refrigeration technologies,” *Renewable and Sustainable Energy Reviews,* vol. 19, pp. 629-651, 2013.

[15] S. He, Y. Li and R. Z. Wang, “Progress of mathematical modeling on ejectors,” *Renewable and Sustainable Energy Reviews,* vol. 13, pp. 1760-1780, 2009.

[16] N. Ruangtrakoon, S. Aphornratana and M. Sriveerakul, “Experimental studies of a steam jet refrigeration cycle; Effect of the pripary nozzle geometries to system performance,” *Experimental Thermal and Fluid Science,* vol. 35, pp. 676-683, 2011.

[17] S. Varga, A. C. Oliveira, X. Ma, S. A. Omer, W. Zhang and S. B. Riffat, “Experimental and numerical analysis of a variable area ratio steam ejector,” *International Journal of Refrigeration* , vol. 34, pp. 1668-1675, 2011.

[18] V. Dvorak and P. Dancova, “An investigarion into air ejector with pulsating primary flow,” *World Academy of Science, Engineering and Technology,* vol. 5, pp. 542-548, 2011.

[19] D. E. Paxson, J. Eilson and T. Dougherty, “Unsteady Ejector Performance: An experimental investigation using a pulse driver,” in *38th AIAA/ASME/SAF/ASFF Joint Propulsion Meeting and Exhibit*, Indianapolis, 2002.

[20] R. Yapici and C. C. Yetisen, “Experimental study on ejector refrigeration system powered by low grade heat,” *Energy Conversion and Management,* vol. 48, pp. 1560-1568, 2007.

[21] K. Chunnanond and S. Aphornratana, “An experimental investigation of a steam ejector refrigerator: the analysis of the pressure profile along the ejector,” *Applied Thermal Engineering,* vol. 24, pp. 311-322, 2004.

[22] A. Selvaraju and A. Mani, “Experimental investigations on R134a vapour ejector refrigeration system,” *International Journal of Refrigeration,* vol. 29, pp. 1160-1166, 2006.

[23] T. Sankarlal and A. Mani, “Experimental investigations on ejector refrigeration system with ammonia,” *Renewable Energy,* vol. 32, pp. 1403-1413, 2007.

[24] R. Yapici, “Experimental investigation of performance of vapor ejector refrigeration system using refrigerant R123,” *Energy Conversion and Management,* vol. 49, pp. 953-961, 2008.

[25] D. Chong, M. Hu, W. Chen, J. Wang, J. Liu and J. Yan, “Experimental and numerical analysis of supersonic air ejector,” *Applied Energy,* vol. 130, pp. 679-684, 2014.

[26] A. Hemidi , F. Henry, S. Leclaire, J. M. Seynhaeve and Y. Bartosiewicz, “CFD analysis of a supersonic air ejector. Part I: Experimental validation of single-phase and two phase operation,” *Applied Thermal Engineering,* vol. 29, pp. 1523-1531, 2009.

[27] Y. Bartosiewicz, Z. Aidoun, P. Desevaux and Y. Mercadier, “Numerical and experimental investigations on supersonic ejectors,” *International Journal of Heat and Fluid Flow,* vol. 26, pp. 56-70, 2005.

[28] K. Chunnanond and S. Aphornratana , “An experimental investigation of a steam ejector refrigerator: the analysis of the pressure profile along the ejector,” *Applied Thermal Engineering,* vol. 24, pp. 311-322, 2004.

[29] I. W. Eames, S. Aphornratana and H. Haider, “A theoretical and experimental study of a small-scale steam jet refrigerator,” *International Journal Refrigeration,* vol. 18, no. 6, pp. 378-386, 1995.

[30] A. Hemidi, F. Henry, S. Leclaire, J.-M. Seynhaeve and Y. Bartosiewicz, “CFD analysis of a supersonic air ejector. part II: Relation between global operation and local flow features,” *Applied Thermal Engineering,* vol. 29, pp. 2990-2998, 2009.

[31] B. J. Huang and J. M. Chang, “Empirical correlation for ejector design,” *International Journal of Refrigeration,* vol. 22, pp. 379-388, 1999.

[32] S. Varga, A. C. Oliveira and B. Diaconu, “Numerical assessment of steam ejector efficiencies using CFD,” *International Journal of Refrigeration,* vol. 32, pp. 1203-1211, 2009.

[33] W. Pridasawas and P. Lundqvist, “A year-round dynamic simulation of a solar-driven ejector refrigeration system with iso-butane as a refrigerant,” *International Journal of Refrigeration,* vol. 30, pp. 840-850, 2007.

[34] H. Vidal, S. Colle and G. d. S. Pereira, “Modelling and hourly simulation of a solar ejector cooling system,” *Applied Thermal Engineering* , vol. 26, pp. 663-672, 2006.

[35] H. D. Kim, J. H. Lee, T. Setoguchi and S. Matsuo, “Computational Analysis of a variable ejector flow,” *J. of Thermal Science,* vol. 15, no. 2, pp. 140-144, 2006.

[36] X. Ma, Z. Wei and O. S. Riffat, “Experimental investigation of a novel steam ejector refrigerator suitable for solar energy applications,” *Applied Thermal Engineering,* vol. 30, pp. 1320-1325, 2010.

[37] Z. Chen , X. Jin, A. Shimizu and C. Dang, “Effects of the nozzle configuration on solar-powered variable geometry ejectors,” *Solar Energy,* vol. 150, pp. 275-286, 2017.

[38] P. R. Pereira, S. Varga, J. Soares and A. C. Oliveira, “Experimental results with a variable geometry ejector using R600a as working fluid,” *International Journal of Refrigeration,* vol. 46, pp. 77-85, 2014.

[39] D.-E. Sun, “Variable geometry ejectors and their applications in ejector refrigeration system,” *Energy* , vol. 21, no. 10, pp. 919-929, 1996.

[40] R. H. Yen, B. J. Huang, C. Y. Chen, T. Y. Shiu, C. W. Cheng, S. S. Chen and K. Shestopalov, “Performance optimization for a variable throat ejector in a solar refrigeration system,” *International Journal of Refrigeration,* vol. 36, pp. 1512-1520, 2013.

[41] H. C. Man, J. Duan and T. M. Yue, “Design and characteristic analysis of supersonic nozzles for high gas pressure laser cutting,” *Journal of Materials Processing Technology,* pp. 217-222, 1997.

[42] W. F. Louisos, A. A. Alexeenko, D. L. Hitt and A. Zilic, “Design considerations for supersonic micronozzles,” *International Journal of Manufacturing Research,* vol. 3, no. 1, pp. 80-113, 2008.

[43] I. W. Eames, A. Milazzo, D. Paganini and M. Livi, “The disign, manufacture and testing of a jet-pump chiller for air conditioning and industrial application,” *Applied Thermal Engineering,* vol. 58, pp. 234-240, 2013.

[44] P. B. Kuttan and M. Sajesh, “Optimization of divergent angle of a rocket engine nozzle using computational fluid dynamics,” *The International Journal of Engineering and Science (IJES),* vol. 2, no. 2, pp. 196-207, 2013.

[45] C. Saengmanee and K. Pianthong, “Design of a steam ejector by co-operating the ESDU design method and CFD Simulation,” in *The First TSME International Conference on Mechanical Engineering* , Ubon Ratchathani, Thailand, 2010.

[46] C. J. Korres, A. T. Papaioannou, V. Lygerou and N. G. Koumoutsos, “Solar cooling by thermal compression the dependence of the jet thermal compressor efficiency on the compression ratio,” *Energy,* vol. 27, pp. 795-805, 2002.

[47] A. L. Addy, J. C. Dutton and C. C. Mikkelsen, “Supersonic ejector-diffuser theory and experiments,” Department of Mechanical and Industrial Engineering, University of Illinois, Urbana, 1981.

[48] G. Flugel, “The design of jet pumps,” Technical report, NACA Technical Memo-randum No:982, 1939.

[49] N. H. Johannesen, Ejector Theory and Experiments, Denmark: Akad. for de Tekniske Videnskaber, 1951.

[50] ESDU86030, Ejectors and jet pumps. Design for steam driven flow, London: Engineering sciences data unit, 1986.

[51] J. Sarkar, “Performance characteristics of natural-refrigerants based ejector expansion refrigeration cycle,” *Journal of Power and Energy,* vol. 223, pp. 543-550, 2009.

[52] D. W. Sun, “Comparative study of the performance of an ejector refrigeration cycle operating with various refrigerants,” *Energy Conversion and Management,* vol. 40, pp. 873-884, 1999.

[53] R. Yapici and H. K. Ersoy, “Performance characteristics of the ejector refrigeration system based on the constant area ejector flow model,” *Energy Conversion and Management,* vol. 46, pp. 3117-3135, 2005.

[54] M. Ouzzane and Z. Aidoun, “Model development and numerical procedure for detailed ejector analysis and design,” *Applied Thermal Engineering,* vol. 23, pp. 2337-2351, 2003.

[55] I. W. Eames, “A new prescription for the design of supersonic jet-pumps: the constant rate of momentum change method,” *Applied Thermal Engineering,* vol. 22, pp. 121-131, 2002.

[56] Y. J. Chang and Y. M. Chen, “Enhancement of a steam-jet refrigeration using a novel application of the petal nozzle,” *Experimental Thermal and Fluid Science,* vol. 22, pp. 203-211, 2000.

[57] H. Zare-Behtash, N. Gongora and K. Kontis, “Effect of primary jet geometry on ejector performance: A cold-flow investigation,” *International Journal of Heat and Fluid Flow,* vol. 32, pp. 596-607, 2011.

[58] G. Hagemann, H. Immich, T. V. Nguyen and A. Eumnov, “Advanced rocket nozzles,” *Journal of Propulsion and Power,* vol. 14, no. 5, pp. 620-634, 1998.

[59] F. S. Kong , H. D. Kim, Y. Jin and T. Setoguchi, “Application of chevron nozzle to a supersonic ejector-diffuser system,” *Procedia Engineering,* vol. 56, pp. 193-200, 2013.

[60] G. Satyanaryana and C. Varun , “CFD analysis of convergent-divergent nozzle,” *Acta Technica Corvineiensis- Bulletin of Engineering,* vol. 6, pp. 139-144, 2013.

[61] B. K. Prafulla, C. C. Babu and S. P. Rao, “CFD analysis of convergent-divergent supersonic nozzle,” *International Journal of Computational Engieering Research,* vol. 3, no. 5, pp. 5-16, 2013.

[62] M. J. Opgenorth, D. Sederstrom, W. McDermott and C. S. Lengsfeld, "Maximizing pressure recovery using lobed nozzles in a supersonic ejector," *Applied Thermal Engineering,* vol. 37, pp. 396-402, 2012.

[63] Y. J. Chang and Y. M. Chen, "Rnhcncement of a steam-jet refrigeration using a novel application of the petal nozzle," *Experimental Thermal and Fluid Science,* vol. 22, pp. 203-211, 2000.

[64] A. K. Ababneh, C. A. Garris, A. W. Jawarneh and Tlila, "Investigation of the Mach number effects on fluid-to-fluid interaction in an unsteady ejector with a radial-flow diffuser," *Jordan Journal of Mechanical and Industrial Engineering,* vol. 3, no. 2, pp. 131-140, 2009.

[65] T. Hanada, A. Nakano, F. Tanigawa and J. Fufita, "Supersonic mixing enhanced by cavity-induced three-dimensional oscillatory flow," *Exp Fluids,* vol. 55, pp. 1711 (1-10), 2014.

[66] K. M. Tacina, "Thrust augmentation in an unsteady supersonic ejector," in *42nd AIAA Aerospace Siences Meeting and Exhibit AIAA,* Nevada, 2004.

[67] C. A. Garris, W. J. Hong, C. Mavriplis and Shipman, "A new thermally driven refrigeration system with enviromnetal benefits," in *33rd Intesociety Engineering Conference on Energy Conversion,* Colorado, 1998.

[68] A. K. Ababneh, A. M. Jayarneh and H. M. Tlilan, "The effects of the secondary fluid temperature on the energy transfer in an unsteady ejector with a radial-flow diffuser," *Heat Mass Transfer,* vol. 46, pp. 95-105, 2009.

[69] T. T. Ng and D. R. Otis, "Experimental investigation of a variable geometry, radial ejector," *Journal of Fluid Engineering,* vol. 101, pp. 491-494, 1979.

[70] E. Rusly, L. Aye, W. W. S. Charters and A. Ooi, "CFD analysis of ejector in a combined ejector cooling system," *International Journal of Refrigeration,* vol. 28, pp. 1092-1101, 2005.

[71] Y. Zhu, W. Cai, C. Wen and Y. Li, "Numerical investigation of geometry parameters for design of high performance ejectors," *Applied Thermal Engineering,* vol. 29, pp. 898-905, 2009.

[72] A. K. Ababneh, C. A. Garris, A. H. Jawarneh and H. Tlila, "Investigation of the Mach number effects on fluid-to-fluid interaction in an unsteady ejector with a radial-flow diffuser," *Jordan Journal of Mechanical and Industrial Engineering,* vol. 3, no. 2, pp. 131-140, 2009.

[73] K. Ariafar, D. Buttsworh, G. Al-Doori and R. Malpress, "Effect of mixing on the performance of wet steam ejectors," *Energy,* vol. 93, pp. 2030-2041, 2015.

[74] T. Sriveerakul, S. Aphornratana and K. Chunnanond, “Performance prediction of steam ejector using computational fluid dynamics: Part 2. Flow structure of a steam ejector influenced by operating pressures and geometries,” *International Journal of Thermal Science,* vol. 46, pp. 823-833, 2007.

[75] N. Ruangtrakoon, T. Thongtip, S. Aphornratana and T. Sriveerakul, “CFD simulation on the effect of primary nozzle geometries for a steam ejector in refrigeration cycle,” *International Journal of Thermal Sciences,* vol. 63, pp. 133-145, 2013.

[76] H. Rahimi, R. Malpress and D. Buttsworth, “Investigation of Radial Flow Ejector Concept through CFD Analysis,” in *20th Australasian Fluid Mechanics Conference,* Perth, 2016.

[77] M. Al-Ajlouni, “An automatic method for creating the profile of supersonic convergent-divergent nozzle,” *Jordan Journal of Mechanical and Industrial Engineering,* vol. 4, no. 3, pp. 404-411, 2010.

[78] J. B. Pearson, D. B. Landrum and C. W. Hawk, “Parametric study of solar thermal rocket nozzle performance,” *NASA Technical Memorandum,* p. 111354, 1994.

[79] D. R. Buttsworth, “Calibration of a gas dynamic model for ejector performance,” in *Proceedings of the 2nd Thermal and Fluid Engineering Conference*, Las Vegas, NV, USA, 2017.

[80] K. Pianthong, W. Seehanam, M. Behnia, T. Sriveerakul and S. Aphornratana, “Investigation and improvement of ejector refrigeration system using computational fluid dynamics technique,” *Energy Conversion and Management,* vol. 48, pp. 2556-2564, 2007.

[81] C. A. Garris, W. J. Hong, C. Mavriplis and A. Shipman, “A new thermally driven refrigeration system with enviromnetal benefits,” in *33rd Intesociety Engineering Conference on Energy Conversion,* Colorado, 1998.

[82] H. Rahimi, D. Buttsworth and R. Malpress, “CFD Study of a Variable Flow Geometry Radial Ejector,” in *the 4th International Conference of Fluid Flow, Heat and Mass Transfer (FFHMT'17),* Toronto, 2017.

[83] L. Wang, C. Wang , W. Hou , H. Zhao and H. Zhang, “Experimental investigation on ejector performance near critical back pressure,” *International Journal of Refrigeration,* vol. 80, pp. 158-168, 2017.